Determination of microbial metabolomics by comprehensive two-dimensional gas chromatography-mass spectrometry and inkjet-MALDI-MS

Dissertation

For the academic degree of

Doctor of nature science

− Dr. rer. nat. −

Presented by

Junjie Li

Submitted to

Applied Analytical Chemistry

University of Duisburg-Essen

2021

All the work was carried out in the period from December 2015 to December 2019 in the working group of Prof. Dr. Oliver J. Schmitz at the Institute for Applied Analytical Chemistry in the University of Duisburg-Essen.
Day of the disputation: 24.08.2021

Reviewer: Prof. Dr. Oliver J. Schmitz

Prof. Dr. Torsten C. Schmidt

Chairman: Prof. Dr. Eckhard Spohr

DOI: 10.17185/duepublico/74914
URN: urn:nbn:de:hbz:464-20211105-082124-6

I hereby certify that I have submitted the present work entitled

" *Determination of microbial metabolomics by comprehensive two-dimensional gas chromatography-mass spectrometry and inkjet-MALDI-MS* "

I have written the thesis myself and have not used any auxiliary materials or sources other than those indicated. The thesis has not been submitted in this or a similar form to any other university. I have not undergone a failed doctoral procedure in this or any other subject.

15.06.2021

_____

Junjie Li

Table of Content

1 Abstract

Metabolome, as the downstream of the genome, the entire set of metabolites in a biological system, describes and reflects the cellular activities more vividly and specifically at the functional level. The procedures of sample preparation for metabolomics studies need to assure reliable and reproducible results. These are particularly challenging, especially for microbial samples, which are sensitive to manipulation and limited in quantity to some extent. Therefore, this study aimed to establish reliable and reproducible sample preparation methods for microbial species allowing metabolomics study in bacteria via mass spectrometric analysis. A gram-negative bacterium, *C. marina*, was chosen for optimizing a protocol from the quenching step to the final derivatization. By applying this, more than 170 intensive signals were detected as a "snapshot" of its intracellular state with acceptable a relative standard deviation (RSD) for most analytes. Based on this, the metabolic response of *C. marina* could be investigated under the artificial oxidative stress by ozone treatment and famishing stress by nutritional starvation. With the comparison in contour plots and the visualization in GasPedal, intracellular pathways involved metabolites such as fatty acids (oleic acid), amino acids (L-cystine) were found to be the potential biomarkers of bacterial intracellular state varying once encountering extreme conditions.

The second goal was to overcome the limitation of bacteria quantity. To this scope, a sample introduction system combined with an inkjet technique was set up and then optimized for the MALDI-MS spotting method. To reduce the "coffee-ring" effect, the inkjet technique was further optimized involved multi-layer introduction. The feasibility of the method was tested by analyzing *E. coli*, which demonstrated that the inkjet printing provides spots homogeneity and possibility to analyze very small amount of bacteria. By inkjet printing, significant signals of *E. coli* metabolites could be obtained with approximately 1000 bacteria. Thus, an alternative introduction method was proposed for bacterial samples on MALDI-MS.

2 Introduction

2.1 Microbial metabolomics

In the 1990s, Collar *et al.* and Montel *et al.* started the pre-metabolome era by applying metabolite profiling to microbiology [1-3]. Followed by Andersen *et al.* and Frisvad *et al.*, their work contributed to analyzing metabolic profiles to compare related species, which proved by providing distinct chromatographic and spectroscopic results [4-6]. In 1998, the keyword "metabolome" was first proposed, considered as a functional tool for understanding the "genome", i.e. the genetic composition of the organism and the "transcriptome" of the expressional profiles [7, 8]. Thus, the era of metabolomics and its application started with microbial systems [8, 9].

There are multiple reasons why microbial metabolomics grew fast and now plays a vital role in the current metabolic studies. For example, compared to multicellular organisms, microbial organisms are simpler and easier to manipulate in general. By taking advantage of this, microbial metabolomics becomes one of the ideal platforms. Such a platform could be utilized for applying and validating assumptions that the development of metabolomics could benefit from [10]. On the other hand, from the point of view of system biology, as shown in figure 1, the metabolome can be considered as the downstream of the genome and thereby may provide insights into the microbial activities and may help to understand microbial interactions and cellular functions. Moreover, the study of the metabolome contributes to integrate biological

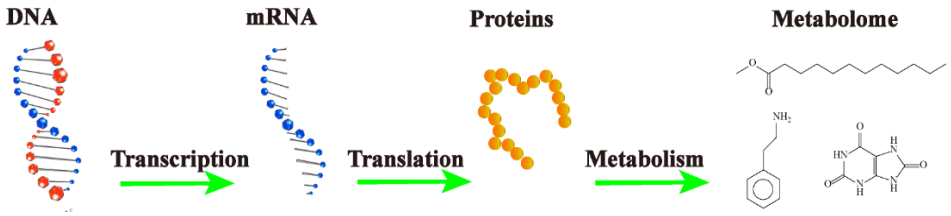

Figure 1 Overview of molecular information in omics level from genotype to phenotype

information from different levels (genome, transcriptome, proteome, metabolome), thus smoothing the path for life scientists.

Saccharomyces cerevisiae was successfully analyzed as a model organism by mass spectrometry-based method for determining its intracellular metabolites by Castrillo *et al.*, who proposed first the idea of metabolic fingerprinting analysis [11]. Also, in 2003, Allen *et al.* pointed out the meaning of extracellular metabolites from *S. cerevisiae* in the medium culture, which was named metabolic footprinting for phenotyping classification [12].

The general workflow of microbial metabolome analysis is depicted in figure 2 [13]. Such a process starts with the cultivation of the cells under defined conditions, followed by the separation of the cells from growing broth. How to separate the extra- and intracellular metabolites and to snap the metabolic activities without affecting metabolic state and cellular integrity would be the primary thinking for a feasible protocol. Thus, a quenching step is crucial for capturing reliable and accurate metabolic

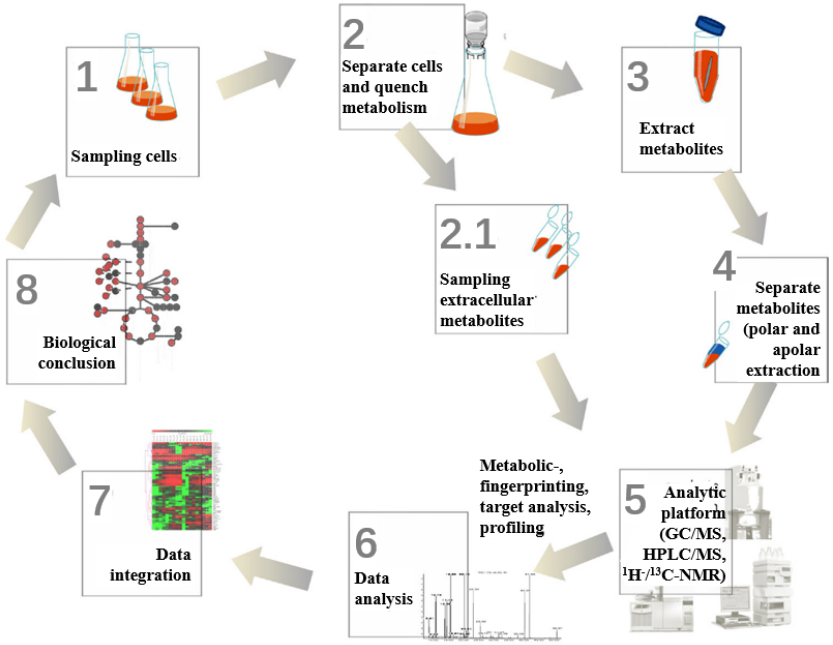

Figure 2 General workflow of metabolome study. For different analyzing targets, the profiling could split into extracellular metabolites (footprinting analysis) and intracellular ones (fingerprinting analysis). After this, the data could be integrated with other information, which draws the conclusion for further research purposes (copy with permission)(Liebke *et al.*) [13]

information at an assigned time point. The intracellular conversion rates are relatively high and not comparable with those metabolites' concentration levels [14]. Therefore, to eliminate those potential enzymatic effects sufficiently, it is necessary to carry out a quenching step as soon as possible and in a short period of time.

There are many ways to inactivate the enzymatic activities during the quenching step. It is well known that organic solvents, too high temperature or low/high pHs lead to the denaturation of enzymes. Tian *et al.* selected methanol, ethanol, acetone, and acetonitrile as the organic quenching solvent and evaluated different combinations. As a result, acetonitrile turned to be the most efficient one [15]. Quenching bacteria at high temperatures typically leads to unwanted membrane damage and leakage compared to those at low temperatures. Due to the temperature dependence of enzymatic activities, sample preparation at relatively low temperature became another choice to reduce the enzyme activities. 60% cold methanol was found to be a sufficient quenching solution as compared to others [16-18]. In contrast, physiological saline was proposed as the substitution to replace the organic solvent with low membrane damage by Wang *et al.* [19], which was considered as a "green" approach for quenching, especially for large-scale sample preparation.

To obtain as much metabolic information as possible, it is crucial that cells are fully lysed, which allows extracting intracellular metabolites with high coverage and recovery. A two-phase extraction mixture combining water, methanol, and chloroform in a specific ratio is one of the most popular strategies. In this case, the water-soluble metabolites stay in the upper phase, and nonpolar or weakly polar ones dissolve in the lower phase. A composition of 79:21:200 water, methanol, and chloroform was reported to be efficient for the water-soluble metabolites of *E. coli* by Wang *et al.* [19]. Nevertheless, Winder *et al.* demonstrated that single-phase extraction by using methanol was slightly better than methanol/chloroform two-phase extraction [17].

2.2 Microbial environmental stress

2.2.1 Oxidative stress

In general, microorganisms could survive and reproduce due to the adaption to optimal environments [20]. However, the balance in such optimum conditions could be broken by any extreme change, defined as “stress”. The responses of microorganisms to the stresses lead to lag time increasing, growth rate reducing, even cell death [21, 22]. Those stresses might include cold or heat shock [23, 24], hyperosmotic pressure [25], acid or organic solvent stress [26, 27], and oxidative stress [28, 29]. Compared to other kinds of stresses described before, oxidative stress results in not physical damage to the bacteria. However, it leads to oxidative damage via the accumulation of reactive oxygen species (ROS), which influences the lipids, nucleic acids, and proteins, resulting in cell toxicity [30]. Typical ROS include superoxide anion (O_2^-), hydrogen peroxide (H_2O_2), and hydroxyl radicals ($OH^{\cdot}$), which could disturb the redox balance of different biological targets [30, 31].

As a powerful oxidant, Ozone has been widely used and considered as one of the most effective antimicrobial agents since the last decades [32, 33]. Once added into aqueous solutions, ozone was decomposed rapidly, followed by the generation of superoxide radicals ($O_2^{\cdot -}$), hydroperoxy radicals ($HO_2^{\cdot}$), and $OH^{\cdot}$ radicals [34]. As shown in figure 3, these radicals would attack the bacterial cell surface by oxidizing amino acids, peptides, or proteins. Once passing through the membrane, it also leads to DNA or intracellular protein damages, impacting the reparation and transcription, resulting in cell lysis or death [35, 36]. Oxidative damage of protein is stepwise depending on the increasing concentrations of ROS and their molecular nature. Carbonylation can reduce the protein activity and induce unfolding. In the worst case, the proteins can be heavily oxidized and cross-linked to each other, which finally leads to aggregation and

functional damage for taking place the proteasomal degradation [37, 38]. Moreover, damage to the DNA may block the activity of the polymerase. Thymine in *E. coli*, for example, was proved to be converted into cis- and trans-5,6-dihydroxy-5,6-dihydrothymine (thymine glycol (Tg)) [39], which was responsible for DNA inactivation and might result in cell death by DNA replication blockage [40].

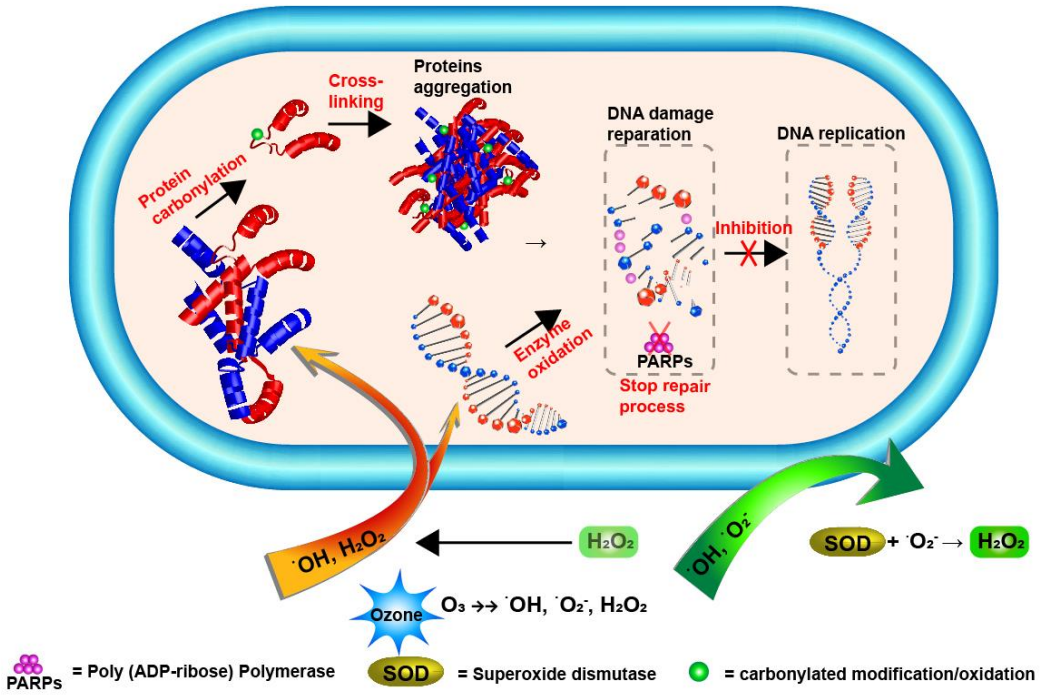

Figure 3 Decomposition of Ozone in aqueous situation. Bacteria cell membrane, intracellular proteins and DNAs become the biological oxidized targets for the decomposed radicals

2.2.2 Starvation stress

The survival of bacteria in natural conditions depends on their physiological states. Typically, in satisfactory environments, bacteria grow exponentially. Once the surroundings are no longer favorable, bacteria start to modify their growing characteristics such as growing slowly or dying [41-43]. Nutrient availability is essential for the survival of bacteria. Compared to the laboratory conditions, the nutrients can be insufficient in the natural environment, which leads to so-called

"starvation stress" [41]. At the beginning of a starvation period, several changes in the characteristics of the might be observed, such as a decreased cell size, increased respiration rate, modification of membrane properties and composition, adherence to surfaces or chemotaxis. Some types of bacteria might degrade many endoenzymes to keep the metabolism stable. However, such stability might collapse after long-time starvation, which would finally result in suspended animation or death [44].

For marine bacteria, the patterns of behavior during starvation are quite species-dependent. Amy *et al.* observed 16 randomly picked isolates obtained from a North Pacific Experiment cruise together with Ant-300, a marine psychrophilic vibrio, representing the most common marine bacteria species [45]. As a result, the patterns of Ant-300 and 7 of 16 isolates have an initial increase followed by a decrease in viable cell numbers. In contrast, the viability in 4 of 16 isolates continued to decrease even after eight weeks. Conversely, 5 of 16 isolates showed patterns with an increasing number of cells from the beginning of the starvation.

2.3 Microorganisms

2.3.1 Cobetia marina

Cobetia marina is a marine bacterium, which was first named as *Arthrobacter marinus* in 1971 by Cobet *et al.* [46]. With growing knowledge, it has been described and named differently, such as *Pseudomonas marina* [47], *Delaya marina* [48, 49], or *Halomonas marina* [50]. In 1996, Dobson *et al.* determined the 16S rRNA sequence of ACAM 21, a representative strain of a biovar of *Halomonas subglaciescola*, which contained all the significant features as formerly named genera *Delaya*, *Halomonas*, *Halovibrio,* and *Paracoccus halodenitrificans*. Thus, a unification was proposed for all these species under the genus *Halomonas* [51]. Several years later, the genus *Halomonas* was developed from 15 to 22 species by intensive study, which attracted more attention to

its family *Halomonadaceae* [52-56]. In 2002, 16S rRNA sequences from seven species of *Halomonas* were resequenced, which demonstrated the results suggesting *Halomonas marina* to be a separate genus from *Halomonas* [57].

Furthermore, those phylogenetic researches indicated that the 23S rRNA sequences of *Halomonas marina* were quite different from other species in *Halomonas*. It was then proposed to be transferred as a new genus, *Cobetia* gen. nov., as *Cobetia marina* comb. nov embedded into the family *Halomonadaceae*. [58] Arahal *et al.* also summarized from other contributors and described the detailed phenotype and genotype of the new classified *Cobetia marina* (*C. marina*). [58] It has general features, including gram-negative, straight, rod-shaped, growing aerobically in the range of 0.5 to 20% (wt/vol) salts, temperatures from 10 to 42 ºC, and preferring culture pH 5 to 10 [58].

Since *C. marina* has a morphology characterized by both exopolymer and flagella, it was selected as a model test strain for studies of bacterial colonization and biofilm formation in biofouling [49]. It has been revealed that the exopolysaccharide is essential for *C. marina* surface colonization [48]. However, previous studies mainly stayed on its phenotypic extracellular characteristics, which barely focused on the metabolic aspect [59]. The analysis of metabolic characteristics of this bacterium might help to understand how anti-biofouling treatment or artificial environmental stress affect its metabolic activity. This combined with former researches may help to get more comprehensive insights on the secondary colonization influenced by the biofilms of *C. marina*.

2.3.2 Escherichia coli

Escherichia coli, a gram-negative, is known as one of the most studied bacteria globally, first isolated by Theodor Escherich [60, 61]. This fast-growing intestinal bacterium was called *Bacterium coli* commune by Escherich at the beginning, which was proposed to

be named *Escherichia coli* by Castellani and Chalmers in 1919, then given official recognition until 1958 [62-64]. After rapid studies on *E. coli*, the complete genome sequence of *E. coli* K-12 was described in 1997 [65].

E. coli is often used as a model organism for its remarkable characteristics, such as being non-pathogenic in most cases. It is able to survive under variable conditions and growing fast on many different nutrients [66]. These advantages were also the reasons why *E. coli* was selected as the experimental object for the establishment and implementation of inkjet introduction in this study.

2.4 Analytical methods for metabolomics investigations

With chromatographic separation, metabolic components could be eluted from the columns at different time points during the measurements. In contrast, measuring without or with poor separation might lead to those extracted metabolites simultaneously arriving at the mass spectrometry detector entrance. Moreover, according to the structures, diverse compounds' ionization capacity makes them charging and responding differently once entering MS. It is then difficult to identify those compounds with similar chemical structures, such as isomeric or isobaric compounds. Thus, the ion suppression phenomenon would occur once analytes compete for available charges. The most ionizable compounds dominate the mass spectra, which affects the whole detection in precision, accuracy, and capacity [67].

2.4.1 Nuclear magnetic resonance spectroscopy

Compared to other metabolic platforms (e.g., LC-MS or GC-MS), there are several advantages for the NMR spectroscopy. Firstly, the analytes could be detected by NMR without chromatographic separation or sample preparation. Moreover, NMR spectroscopy is capable of large-scale or high throughput metabolic samples due to its

high automation and reproducibility for routine identification. Thirdly, nondestructive analysis enables NMR to measure living cells for real-time metabolite profiling, which could hardly be realized by LC-MS or GC-MS [68].

Nicholson's group contributed to the metabolic fingerprint analysis with NMR for biofluids such as urine and plasma. By monitoring the compositions of biofluids, the metabolic profiles were recorded corresponding to the extracellular stress from toxicity or disease. The biomarkers were identified successfully, which fluctuate in response to such stress [69]. Palama *et al.* proposed a fast and reliable NMR-based approach to rapidly distinguish by metabolic profiling of extracellular metabolites among six different bacterial species. In this case, the potential of NMR was demonstrated for the footprinting analysis of bacteria in clinical diagnosis [70].

However, NMR also has some drawbacks, especially its sensitivity, which is less sensitive for the factor from 10 to 100 compared to other MS techniques [71]. Besides, the peak overlapping in NMR also leads to challenges for those non-target analyses of compounds in complex samples. Although two-dimensional NMR was proposed to solve this problem, the sensitivity and throughput were sacrificed compared to one-dimensional NMR [72].

2.4.2 Liquid chromatography coupled to mass spectrometry

Coulier *et al.* proposed using ion-pair liquid chromatography coupled to electrospray ionization mass spectrometry (IP-LC-ESI-MS) to simultaneously quantify several important metabolic classes from *Bacillus subtilis* and *E. coli* [73]. Hexylamine was utilized as the ion-pairing agent under optimized pH values to obtain better retention and peak shapes than reverse phase (RP)-LC-MS [73].

To achieve lower detection limits, a nanoscale IP-RP-HPLC-MS method was developed by Kiefer *et al.* with tributylamine as the ion-paring reagent. The ion suppression was lower by taking advantage of the small injection volume for the nanoelectrospray system, which enabled identifying of 20 ± 4 metabolites with 1.5 ng cell dry weight and 157 ± 5 metabolites with 150 ng cell dry weight from *Methylobacterium extorquens* [74].

HILIC mode provides better separation for polar compounds compared to RP mode. Therefore, a HILIC approach was presented by Fei *et al.* for the extraction of *Sinorhizobium meliloti*. It demonstrated a coverage of 92.2% of detectable metabolome for such gram-negative bacterium [75].

2.4.3 Gas chromatography coupled to mass spectrometry

For the metabolomics research, columns with limited coating materials were applied in GC-MS, such as DB-5, TR-5, Rtx-5 with 95% dimethyl/5% diphenyl polysiloxane DB-5MS, Rtx-5sil MS with more inert polysilarylene [76].

GC-MS is mainly used to separate volatile and thermal stable analytes. In contrast, polar metabolites such as amino acids, free fatty acids need to be derivatized by alkylation or silylation before analysis. For example, silylating a polar functional group with trimethylsilyl (TMS) is to substitute its active hydrogens (in -OH, -COOH, NH, $-NH_2$, and -SH groups) by TMS group [77]. It increases the volatility of the analytes by reducing the dipole-dipole interactions. Furthermore, chromatography resolution and MS identification would be improved by increased molecular fragments [76]. The silylated derivatives were formed as shown in the equation below:

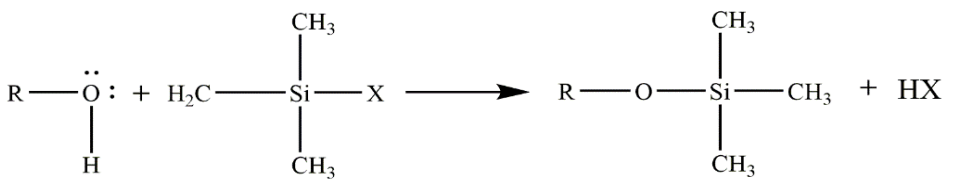

(1)

In the case of trimethyl-chlorosilane (TMCS), “X” is the -Cl group, which reacts with the substituted group from samples [77].

As described by Kataoka *et al.*, silylation contributed to the volatility and stability of derivated compounds, which then dramatically improves the peak shape during measurements [78]. Chen *et al.* and Lin *et al.* also reported that some hydroxyl and amino compounds were able to be measured by GC with the help of silylation at the temperature range of 200 to 300 ºC [79, 80].

There are many derivatizing reagents for the silylation, including Hexamethyldisilzane, Trimethylchlorosilane, Trimethylsilylimidazole, Bistrimethylsilyltrifluoroacetamide (BSTFA), N-Methyl-N-(trimethylsilyl) trifluoroacetamide (MSTFA), and N-Methyl-N-t-butyldimethylsilyltrifluoroacetamide. As mentioned before, alcohols and acids would be silylated into trimethylsilyl ethers or trimethylsilyl esters once properly reacted with these reagents.

Except for the solvent system, the derivatization reagent efficiency could also be influenced by the catalyst additive, such as pyridine used in the silylation. These catalysts increase the reactivity of the derivatization reagent and drive the reaction forward [77]. Importantly, such derivatization must be proceeded without water interfering. Otherwise, the reaction might be slow down or terminated. In some cases, even a little moisture would decompose the TMS reagent or newly formed derivatives [81].

Since the concept of metabolomics was proposed in the 1990s, the research interests focused on metabolite profiling. It has paved the way to followed microbial metabolomics. *Corynebacterium glutamicum*, a gram-positive bacterium, was analyzed with a GC-MS method presented by Strelkov *et al.* until 2004. In this method, pyridine was utilized as the catalyst for the reagent MSTFA in the derivatization step. Out of 330

significant peaks, 121 different metabolites were identified with high reproducibility [82].

Koek *et al.* later demonstrated a method with oximation and silylation on GC-MS, which was validated for the cell extracts of *Bacillus subtilis*, *Propionibacterium freudenreichii,* and *Escherichia coli*. Metabolites such as alcohols, aldehydes, amino acids were detected and showed high linearity for most compounds [83].

2.4.4 Advance of two-dimensional gas chromatography in metabolomics

Conventional GC provides adequate sensitivity and linearity for some analytical detection. However, it cannot resolve analytes in complex samples, especially for those in biological extracts. Liu and Philips developed the comprehensive two-dimensional gas chromatography (GCxGC) with a thermal desorption modulator, which generates a much higher peak capacity than one-dimensional GC [84].

In principle, the improvement of comprehensive GCxGC depends on the orthogonality formed by two columns, which then multiplies the peak capacity sufficiently [85]. GCxGC was evolved from GC-GC, which is so-called “heart-cutting” since 1958 proposed by Simmons *et al.*[86].

Such heart-cutting method was developed for the target analysis that the selected fractions would be transferred to the second column after eluted from the first column. Although the heart-cutting method could enhance the resolution compared to GC, it becomes inadequate once the researchers are more concerned about the unknowns in the whole sample than those known targets.

If the peak capacity of GC with a single column were n, the one in the comprehensive GCxGC, in orthogonal separation, would be $n_1 \times n_2$ instead of $n_1 + n_2$ in heart-cutting GC-GC (peak capacity n_1 of the first dimension, n_2 of the second dimension). In this so-called "orthogonal separation", both dimensions need to be independent and uncorrelated in separation mechanisms and retention times. To obtain the orthogonality of both columns, each column's polarity should be different, such as the combinations of nonpolar-polar or polar-nonpolar [87]. Thus, the peak distribution could also be improved to obtain optimal peak capacity in actual measurements.

To realize such "heart-cutting", the modulator is a critical factor for GCxGC, which was designed for transporting the sample from the first column to the head of the second column. In principle, the modulator is responsible for continuously collecting eluent from the first column, then trapping it into small fractions. Moreover, each fraction would be refocused and then injected into the second column in a regular time interval, so-called modulation time. A peak from the first dimension would be typically fractionated into 3 or 4 times before reaching the second column's head. Thus, the modulator enables the peak from the first dimension to be further separated in the second dimension [88].

On the other hand, the separation time on the second column needs to be estimated for choosing the proper modulation time, which is to avoid the so-called "wrap-around effect". The fraction reinjected into the second dimension might influence the separation of the former fraction or even result in overlaying if it was released before the former fraction eluted from the second column. Therefore, usually, the modulation time should be set longer than the second dimension eluting time.

There are two basic classes of modulation interfaces, thermal-based and valve-based interfaces. As a more common one, the thermal-based interface modulation could be realized by two types of modulators, the heat and cryogenic modulator [89]. The heat

modulator drives trapped fractions by rapidly heating with electrical current. In contrast, the cryogenic modulator traps the fractions by cryojet with liquid gases such as nitrogen or CO_2, then remobilizes them with a hot-jet air stream [90]. In this study, a modulator utilizing liquid nitrogen for trapping analytes fractions was adopted.

For a GCxGC run, as shown in figure 4 [91], peaks from the first column were cut into small fractions in a certain modulation period. Each fraction was then separated on the second column to generate a second dimension chromatogram. These second dimension chromatograms were stacked to get a 2D chromatogram, with the x-axis representing the retention time on the first dimension and the y-axis for the second dimension. With GC image software, such a 2D chromatogram could be visualized as a 2D contour plot or even a 3D plot.

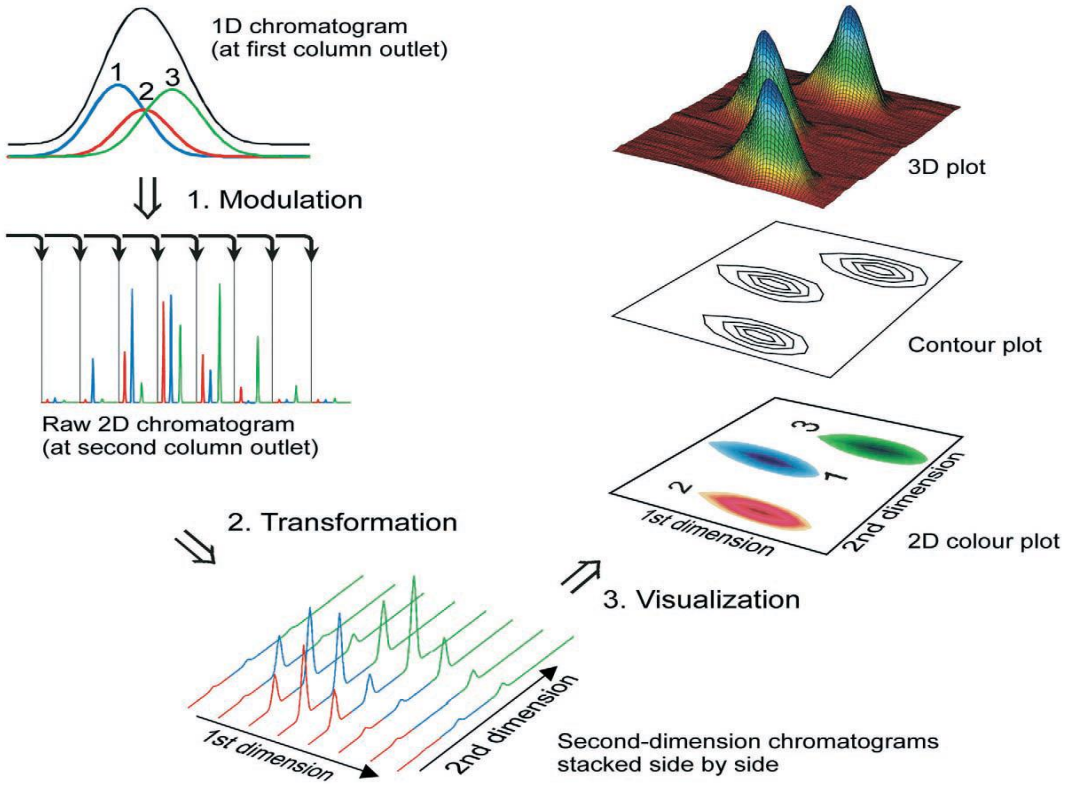

Figure 4 Workflow of GCxGC modulation and its data visualization (copy with permission) [91]

For complex samples, the orthogonality formed by implementing two complementary separations mechanisms (GCxGC) could provide more selectivity and overall information in equivalent time compared to the conventional one-dimensional GC

system [92-96]. In previous work, the Lidstrom group's research demonstrated the capability of mass-based GCxGC on profiling and identifying gram-negative bacteria species by determining those derivatives of water-soluble metabolites such as amino acids, amine, and sugars [97-99]. According to Kamatou *et al.*, later in 2010, GCxGC was proved to have superior separation capacity, especially for complex matrix compared to the conventional one-dimensional GC [100].

2.4.5 Matrix-assisted laser-desorption ionization mass spectrometry

Since the 1980s, the development of matrix-assisted laser desorption/ionization (MALDI), especially coupled to time-of-flight (TOF) mass spectrometry (MS), has provided high applicability for the identification of large biomolecules [101-104]. Compared to the conventional harsh ionization methods [105], such a soft ionized technique offers an alternative approach for rapid and accurate detection in many applications involving bacteria, such as clinical identification [106, 107], antibiotic resistance observation [108], and biomarkers characterization [109].

Both ESI and MALDI are capable of analyzing large biological molecules. However, there are some advantages of MALDI-TOF MS compared to ESI-MS. First, MALDI produces single charged ions, which reduces the complexity of data interpretation. Secondly, chromatography separation is unnecessary for MALDI, unlike ESI-MS. Thus, highly automated MALDI-TOF is suitable for large-scale analytical work [107].

In MALDI analysis, the most common method for sample loading is the dried droplets method. Usually, a liquid sample was mixed with a saturated matrix solution dissolved energy-absorbent organic compounds. Such mixture is typically in microliter scale, which then dropped onto MALDI plate. After being dried with air or nitrogen stream under ambient temperature [102], the sample and matrix is co-crystallized [110]. Then,

the matrix/analyte mixture were rapidly heated up by a brief laser pulse, leading to the matrix molecules becoming an excited state and carrying the analyte molecules into the gas phase. The analyte molecules are single protonated by matrix molecules and accelerated to reach the analyzer [110]. To date, α-cyano-4-hydroxycinnamic acid (CHCA), 2,5-dihydroxy benzoic acid (DHB), and 3,5-dimethoxy-4-hydroxycinnamic acid (SA, sinapinic acid) were demonstrated to be the most sufficient matrices for microbiological study.

In some cases, the number of microorganisms is limited for the sample preparation according to a standard extraction protocol. Therefore, direct bacterial profiling (DBP) was proposed as an "intact-cell" approach for the rapid identification of bacteria with MALDI-TOF-MS. The bacterial colonies were picked from the agar plates and mixed with CHCA matrix, then dried in the air for further instrumental analysis. In 1996, Holland *et al.* using the DBP method to distinguish five different bacteria from their own unknown species, including *Enterobacter cloacae, Proteus mirabilis, Shingella flexneri, Escherichia coli,* and *Serratia marcescens* [111]. Besides, some gram-negative species such *Vibrio* spp., *Yersinia* spp., and *Neisseria* spp. were demonstrated to be successfully identified from the subtyping by DBP [112-114].

To achieve better ionization, the sample preparation method for depositing of sample and matrix is an important factor for the protocol. In 2007, four different deposition methods were compared by Liu *et al.* At first, the pre-mixture of sample and matrix was applied onto the plate and dried. Secondly, a matrix pre-layer was formed by the diluted matrix deposition then applied with the pre-mixture of sample and matrix. Thirdly, a two-layer method was involved, the deposition of CHCA in acetone as the first layer followed by the pre-mixture application of CHCA and sample as the second layer on its top. Fourthly, a dried-droplet method was used that the sample solution was dropped first and dried, which was then overlaid by a layer of CHCA matrix. As a result, *Yersinia pestis* was analyzed with deposition methods mentioned before, which revealed that the

dried-droplet method showed the best performance in reproducibility by enhancing the sample's homogeneity [115].

Furthermore, a technique so-called "compressed sample" (CS) was developed by Hyzak *et al.* in 2011. Compared to the conventional dried droplets method, the CS technique was utilized with a solvent-free deposition, which provides a more uniform distribution of analytes by a drilling structure. The quantitative analysis of synthetic peptides and polymers could be proceeded with such technique with relative standard deviations less than 8% and correlation coefficients higher than 0.982 [116]. Besides, Hyzak *et al.* improved the CS technique in 2013 with some optimization, such as homogenization of electrical field brought by the drills, additive of metal powder to the sample/matrix mixture, and adaptation of a laser raster. These improvements allowed the more precise result and higher detection range of peptides molecular weight instead of 3500 DA than before [117].

2.5 Inkjet technique and its advances

In the 1980s, the term so-called "cytoscription" was proposed by Klebe *et al.*, which adopted the inkjet for precisely positioning cells to generate single cells [118]. After that, the interest in inkjet printing was extended from mechanical electronics to the bioengineering fields [119]. Two main types of inkjet dispensers are generally involved in cellular printing, thermal and piezoelectric driving, shown in figure 5 [120, 121]. Regarding the thermal printing, the air bubbles are heated up by a thermal resistor, leading to the expansion of the bubbles and expels liquid drops. In the piezoelectric technique, the liquid droplets are squeezed out of the nozzle by the charging crystal made by piezoelectric material [122].

Xu *et al.* proposed the possibility of using a thermal inkjet printer to fabricate *E. coli* colony arrays and to position the mammalian cells such as Chinese Hamster Ovary as

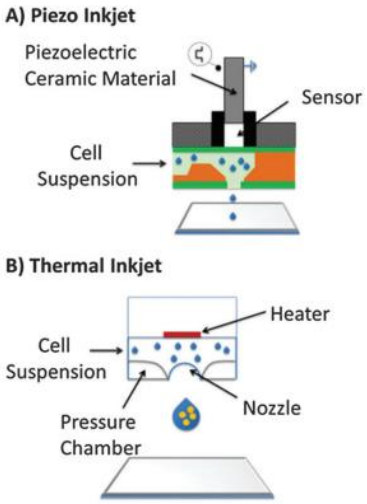

Figure 5 Inkjet printing technology (A) piezoelectric printing (B) thermal printing (copy with permission) [122]

pre-designed patterns [123, 124]. Saunders *et al.* simulated the delivery of human fibroblasts (HT1080) by piezoelectric drop-on-demand inkjet method and observed them under different stresses that occurred during the printing process [125]. To avoid heat damages, Nakamura *et al.* presented an application of electrically driven piezo inkjet in tissue engineering. The bovine endothelial cells were then successfully transferred from the cell suspension onto the culture disks in inkjet droplets. It turned out to an alternative for the migration and on-site cultivation on individual tiny dots of living cells [126].

After years of research, piezoelectric printing has been demonstrated to be a better choice for microorganisms patterning. A setup involved a piezoelectric inkjet printer with an XY stage was presented by Merrin *et al.* for multi-strain bacteria patterning [127]. *E. coli* strain MG1655, as the object, was printed in the single droplets by Choi *et al.* with a commercially available inkjet printer, obtaining an average of 10 cells of *E. coli* in a single droplet. In this case, inkjet printing technology was useful for investigating bacterial cell-to-cell communication due to the high resolution and pre-defined order [128].

Except for printing droplets to observe living organisms by microscopy, the inkjet printing technique could also be applied for the sample preparation or introduction for some detection techniques, such as MS [129]. The rat brain tissues were sectioned first, then coated by matrix solution through a chemical piezoelectric inkjet printer. Such coated tissues were ready to be detected by MALDI TOF/TOF for MALDI imaging [130].

Inkjet printing technique was also applied for ESI-MS. In 2012, Luo *et al.* optimized the conventional ESI droplets introduction by adopting a piezoelectric inkjet printer with a pulse generator to form the droplets. With such a printer, the volume of droplets and their location on the probe could be accurately regulated. [131].

To date, many inkjet printing techniques have been applied to the introduction of bacteria onto the substrate, such as droplet-based clonal culturing [132], multi-strain bacteria automated printing [127], and multi-layer printing for anti-microbial test [133]. Thus, the feasibility of inkjet introduction for bacteria onto the MALDI plate has been validated. It offers an alternative introduction platform in MALDI detection for some advantages, such as high throughput, automated sample loading, and adjustable volume by controlling the number of droplets.

2.6 “Coffee-ring” effect

The existence of heterogeneous distribution resulting from the droplets method mentioned above was reported by Vorm *et al.* [134], which leads to poor shot-to-shot repeatability and less sample-to-sample reproducibility. Such heterogeneity forms so-called “sweet spots” or “hot spots”, the tiny spot area with concentrated analyte molecules in sample deposits, which could increase the measuring time and difficulty to obtain accurate quantitation results [135].

Not only “sweet spots”, but ring-like fashion surrounding the sample spot has also been observed; such phenomenon could be attributed to the so-called “coffee-ring” effect [136], which formed due to the movement of capillary outward flow during evaporation [137]. By this flow, the solute and suspended non-volatile particles might be carried to the edge of the droplet as evaporation proceeds [136]. Thus, the homogeneity of the MALDI spot could be influenced by such a “coffee-ring” effect, which attracts many researchers to find out solutions in different fields.

2.7 Aim of the thesis

Bacterial metabolic phenotyping is a powerful technique to investigate the metabolic state of selected bacterial populations and their corresponding responses under stresses. Over the last few decades, many protocols about microbial sample preparation have been proposed. However, the previous studies barely focused on protocols for preparing samples for two-dimensional GCxGC analysis, which have advantages in peak capacity, sensitivity, and visualization. Furthermore, the introduction methods were seldom implemented for microbial studies, which are characterized by limited sample availability, or for real-time analysis by direct injection to the MS detector.

This study aimed to establish reliable and reproducible sample preparation methods for microbial samples to allow metabolomics studies in bacteria via mass spectrometric analysis, possibly revealing metabolic state or corresponding responses under stresses.

Furthermore, sample introduction of those samples with a limited number of microorganisms needs to be taken into account in the real microbial analysis. In this case, inkjet printing could be utilized as an alternative with optimization.

Thus, the goals could be specified as follows:

- Development and optimization of routine sample preparation protocols for

GCxGC-MS metabolic analysis of microbial samples by taking *C. marina* as a research object for the application of gram-negative bacteria

- Studies on the influence of ozone treatment on the metabolome of *C. marina*
- Establishment of sample introduction system for MS analysis by utilizing an inkjet printer as introducing device
- Optimization of an inkjet technique for MALDI spotting to reduce the "coffee-ring" effect and improve the sensitivity by controlling the number of the droplets
- Application of inkjet introduction for the MALDI-MS analysis of *E. coli* and comparison to conventional manual spotting method

3 Material and Methods

3.1 Microbial culture

3.1.1 Cobetia marina

C. marina used in this study for metabolic analysis was incubated by Dr. Rumancev from Ruhr University Bochum (Bochum, Germany). *C. marina*, strain DSM 4741, an aerobic, gram-negative bacterium, was obtained as dried culture from DSMZ ("Deutsche Sammlung von Mikroorganismen und Zellkulturen", German Collection of Microorganisms and Cell Cultures GmbH, Braunschweig, Germany), frozen stored in marine broth (MB) (2216, Difco, Augsburg, Germany) containing 20% glycerol at -70 ºC. Frozen bacteria were streaked onto marine agar (MA) plate as shown in figure 6, which was prepared with the addition of 2% Bacto agar (Difco) to MB. The streaking tools and methods were shown in figure 6. These stock cultures were stored at 4 ºC for up to 3 weeks. For each sample, a single colony from an agar plate was inoculated into 20 mL sterile MB and shaking on a vibrational table (65 rpm) overnight at room temperature around 20 ºC.

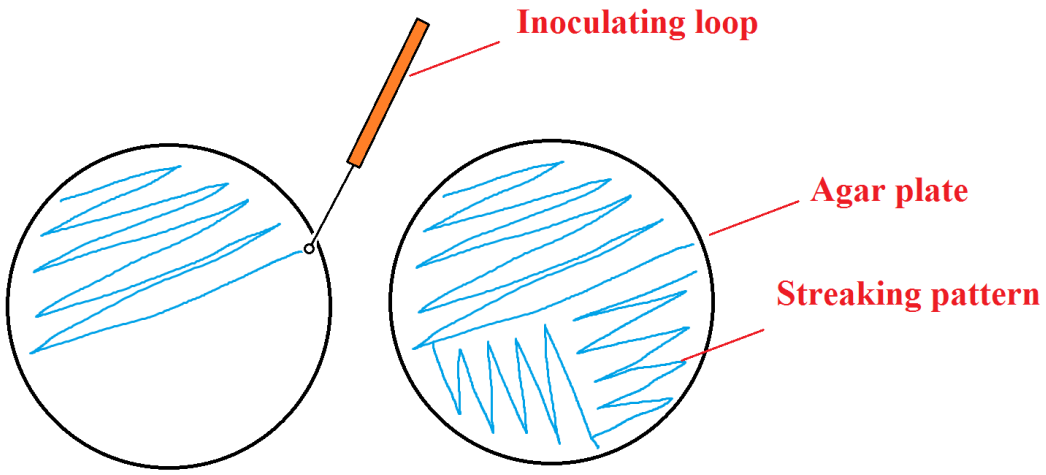

Figure 6 Bacteria streaking with inoculating loop and its patterns on agar plate

The growing condition of the bacteria was quantified as the optical density at 600 nm wavelength (OD_{600}) using a spectrophotometer (Du-70, Beckman Coulter, Krefeld, Germany). As shown in figure 7, the optical density (k = 600 nm) of *C. marina* was determined by the working group of Prof. Rosenhahn (Ruhr-University Bochum) [138]. After overnight (≈12h), *C. marina* growing reached the stationary phase with an optical density of OD_{600} >1. According to the counting method under microscopy, the density of bacteria was ≈ 108 cells/mL at OD600 of 1.

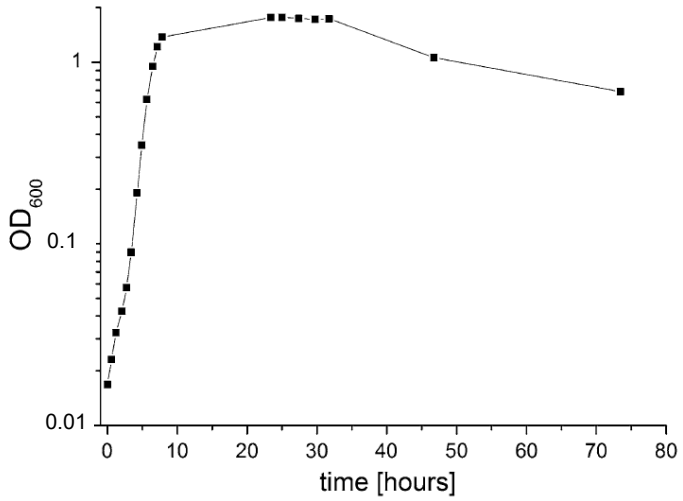

Figure 7 Growth curve of Cobetia Marina in MB with optical density OD_{600} (measured at 600 nm wavelength) from Prof. Rosenhahn group

3.1.2 Escherichia coli

For the inkjet and MALDI-MS experiments, the *E. coli* strain ATCC 25922 purchased from Anxinkang Co., Ltd. (Beijing, China) was used. Bacteria stored in glycerol were recovered by streaking directly on the agar plate with a loop. The plate was then placed at 37 ºC in the bacteriological incubator. Before the experiment, a single colony was picked from the plate and cultivated within Lysogeny broth (LB) medium at 37 ºC, continuously shaking at 175 rpm. LB broth for the cultivation consists of tryptone (10 g/L), sodium chloride (10 g/L) and yeast extract (5 g/L), which were purchased from Shanghai Macklin Biochemical Co., Ltd. (Shanghai, China). The optical density (OD)

of bacteria was determined by UV-visible absorption spectroscopy at 600 nm with a spectrophotometer. Typically, *E. coli* were used for the experiment when OD600 reached about 1, which is approximate 5 x 10^8 cells mL^{-1} culture.

3.2 Sample preparation

3.2.1 Reagents

The commonly used reagents would follow the description below if not stated otherwise. Deionized water was purified using a Millipore system (Milford, MA, USA). MS grade methanol was purchased from Tedia (Fairfield, OH, USA). Sodium chloride (NaCl), chloroform, phosphate-buffered saline (PBS) in tablets, pyridine, hexane, methoxyamine hydrochloride, N-methyl-N-(trimethylsilyl)-trifluoroacetamide (MSTFA) and N,O-bis-(trimethylsilyl)-trifluoroacetamide (BSTFA) with 1% trimethyl-chlorosilane (BSTFA:TMCS, 99:1), boron trifluoride-methanol (BF3-MeOH, 14% in methanol) were purchased from Sigma-Aldrich Chemie GmbH (Darmstadt, Germany).

Ozone-containing gas was produced onsite with an ozone generator (BMT 802 X, BMT Messtechnik, Berlin, Germany; feed gas: O_2 6.0, Linde, Duesseldorf, Germany), which was bubbled into ice-cooled ultrapure water as shown in figure 11. Potassium indigotrisulfonate purchased from Sigma was dissolved in ultrapure water for a 10 mM indigotrisulfonic acid solution.

For the MALDI-MS analysis, the matrix solution, acetonitrile (ACN) (HPLC grade) and trifluoroacetic acid (TFA) (HPLC grade), α-cyano-4-hydroxycinnamic acid (CHCA) and sinapinic acid (SA) were from Merck KGaA (Darmstadt, Germany). The calibrants were obtained from Sigma-Aldrich Chemie GmbH (Munich, Germany)

including adrenocorticotropic hormone fragment 18-39, insulin B chain, insulin, cytochrome C and apomyoglobin.

3.2.2 Starving stress treatment

As described in figure 8, 20 mL of overnight growing *C. marina* was diluted by a factor of 1:10 with MB medium into 12 batches. The diluted bacteria were regrown with both MB and artificial seawater. The artificial seawater (ASW, Instant Ocean, Mentor, Ohio, USA) was prepared according to the manufacturer's instructions. In about 5 hours, the OD_{600} of regrown bacteria reached≈0.1, which was then combined together in one falcon tube and centrifuged at 2000 *g* for 3 min. The supernatant was removed with pipette followed by resuspension with both MB and ASW. The bacteria resuspended in ASW would starve due to lack of nutrients. Accordingly, those resuspended in MB would keep normal state as control. The starvation process typically lasts for 30 minutes. After this, both starved bacteria and control bacteria were proceeded to further sample preparation.

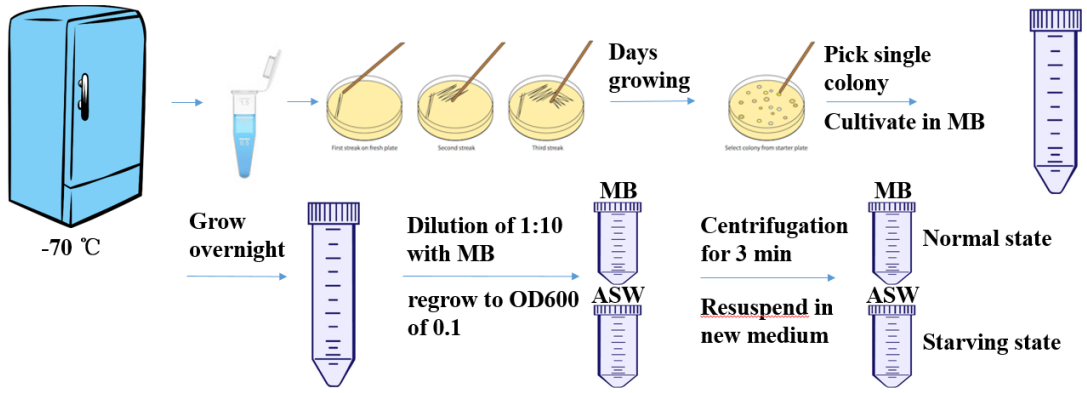

Figure 8 Process of famishing the bacteria by resuspending within ASW

3.2.3 Ozone stress treatment

The ozone experiment was performed with Katharina Hupperich from Prof. Dr. Torsten C. Schmidt research group (University of Duisburg-Essen, Essen, Germany). In this

experiment, ozone was produced by atomizing oxygen in a corona discharge. Therefore, an oxygen supply was necessary for the ozone generator. As shown in figure 9, the ozone was then continuously purged into the ultrapure water to obtain an ozone stock solution at a stable concentration. (The appearance of the generator shown in Appendix figure S 1)

The ozone stock solution concentration was determined by UV absorption at 258 nm using a UV-1650PC spectrophotometer (Shimadzu, Kyoto, Japan). The concentration of ozone was then calculated according to the equation of the Lambert-Beer law:

$$[O_3] = \Delta A_{258}/\varepsilon_{ozone} \quad (2)$$

Where ΔA_{258} represents the difference between the reference and sample absorption. ε_{ozone} is the molar absorption coefficient of ozone at 258 nm (2950 $M^{-1}{\cdot}cm^{-1}$).

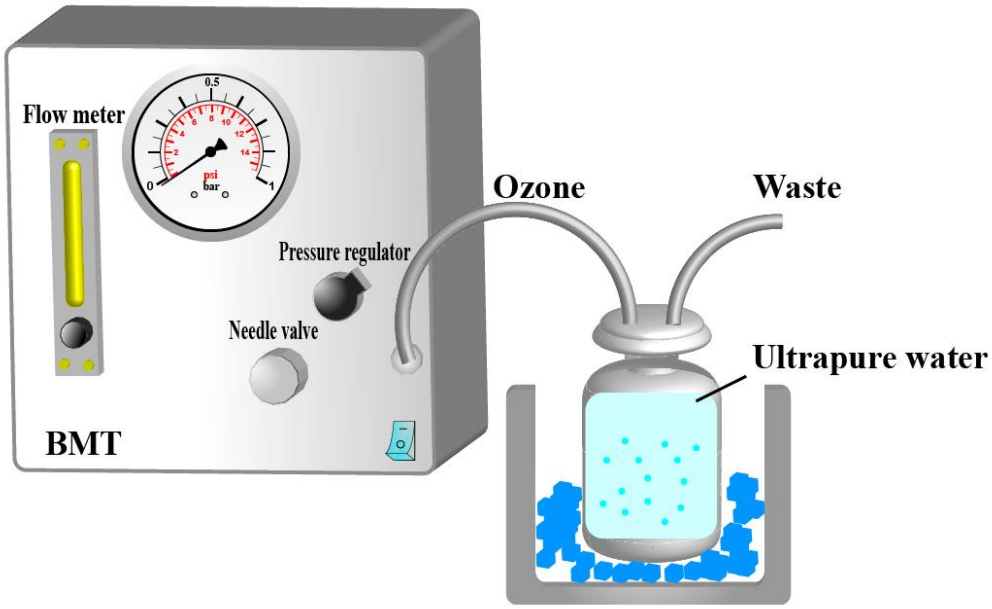

Figure 9 Setup of the ozone generator. The ozone stock solution was in ultrapure water

Before spiking ozone into the real bacteria culture, the depletion of ozone in the medium was measured according to Bader *et al.* by UV adsorption at 600 nm [139]. As shown in figure 10, the indigotrisulfonic acid solution in dark blue would react rapidly with ozone by cleaving the double bond, producing colorless isatin sulfonic acid. Compared to indigotrisulfonic acid, isatin sulfonic acid does not absorb UV light at 600 nm. The chemical formula is shown below:

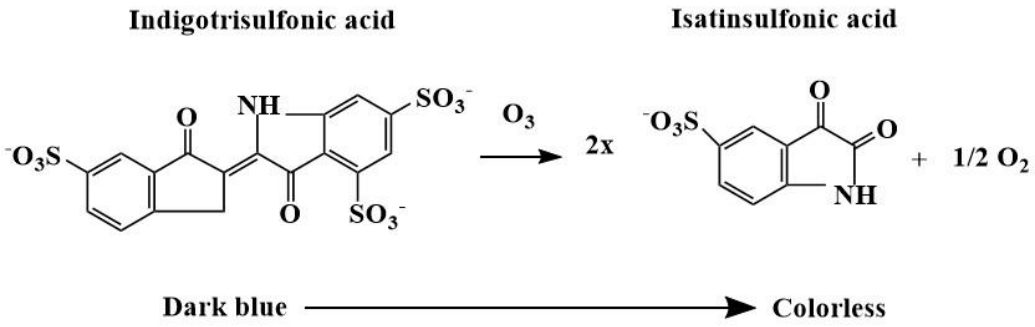

Figure 10 Reaction of Indigotrisulfonic acid with ozone

The detailed protocol for ozone depletion was described in Appendix 1. The reference was a blank sample with the indigo solution before spiking ozone. Thus, the difference between absorption of the reference and those samples reveals the amount of indigo acid consumed by ozone. Therefore, the ozone concentration in the depletion test was calculated as equation below:

$$[O_3] = \Delta A_{600} / \varepsilon_{\text{indigotrisulfonic acid}} \quad (3)$$

Where ΔA_{600} represents the difference between the absorption of reference and spiked samples due to the reaction. $\varepsilon_{\text{indigotrisulfonic acid}}$ is the molar absorption coefficient of indigotrisulfonic acid at 600 nm (20000 $M^{-1} \cdot cm^{-1}$).

To stress the bacteria, the ozone stock solution was spiked with a gastight syringe (Hamilton, Reno, USA) into the bacteria sample to obtain ozone concentrations of 500

μM and 600 μM. The samples were then kept under stress for 10 min before further sample preparation. A bacteria sample without ozone dosage was prepared as a control sample.

3.2.4 Minimal inhibitory concentration determination

To confirm the status of the bacteria after ozone stressing, the minimal inhibitory concentration (MIC) determination was performed with Dr. Rumancev. Four different concentrations were tested with the final ozone concentration of 170 μM, 500 μM, 600 μM, and 1000 μM on 48-well plates. Figure 11 shows the diagram of the MIC test. There were 6 parallels for the same ozone dosage from row A to F. The initial volume of bacteria culture was 500 μL in the first well of each row, which would be spiked with

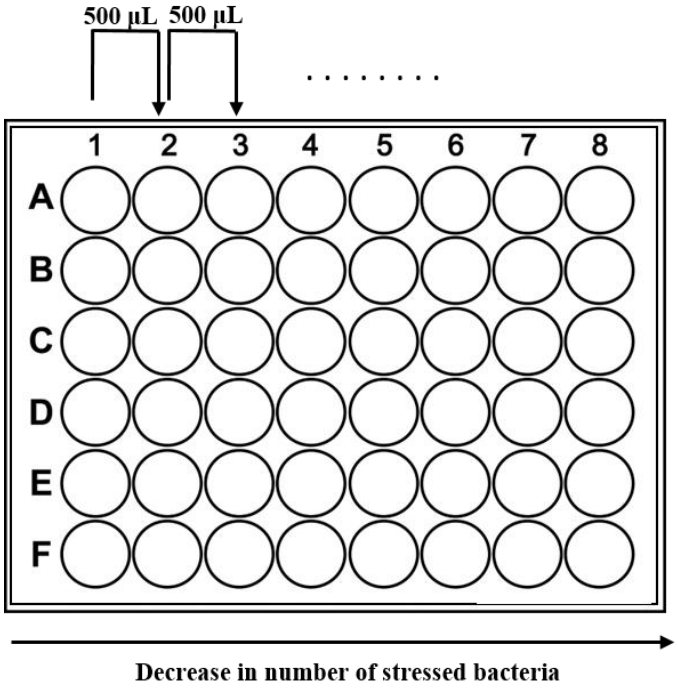

Figure 11 Workflow of MIC test. The wells in the first column was spiked with ozone stock solution. The initial volume of the bacteria culture in the first well was 500 μL. After spiking with 500-μL ozone stock solution and mixing, 500 μL of mixture was transferred to the next well in the same row, which was repeated until column 6. From row A to F were six parallel repeated for the same dosage.

another 500-μL ozone solution. These ozone solutions were prepared in advance to

reach the final concentrations (170 μM, 500 μM, 600 μM, and 1000 μM) in the first well after mixing with bacterial cultures. For example, on the plate for 170-μM ozone dosage, 500-μL bacteria culture in A1 was first spiked with 500-μL ozone solution with the concentration of 340 μM (bacteria culture:ozone solution, 1:1 in A1). 500 μL of this mixture was then transferred to A2 to obtain another ratio of 3:1. Accordingly, each time 500-μL mixture was pipetted into the next well. In the end, the ozone concentrations in the same row were decreasing with such series dilution. The 48-well plates with different initial dosages were then shaken for 24 h at room temperature.

3.2.5 GCxGC-MS

The analysis of *C. marina* metabolites was performed using a GCxGC-Shimadzu QP-2010. The standard setup and settings were mentioned below if no particular statements. For the first dimension, a Rxi-5sil MS column (30m x 0.25mm x 0.25 um, Restek, USA) was used. A middle polar Rxi-17sil MS column (1 m x 0.15 mm x 0.15 μm, Restek, USA) was applied in the second dimension. In general, the modulation time of the dual-jet cryogenic modulator was 3.8 s. Helium was used as carrier gas with a constant flow of 1.09 $mL \cdot min^{-1}$. 1 μL of the derivatized sample was injected at 280 ºC with a split ratio of 1:1. The oven for both columns was heated up from 80 ºC (5 min hold) to 300 ºC (15 min hold) at 5 ºC min^{-1}. The transfer line and ion source were kept at 310 ºC and 200 ºC, respectively.

3.2.6 Matrix-assisted laser desorption ionization (MALDI)-MS

The MALDI-MS experiments were finished with the help of Prof. Jinming Lin's research group (Tsinghua University, Beijing, China). MALDI-MS analysis was performed by an AXIMA Performance MALDI TOF/TOF mass spectrometer (Shimadzu Co. Ltd. Kyoto, Japan).

All MALDI experiments were performed with a 337 nm nitrogen laser at 120 V power. The data were collected in the positive mode with the scan range from 2000 to 12000 m/z. MALDI data was obtained from an average of 20 mass profiles, and each profile resulted from 20 laser shots at 5 Hz.

3.2.7 Inkjet for MALDI-MS

3.2.7.1 Inkjet setup

Inkjet components were obtained from Fuji Electrics Systems Co., Ltd. (Tokyo, Japan). The MMU-30X, electromotive x-y stage, was self-assembled, and parts of this platform were purchased from Chuo Precision Industrial Co., Ltd. (Tokyo, Japan). For the sample/solvent solutions loading, a 75-mm glass tube was applied and provided by Funakoshi, Co. (Tokyo, Japan). The droplets were visualized with a microscope (Leica DMI 4000 B, Wetzlar, Germany) and a charged-coupled device (CCD) camera (Leica DFC 300 FX, Wetzlar, Germany). A Laboratory-made software was programmed to control the inkjet waveform, such as pulse driving voltage, pulse time, and the number of droplets formed by the nozzle. The x-y stage movement of the sample introduction platform was controlled by another laboratory-made software.

3.2.7.2 Sample introduction for MALDI plate by inkjet

Before starting, 10 mL of *E. coli* ($OD_{600} \approx 1$) was transferred into a 50-mL falcon tube and centrifuged at 2000 *g* for 3 min to remove the broth. The bacteria pellet was then washed twice with 10 mL of deionized water to eliminate the nutrient broth, followed by centrifugation at 2000 *g* for 3 min to remove the supernatant. The pellet was resuspended with 5 mL deionized water then loaded in a glass tube, as shown in figure 12A for the introduction. The components of the inkjet device, such as the inkjet fixer

and the piezo ceramic, were illustrated in figure 12B. The microscope and CCD camera mentioned for observing were shown in figure 12C.

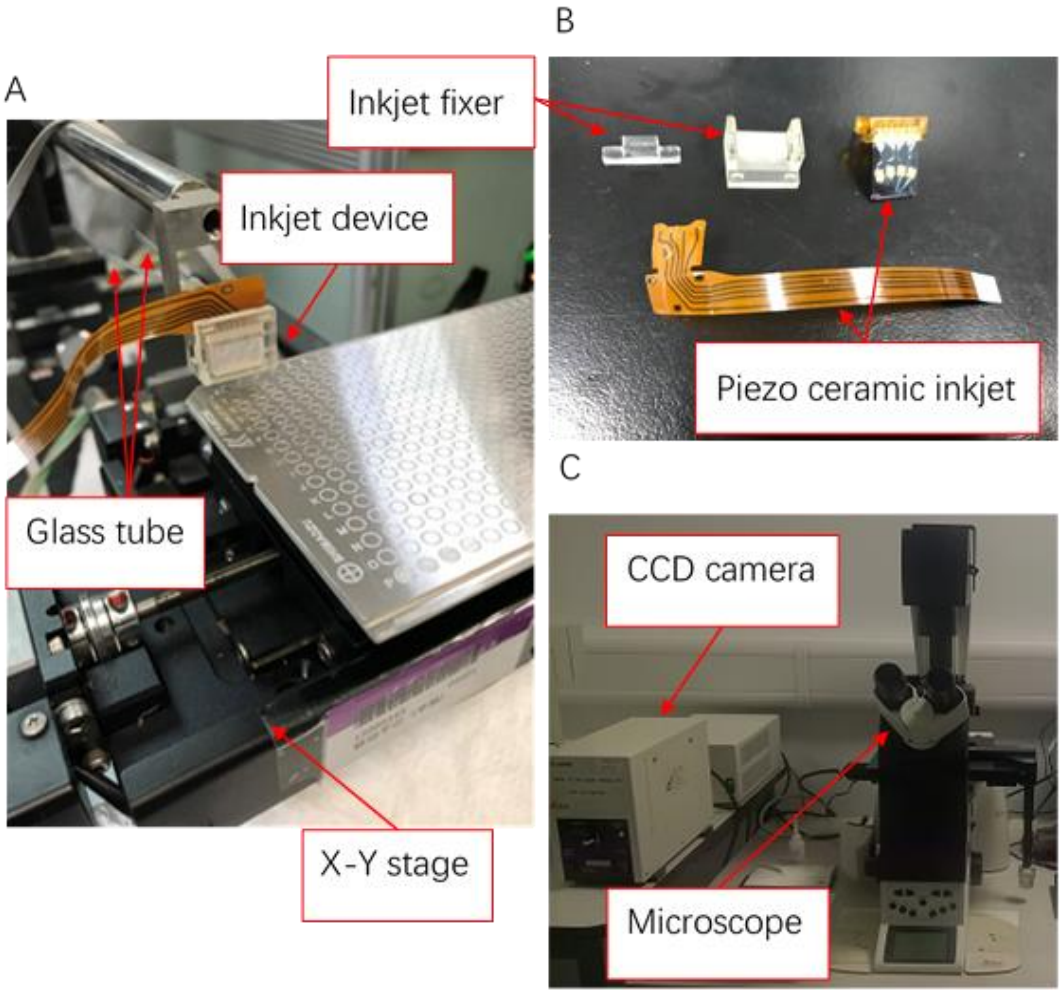

Figure 12 Setup of inkjet coupled with x-y stage. (A) inkjet device (B) inkjet components (C) microscope and CCD camera for the observation of dried droplets on glass

3.2.8 Droplets formation

3.2.8.1 Droplets prepared for MS analysis

As reported by Chen *et al*. [140], it has been demonstrated that the droplets formed with a solvent of 50% methanol/water were successfully introduced for the single-cell analysis on electrospray ionization mass spectrometry. The inkjet device was optimized

with the setup to adapt this for bacteria analysis in figure 13. The tungsten needle (ST-20-2, GGB Industries Inc., USA) (figure 13C) was placed about 1 cm under the inkjet nozzle, as shown in figure 13A. The high voltage of 2500 V on the needle tip would immediately ionize the falling droplets and then transfer them towards the metal plate (replacement of MS in this case) placed in front.

The formation of droplets was controlled by the pulse generator, which was influenced

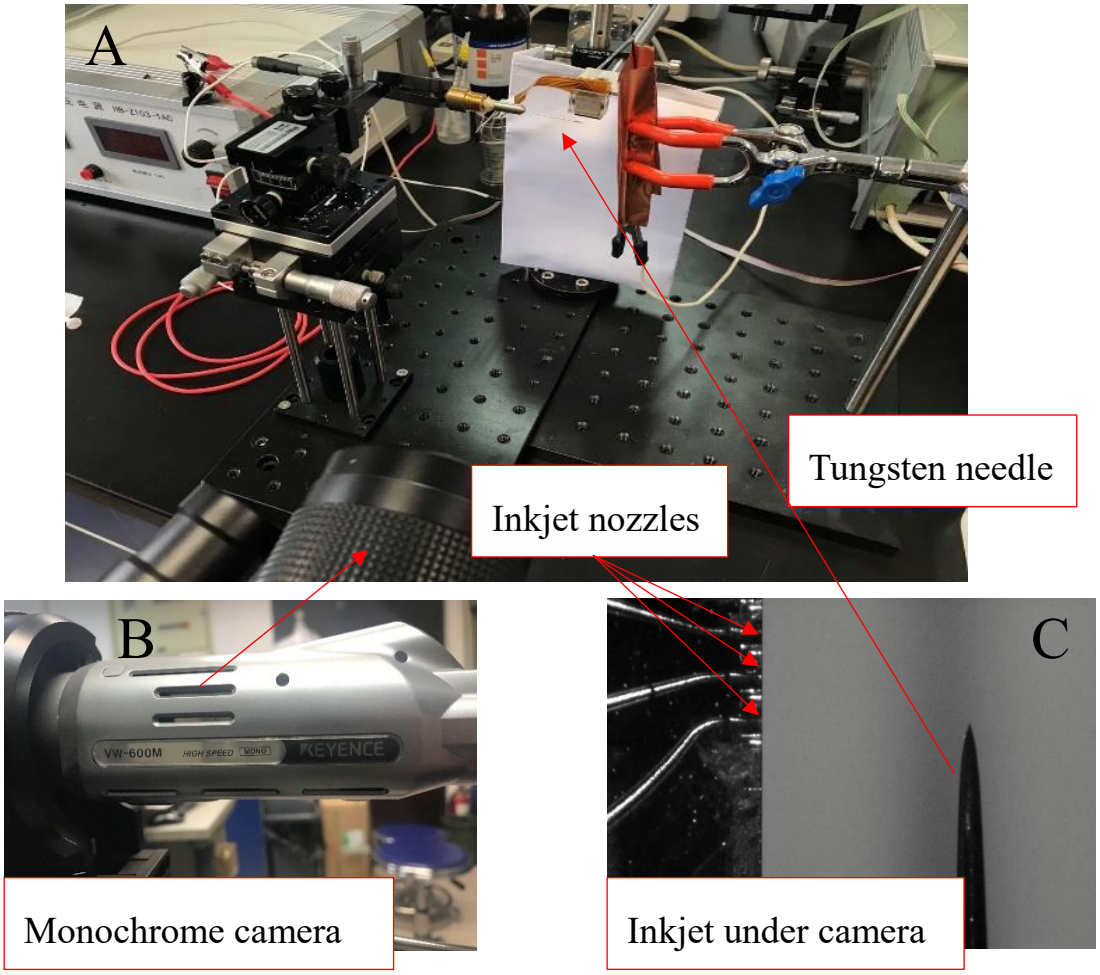

Figure 13 Setup for the observation of droplets formation by monochrome camera

by two parameters, the current pulse and driving voltage. Different parameters were compared by monochrome pictures in this study, captured by a high-speed monochrome camera shown in figure 13B (Keyence VW600M, Tokyo, Japan).

3.2.8.2 Droplets prepared for the “coffee-ring” effect observation

To evaluate the “coffee-ring” effect, the observation of droplets crystallization on indium tin oxide (ITO) glass was realized by the Leica microscope with the CCD camera as mentioned in 3.2.8.1. The crystallization on the MALDI plate was recorded by the MALDI camera. The crystallization of different MALDI matrices such as DHB, CHCA, and SA was observed under the microscope. The droplets of the matrices were

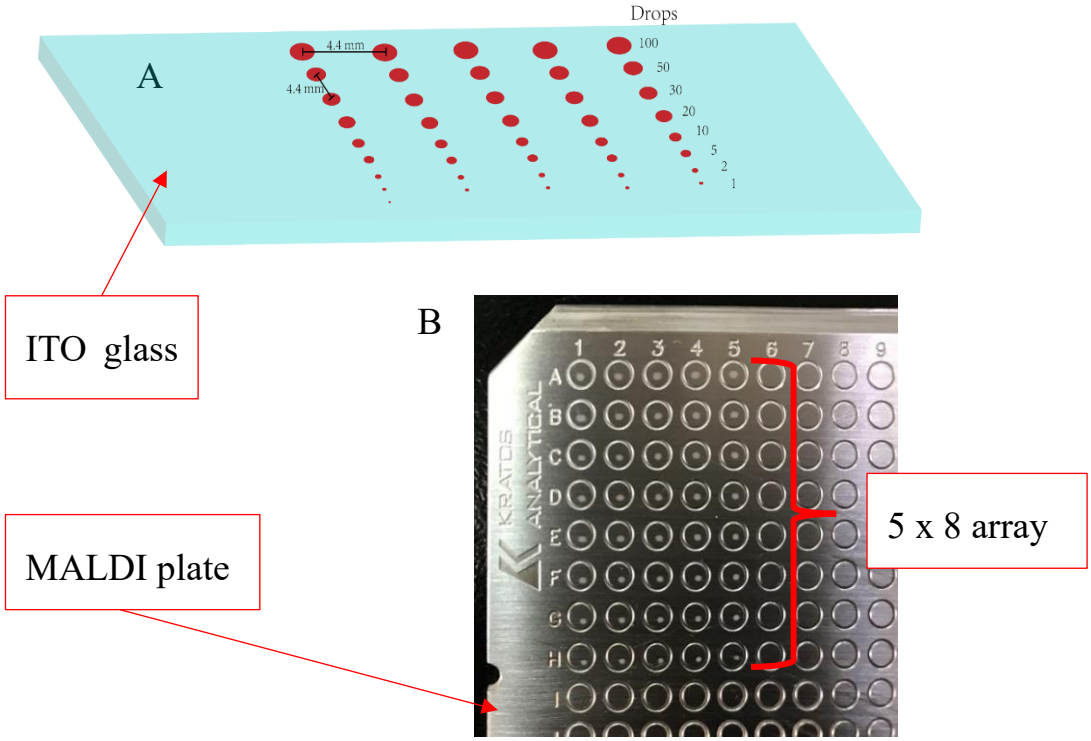

Figure 14 Inkjet printed arrays on (A) ITO glass and (B) MALDI plate for “coffee-ring” effect

printed in a 5x8 array printing, as shown in figure 14. For the array on the ITO glass, each spot has a distance of 4.4 mm, containing different amounts of drops (from 1 to 100). It was similar for spotting on the MALDI plate, but the distance was adjusted according to the single spot area on the plate. Unless otherwise described, the composition of matrix solvent was 70:30 (ACN:H_2O).

As shown in figure 15A, the “coffee ring” after crystallization on the ITO glass was recorded on the scale of 100 µm with the CCD camera. In figure 15B, the droplet was spotted in the middle of the MALDI target and observed by the camera.

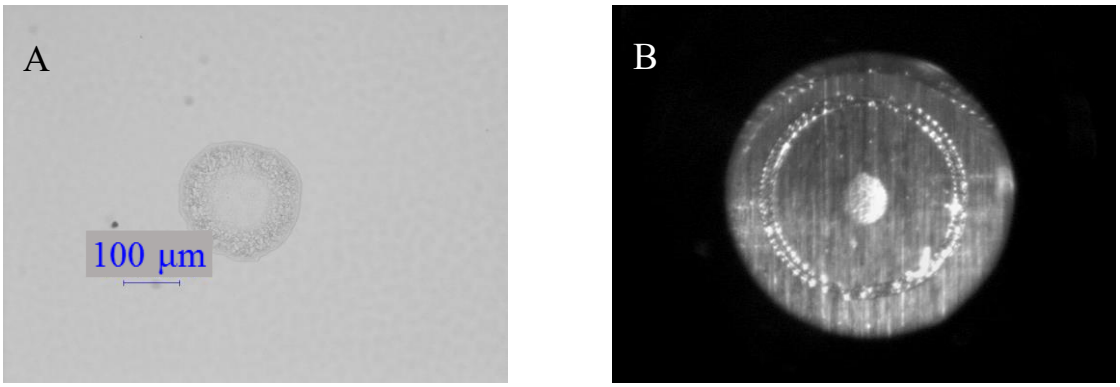

Figure 15 Observation of droplets crystallization (A) via Leica microscope (B) under MALDI camera

3.3 Software

3.3.1 General software list

Table 1 Software list

Type	**Name**	**Company**
GC software	GCMSsolution 2.4	Shimadzu
Database	NIST05	NIST USA
2D contour plot software	GC Image 2.3	Shimadzu
2D contour plot software	GasPedal	DECODON
MALDI software	Biotech Axima Assurance 2.9.3	Shimadzu
Drawing software	ChemDraw Professional 15.0	CambridgeSoft
Graphic software	Adobe illustrator	Adobe
Citation software	Endnote X9	Clarivate Analytics
Inkjet software	Lab-made	Tsinghua University
X-Y stage control software	Lab-made	Tsinghua University

3.3.2 GasPedal

The GasPedal, developed by DECODON, is built upon Delta2D, mainly for data analysis of GCxGC. Collecting the features from plotting images enables the visualization of the difference between images directly instead of traditional spot-to-spot work. Once the contour plots from GC Image were obtained, these plots could be imported into the GasPedal for its standard workflow. For the first step, the so-called "warping image" needs to be applied for interesting images shown in figure 16. In this step, the GasPedal recognizes those plots represented for the same substance and warps

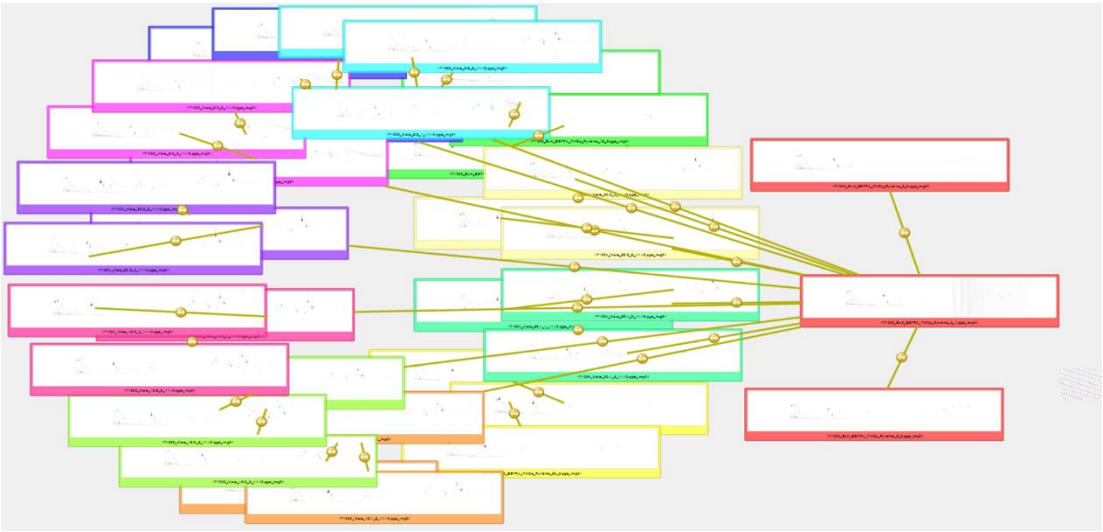

Figure 16 Diagram of warping image, for example, the same color represents for the same sample group, which were warped to locate the same substance in independent image of each group

them to the same position across the images. Each color represents the parallels in the same sample group. The yellow lines connecting two different images are the vectors generated after the warping process, indicating the warping target of each imported image. Such a warping process is one of the key advantages of GasPedal, which could avoid errors caused by the traditional observing method with the naked eyes and save plenty of time.

The other important function is provided for the quantitative analysis based on warped images. Once the same substance was located on warped images, these images could be combined, so-called “fusing image” shown in figure 17.

After being fused, a new image would be generated, which contains all the features of target images before fusing. Any spot from the same substance located in the same position on chosen warped images would be attributed to a new spot on the fused image. The intensity of such a new spot would be considered the overall value as 1. Those contributions from each original spot would be computed into a certain percentage, which was then applied for the quantitative analysis by comparing between contributed percentages.

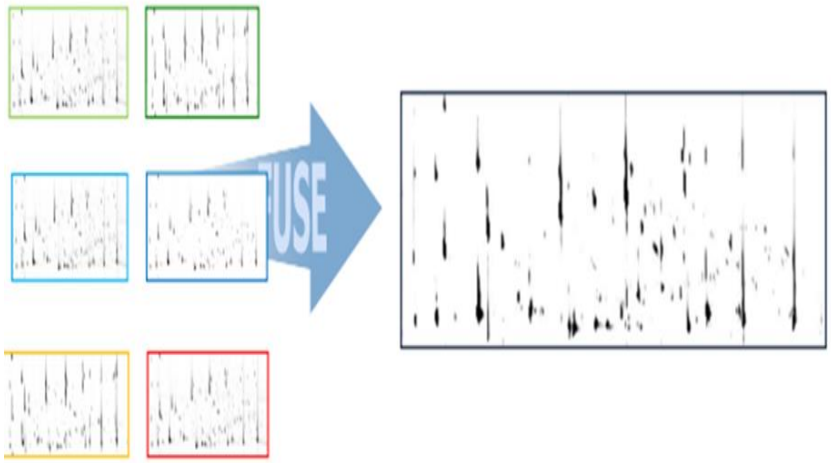

Figure 17 Diagram of fusing image process from the warped images to a fused one

3.3.3 Inkjet control interface and its programming

The requite parameters of the inkjet device were given in a lab-made software invented by the research group of Prof. Lin in Tsinghua University. As illustrated in figure 18, the detailed parameters could be specifically adjusted, including the port of controlling PC and inkjet platform, the inkjet channel, and the number of droplets released within

single printing. The inkjet movement could be programmed by inputting the numbers of rows, columns, spotting distance, and dwell time for switching rows accordingly. Thus, the applied inkjet system could be customized according to the research purpose.

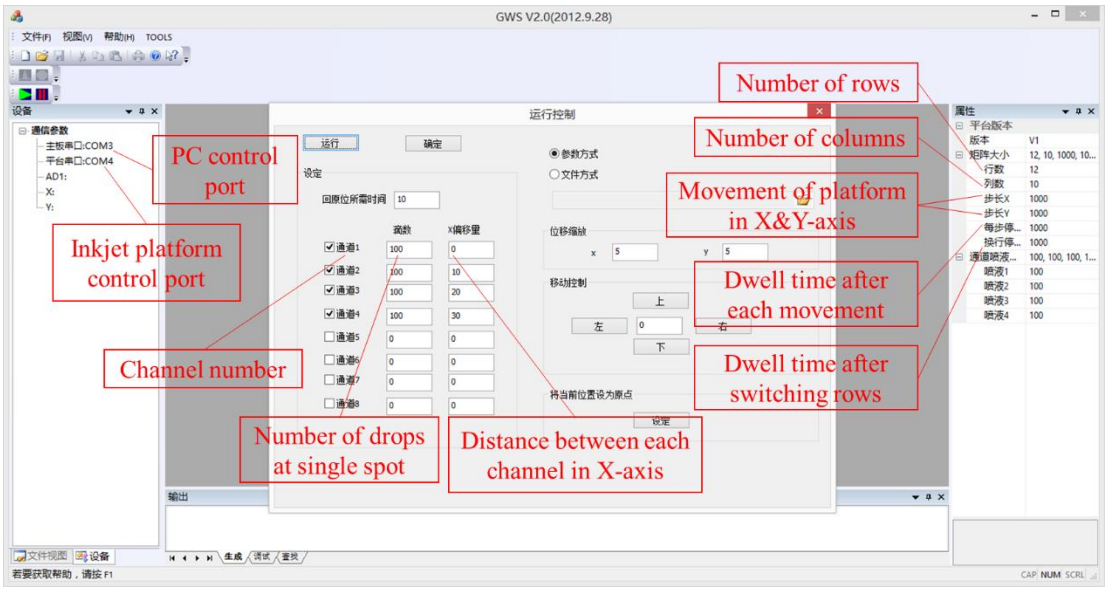

Figure 18 Inkjet control interface

4 Results and Discussion

4.1 Detection of intracellular metabolites from *C. marina*

To analyze the intracellular metabolites of *C. marina*, a proper sample preparation protocol for the identification of the metabolites with high coverage and repeatability was required. As mentioned in section 2.1, there are many approaches to inactivate the bacteria cells during the quenching step. However, to date, there was no published protocol for the metabolic study of *C. marina*, especially for the details from quenching to derivatization steps. Therefore, a stable and robust protocol needed to be developed first, which was crucial for carrying out further investigations.

In addition to analyzing the metabolome under steady state conditions, the aim of this study was also to investigate the metabolic behavior of *C. marina* under different stresses for improving the understanding of its response to the environment. Therefore, additional experiments such as treating *C. marina* with ozone and starving stresses were carried out to find out changes in metabolic profile, which might give a hint for understanding the response of *C. marina* to environmental stresses.

4.1.1 Sample preparation

In general, as illustrated in figure 19, the preparation workflow of bacteria metabolic analysis was started with the cultivation of bacteria and ended with derivatization of extracted metabolites [141]. As mentioned in section 3.1.1, the cultivation work of *C. marina* was carried out in collaboration with Prof. Rosenhahn´s group at Ruhr-University Bochum. If not otherwise indicated, all the *C. marina* samples described in this thesis were cultivated overnight ($\approx$ 12 h) with $OD_{600} > 1$. Further steps of sample treatment are described in detail in the following sections. Unless otherwise described,

all operations were performed at 0 °C. All used reagents and containers were set to 0 °C if possible.

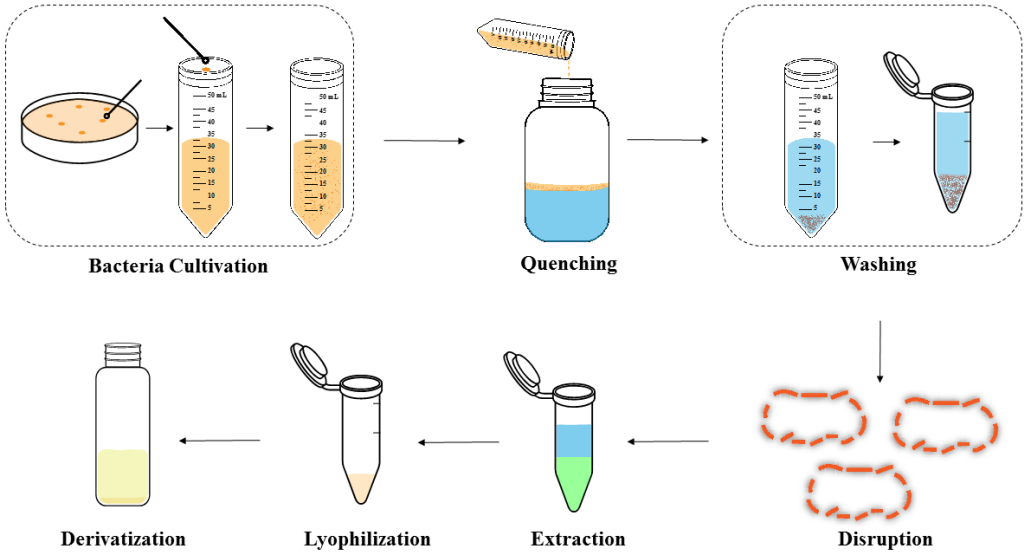

Figure 19 Basic workflow of bacteria sample preparation for intracellular metabolites

4.1.1.1 Quenching

To inactivate the enzyme activity, a quenching step is necessary as the first step of sample preparation. It is crucial to stop the potential enzymatic effect immediately for a snapping view of the endo-metabolome at a particular time. Low-temperature treatment would be one of the best solutions to achieve this purpose. An environment friendly method proposed by Wang *et al*. was adapted for the quenching step of *C. marina* [19]. 100 mL of deionized water containing 0.85% NaCl were placed in a plastic cubic bottle and frozen into an ice block. Bacteria culture was poured onto the ice surface, and then the whole ice block needs to be manually crashed into pieces after fresh bacteria culture poured onto its surface. However, it is difficult to crush the ice without damaging the bacteria. Instead of crushing, another alternative is to increase the contact time with the ice surface from seconds to minutes. As shown in figure 20, most of the bacteria settled near the ice block's surface after about a minute because they were less mobile at low temperature. The bottom layer of the bacterial culture was

frozen into less solid ice, making it difficult to transfer the quenched culture for the next step just by shaking and pouring. Moreover, this frozen layer causes a scattered distribution in the culture that may cause the quenching to be unevenly distributed.

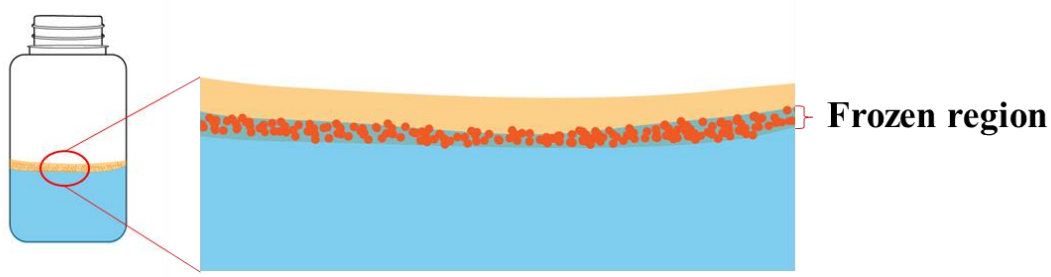

Figure 20 Status of bacteria and its culture after poured onto the ice block surface

To avoid this, ice bulks (obtained by freezing deionized water containing 0.85% NaCl in a plastic cube tray) were used instead of one single piece of frozen ice. As shown in figure 21, the ice bulks were placed inside the cubic bottle. As a result, the bacteria were distributed around the ice bulks, which increased the contact surface between ice and bacteria without crashing them. The cubic bottle was placed in the fridge at - 80 °C for 3 minutes. After this, the quenched culture could be easily transferred into 50-mL

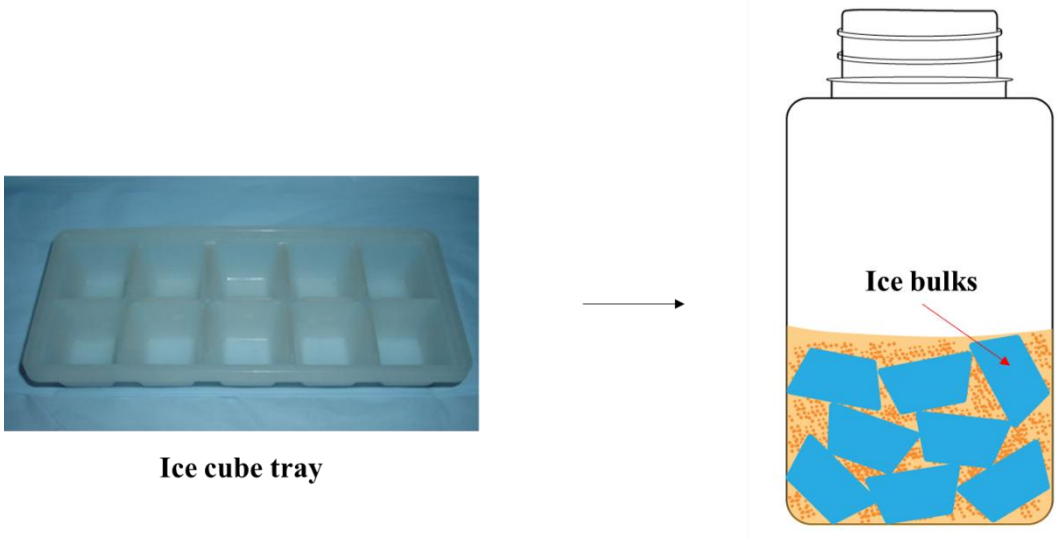

Figure 21 Ice bulks used in quenching treatment

prechilled falcon tubes in aliquots of 20 mL. These aliquots were then centrifuged to separate the bacteria pellet from the supernatant of melted ice and the culture medium.

According to published procedures, *E. coli* should be centrifuged at 9000 *g* for at least 2 minutes [142]. In contrast, it has been found here that centrifuging at 2000 *g* for 4 min was enough for *C. marina* to precipitate as a cell pellet and adhere steadily to the tube wall. A lower centrifugation speed also reduces the risk of metabolite leakage from the cells, which is due to an increased weakness of the bacterial cell membrane after a low-temperature stimulation. Thus, such an optimized "green" quenching method was used to analyze *C. marina* in this thesis.

4.1.1.2 Bacteria cell washing

A washing step was considered necessary to eliminate the influence of extracellular metabolites and residuals of cultivation nutrients after quenching the bacteria except for those quenched with cold methanol [143]. Since a green quenching step was adopted, the washing step with PBS was indispensable, according to Wang *et al.* [142]. After washing with PBS solution, the cell pellets were more loosely bound to the tube wall. This was probably due to the centrifugation speed, which was insufficient. However, to keep the cell intact during the centrifugation step, the centrifugation speed needs to be as low as possible. Therefore, it was step-wise increased starting from 3000 *g* to 8000 g. From this test, it turned out that a centrifugation at 8000 *g* for 3 min was showing a satisfying cell pellet adhesion with the lowest speed in a relatively short time period. The comparison between centrifugation at 3000 *g* and 8000 *g* was shown in Appendix, figure S2. The washing step was repeated first with 30-mL PBS, and then after removal of the supernatant the pellet was resuspended in 1.5-mL PBS and transferred into 1.5-mL centrifuging tube, and centrifuged again. This last step was carried out to minimize

the potential unremoved residuals from the first centrifugation step and exclude most of the contamination.

4.1.1.3 Cell disruption & metabolites extraction

To increase the number of detectable intracellular metabolites, the bacteria need to be adequately disrupted before the extraction. Wang *et al.* compared sonication and bead-beating disruption for a successful analysis of different groups of metabolites from *E. coli*. They found that the mechanical forces could improve the extraction efficiency for metabolic compounds such as amino acids, nucleosides or fatty acids [142]. In this study, glass homogenizer and Speedmill Plus were compared for the disruption method.

There were several drawbacks found by operating with the glass homogenizer, as shown in figure 22A. At first, it was necessary to grind the samples more than 30 times for sufficient cell wall breaking. Moreover, this method was also time-consuming, especially for experiments with a number of replicates. Once grounded into pieces, the bacteria cell residues stick to the glass wall, which makes it difficult to clean the vessels even with isopropanol between one sample and the next. The Speedmill apparatus is shown in figure 22B and uses beads to crash samples in a single tube. In this system, each sample is lysed in an individual lysis tube where the cells are uniformly broken. Since the surfaces of the beads are less adhesive for biological matters as compared to glass, the mixture after disruption could be more readily transferred by pipette to a 1.5-mL centrifuging tube. Thus, the sample loss could be reduced to a considerably low level.

Cell disruption was carried out in 0.5 mL of a mixture containing chloroform, methanol, and water (100:21:79, v/v/v). In fact, even with such a lysis tube, it is unavoidable to have residues during the transfer process of the disrupted sample, which could lead to the sample loss of some polar metabolites not dissolving in chloroform. Therefore, the

disruption reagent and extraction reagent (as described in the extraction section) were prepared as the same composition, which minimizes the sample loss at this step.

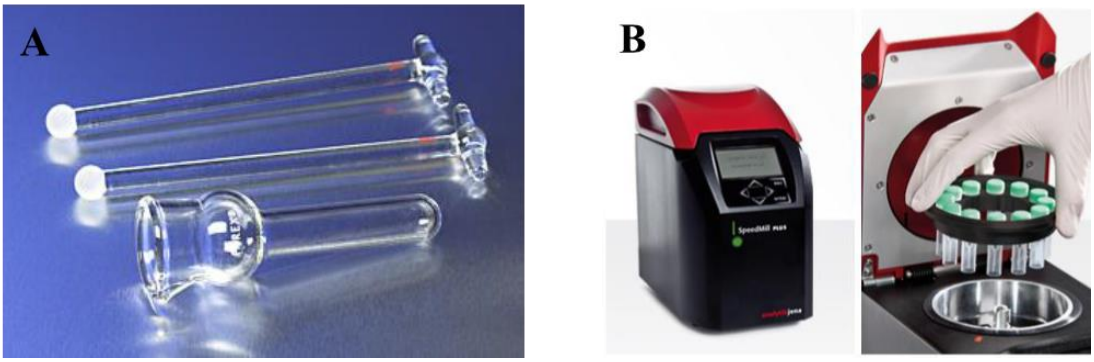

Figure 22 Cell disruption by (A) glass homogenizer and (B) lysis tube in Speedmill

In this study, a two-phase extraction strategy was used, as recommended by many researchers. A solvent mixture of water, methanol, and chloroform was used, whereby the water-soluble metabolites were extracted into the upper phase and the non-polar or weakly polar ones into the lower phase [144, 145]. 500 µL of an extraction reagent, the same as the mixture added during disruption, was added to the disrupted sample, followed by centrifugation at 13360 *g* for 10 min. After the centrifugation, 400 µL of the upper phase was then collected, followed by re-extracting the lower phase with a maximum of 0.5-mL MeOH/H_2O (21:79, v/v). Two 400-µL upper phase extracts were combined and stored at - 80 °C for further steps.

4.1.1.4 Lyophilization

It has been revealed by Fisher *et al*. that freezing-drying techniques were sufficient for solution removal in metabolite analysis [146]. To assure the success of the derivatization, it is necessary to minimize the sample moisture, which is occurring in particular after overnight storage at - 80 °C. Therefore, the frozen extract was lyophilized at approximated - 45 °C for 24 hours in a vacuum lyophilizer (Alpha 1-2 LDplus).

4.1.1.5 Derivatization

According to Fiehn *et al*., silylation was considered to be more applicable and operable than other derivatization strategies [147]. MSTFA and BSTFA are two of the most commonly used derivatization reagents for silylation. They replace acidic protons from hydroxyl, carboxyl, amino, and thiol groups with trimethylsilyl group to obtain molecules with high volatility and thermal stability, which are optimal for GC analysis [148]. In this case, silylation with BSTFA and 1% TMCS was carried out for the metabolic extract of *C. marina*. BSTFA has similar silylation strength to MSTFA, which provides similar reaction and silylation rates. Once combined with TMCS, the reactivity was increased compared to derivatization with BSTFA only [149]. For potential metabolites detected by GC-EI-MS, there are many applications of BSTFA for the organic compounds, such as fatty alcohols, phenolic compounds, fatty acids, amines, sugar, and sugar alcohols [160]. These organic compounds are very likely metabolites of bacterial enzymatic activity, which are of major interest in this study.

For the derivatization, 100 µL of pyridine (with 25 mg/mL methoxyamine hydrochloride) was added to the lyophilized extract, then incubated at 60 °C for 60 min. Then, 100 µL of TMS reagent (BSTFA:TMCS, 99:1, v/v) was added and heated at 60 °C for another 60 min.

4.1.1.6 Optimized routine protocol

The optimized protocol is described below in detail.

Bacteria sample treatment

1. Freeze 100-mL 0.85% NaCl frozen in ice cube tray at -80 ℃ into small bulks and then transport them into plastic cubic bottles

2. Pour approximately 200-mL over-night culture ($OD_{600} \approx 1$) into the bottle against the ice surface and stand at - 80 ℃ for 3 min
3. Gently aliquot quenched culture into 20 mL in 50-mL prechilled falcon tubes
4. Centrifuge the tubes at 2000 *g* for 4 min
5. Remove the liquid and resuspend the pellet gently first with 30-mL prechilled PBS solution
6. Centrifuge the tubes at 8000 *g* for 3 min then remove the liquid
7. Resuspend the pellet gently with 1.5-mL PBS, then transfer it into 1.5-mL prechilled Eppendorf tube
8. Centrifuge the tubes at 8000 *g* for 3 min, then remove the liquid
9. Add 0.5 mL of the mixture containing chloroform, methanol, and water (100:21:79, v/v/v) to resuspend the pellet, then transfer it into a lysis tube
10. Disrupt cell by placing the lysis tube in Speedmill at continuous mode for 1 min
11. Transfer disrupted sample into clean 1.5-mL prechilled Eppendorf tube and add another 0.5 mL of mixture at step 9 then vortex for 30 seconds
12. Centrifuge the Eppendorf tubes 13360 *g* for 10 min
13. Collect 400 µL of upper phase then add another 0.5 mL of MeOH/H2O (21:79, v/v) for re-extraction
14. Combine two 400-µL extracts and store them at - 80 ℃
15. Lyophilize the overnight frozen sample at approximated - 45 °C for 24 h in vacuum with freezing dryer Alpha 1-2 LDplus

Derivatization

16. Add 100 µL of pyridine (with 25 mg/mL methoxyamine hydrochloride) to the lyophilized extract and Incubate at 60 °C for 60 min
17. Add 100 µL of TMS reagent (BSTFA:TMCS, 99:1, v/v) to the sample above and heat it at 60 °C for 60 min.
18. Vacuum dry the derivatized sample with a Thermo Scientific concentrator.

19. Add 100 µL of hexane to dried sample and transfer it to a GC vial with a 200-µL insert for the further GCxGC analysis.

4.1.2 Repeatability validation

The sample preparation protocol for the intracellular metabolites of *C. marina* should be applied in routine analyses. Therefore, to assure data reliability, it is necessary to determine its repeatability. The repeatability of the bacteria sample preparation method was investigated for three groups with different culture volumes (5-mL, 10-mL, and 30-mL) with bacteria $OD_{600} \approx 1$. The samples with different volumes were measured in triplicates with the methods mentioned in section 3.2.5.

To get a better overview of GC images, the software GasPedal was employed for the data comparison. Original data was obtained as 2D contour plots by the software GC Image, which was then imported into the GasPedal. The fused images combine those features, including spots positions and intensities from selected images. To compare o inter-and intra-sample variability, the warping strategy, as mentioned in section 3.3.2, was applied. After being warped, the peak areas of the same substance in the same position were summed up then indicated in the fused image. Thus, the spot area on a single image could be normalized by the equation below:

$$P_{single} = Peak\ \ area_{single} \div Peak\ \ area_{sum} \quad (4)$$

Furthermore, the relative standard deviations (RSDs) of P values were applied to reveal the repeatability.

As indicated in figure 23, the signals with relative standard deviation (RSD in %) less than 30% (represented in green and yellow) were 150 (94.9% of all signals) in 5-mL culture group, 141 (94.6%) in 15-mL culture group and 159 (96.3%) in 30-mL culture

group. These results are comparable with those from Maifiah *et al*. for their study on *Acinetobacter baumannii* with RSD% of 22% for metabolites extracted by chloroform/methanol/water [150]. These results also imply that the sample preparation

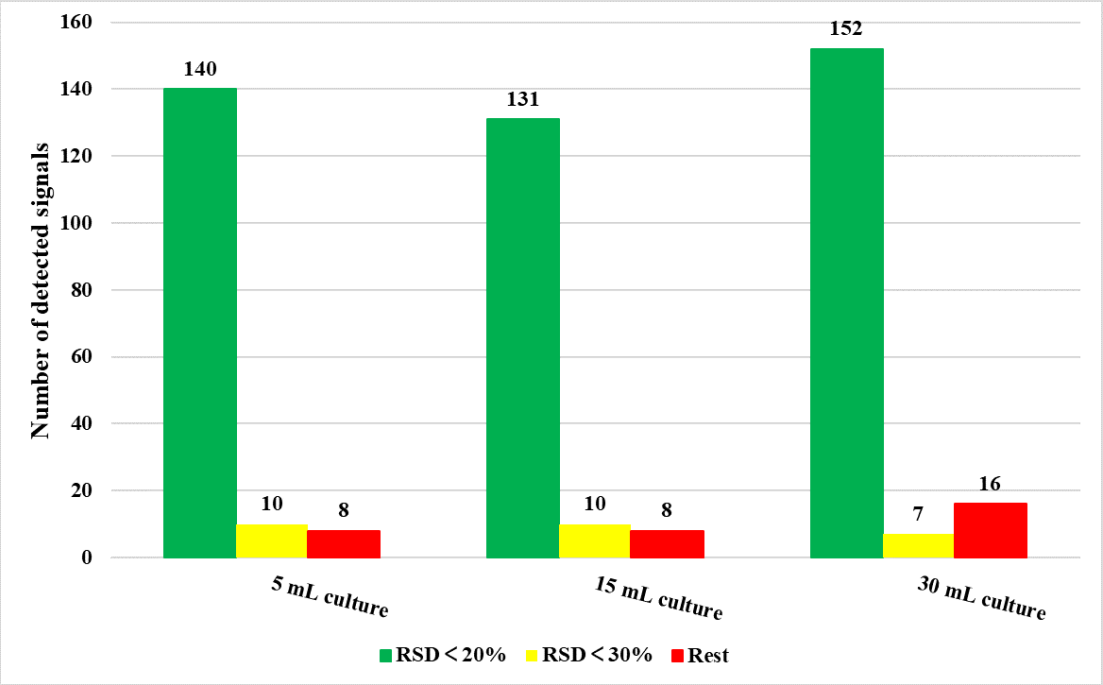

Figure 23 Repeatability validation of bacteria sample in triplicates measurements

for the intracellular metabolites of *C. marina* is repeatable and reliable for the research purpose.

4.1.3 Identification of metabolites with GCxGC-MS

With the instrumental parameters mentioned in section 3.2.5, 1 µL of the derivatized extracted sample was injected into the GCxGC-MS for metabolic analysis. At first, the raw data were visualized in GC Image as a contour plot. More than 170 intensive signals could be detected, which represents an overview of the intracellular metabolic state of *C. marina* as a "snapshot". The retention times in both dimensions were employed to search those intensive spots in the total ion current (TIC) chromatogram. The MS spectra were compared with the NIST library, which contains suggested substances with match factors (i.e., indexes of similarity). Compared with the literature and NIST

database, those compounds as potential metabolites with match factors ≥ 80 were selected and listed in table 2.

Two zones, A and B, were circled in figure 24, which imply different groups of metabolites. For example, as shown in table 5, amino acids such as L-cystine (50), L-aspartic acid (72), etc., were located in zone A. In zone B, there was the alkane group including eicosane (138), docosane (148), etc. Besides, fatty acid metabolites such as butanoic acid (17), succinic acid (31), and oleic acid (152) were detected with high match factors. Similar to previously reported work [151], the intracellular metabolites of *C. marina* show distributions in defined classes. The majority of the detected metabolites were separated well without co-elution. The orthogonality and optimized parameters of the instrument reduced the interference and brought advantages for the qualification and quantification of such derivatized samples.

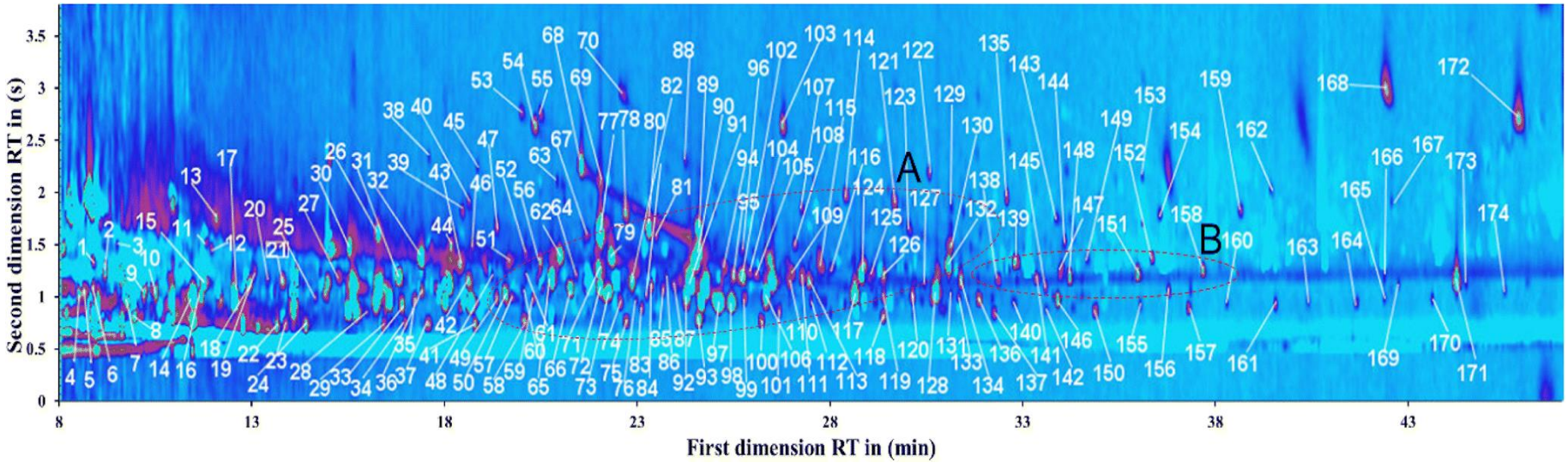

Figure 24 Contour plot from GC Image. Intracellular metabolites of *C. marina* were detected as spots in the plot. The x-axis represents the retention time (min) for the first dimension. The y-axis represents the retention time (s) for the second dimension

Table 2 Potential intracellular metabolites of *C. marina* according to the NIST library

Spot number	**Suggested metabolites**	**Retention times**		**Match factor**
		1st D (min)	**2nd D (s)**	
4	Octanol	8.54	2.54	86
7	Propanoic acid	9.81	2.42	92
11	Pentanoic acid	11.90	2.98	91
14	Glycine	11.52	2.50	93
17	Butanoic acid	12.66	2.46	93
19	Isoleucine	13.17	2.74	80
25	Methylmalonic monoamide	14.75	2.46	80
31	Succinic acid	16.90	2.66	91
48	Glutaric acid	19.37	2.70	87
50	L-Cystine	19.69	2.54	80
57	Beta-Alanine	19.88	2.50	82
59	L-Homoserine	20.45	2.46	80
61	Threonine	20.26	2.66	81
65	Aminomalonic acid	20.96	2.70	90
66	Malic acid	21.40	2.58	91
68	L-Proline	21.72	3.78	80
71	L-Methionine	22.16	2.74	89
72	L-Aspartic acid	22.22	2.58	87
78	Alanine	22.86	3.30	91
90	L-Phenylalanine	24.76	2.90	86
91	Glutamic acid	24.57	2.62	83
106	l-Lysine	26.53	2.50	89
112	D-Galactose	27.73	2.46	80
117	L-Ornithine	28.87	2.50	93
120	D-Glucose	30.39	2.50	86

121	Adenine	29.89	3.38	84
132	L-Tyrosine	31.34	2.78	92
133	Octadecanamide	31.60	2.46	80
138	Eicosane	32.61	2.62	80
143	Oleanitrile	34.13	3.26	88
148	Docosane	34.51	2.66	89
149	Myristic acid amide	34.95	2.86	80
151	Tetracosane	36.28	2.70	90
152	Oleic acid	36.66	2.86	88
158	Hexacosane	37.99	2.74	87

As reported by Winder *et al.*, amino acids such as glycine (14), phenylalanine (90), and glutamic acid (91) were found in *E. coli.* strain MG1655 with relatively high responses compared to other detected intracellular metabolites [17]. On the other hand, Li *et al.* differentiated bacteria with fatty acids measured by GC/MS/MS [152]. Oleic acid (C18:0)(152) was confirmed in three bacteria, including *E. coli.*, *Francisella novicida*, and *Bacillus subtilis*, which was considered a common long-chain fatty acid in bacteria [152]. Fatty acid C14:0 was also observed in these three bacteria. In this study, its amide - myristic acid amide (149) was found to present in *C. marina*.

4.2 Metabolic response to the ozone stress

As described in section 3.2.3, cultivated *C. marina* was spiked with different ozone dosages to evaluate its metabolic response under oxidative stress. A MIC test was performed to ensure that the bacteria were stressed but not dead after ozone treatment, as mentioned in section 3.2.4. Thus, the proposed protocol could be applied to help understanding its metabolic change under stress. The overall working flow of ozone treatment was described in Appendix figure S 3.

4.2.1 Status of bacterial cells after MIC test

To confirm the activity and cell integrity of the bacteria after ozone treatment, those bacteria in the first rows of each plate were streaked and re-cultivated on the MB agar plates. For example, the bacteria treated with 500-µM ozone were cultivated and shaken for 24 h at room temperature. The 48-well plate was photographed from its bottom to observe the ozone-treated bacteria compared to sterile and growth control. As shown in figure 25, taking row A as an example, the colors of bacterial culture were increasingly turbid with decreasing ozone concentration from A1 to A6. Less aggregation of bacteria was found from A1 to A5 compared with A6, which has the least ozone-stressed bacteria. It reveals that an increasing living activity could be found by decreasing stress. The influence of ozone stress treatment on metabolic activity might lead to the reproduction declining of bacteria even after a long period. For A1 and A8, a clear difference could be observed between bacteria with (A1 to A6) and without ozone dosages (A8), which could be due to the suppressed growth of bacteria by the ozone treatment. It also reduces the chance for the bacteria to aggregate together.

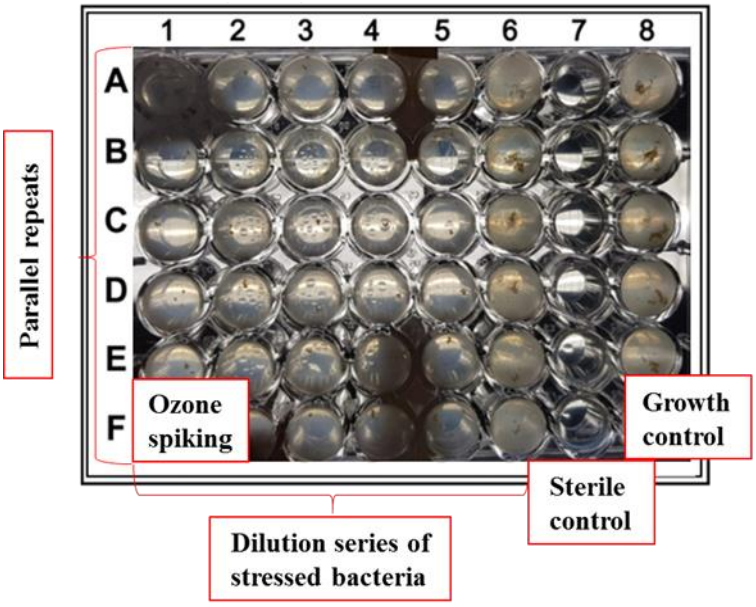

Figure 25 Sample in 48-well plate with ozone dosage of 500 µM after 24h shaking. In column 1 to 6 were the dilution series by the ratio of 1:2. Column 7 and 8 show the sterile control without bacteria and the bacteria culture without ozone treatment, respectively

The bacteria culture from the 48-well plate above was streaked on MB agar plates to investigate their activity by regrowth. After overnight regrowing, the colonies were observed in four separated sections, as shown in figure 26. Those bacteria that encountered different stress were streaked in different sections, which all formed yellow-white dots from highly (1000 µM) to less stressed (170 µM) samples. By the comparison of ozone-treated bacteria streaked and growth control sections, it was found that the stressed bacteria could regrow similarly to non-treated bacteria in the same condition. On the other hand, there were no colonies found in sterile control sections showing that there was no cross contamination. Thus, it was proven that the *C. marina* was merely stressed by ozone and not directly inactivated by cell membrane damage. Accordingly, the intracellular state could change to resist the stress and survive during the attack of ozone.

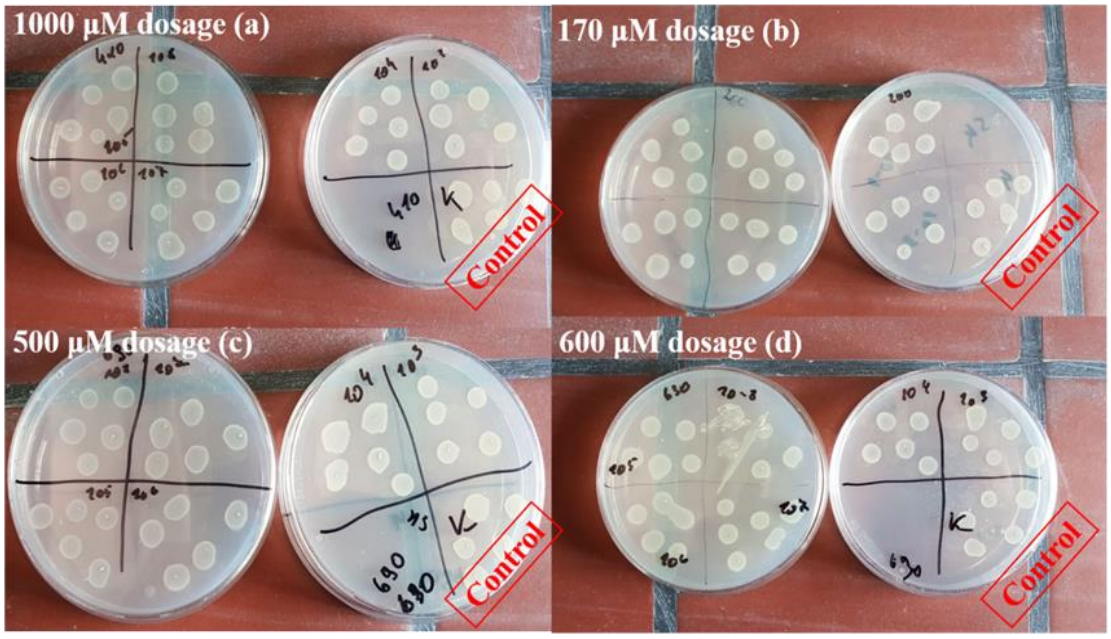

Figure 26 Regrowth of *C. marina* culture on the MA agar plate after ozone treatment. Bacteria with ozone dosages of (a) 1000 µM, (b) 170 µM, (c) 500 µM and (d) 600 µM were streaked in four different plates. The yellow-white dots were colonies formed by room-temperature incubation. Each plate contained four sections. On the first plate of each dosage, there were four parallels. On the second plate, there were another two parallels, growth control (in red) and sterile control (no colonies grown)

4.2.2 Intracellular state variation induced by ozone stress

Based on the MIC test conclusion, the ozone treatment was not lethal but obviously influenced the living state of *C. marina*. A non-target analysis with GCxGC-MS at scan mode was performed to verify such physiological change as described in section 3.2.5. Three contour plots of ozone-treated (two different ozone dosages) and non-treated samples were selected for further comparison, shown in figure 27. There is a clear trend that the detected signals became less in number and weaker in intensities once the ozone treatment was applied. Furthermore, the effect was amplified for some metabolites once the ozone dosage was increased from 500 µM to 600 µM.

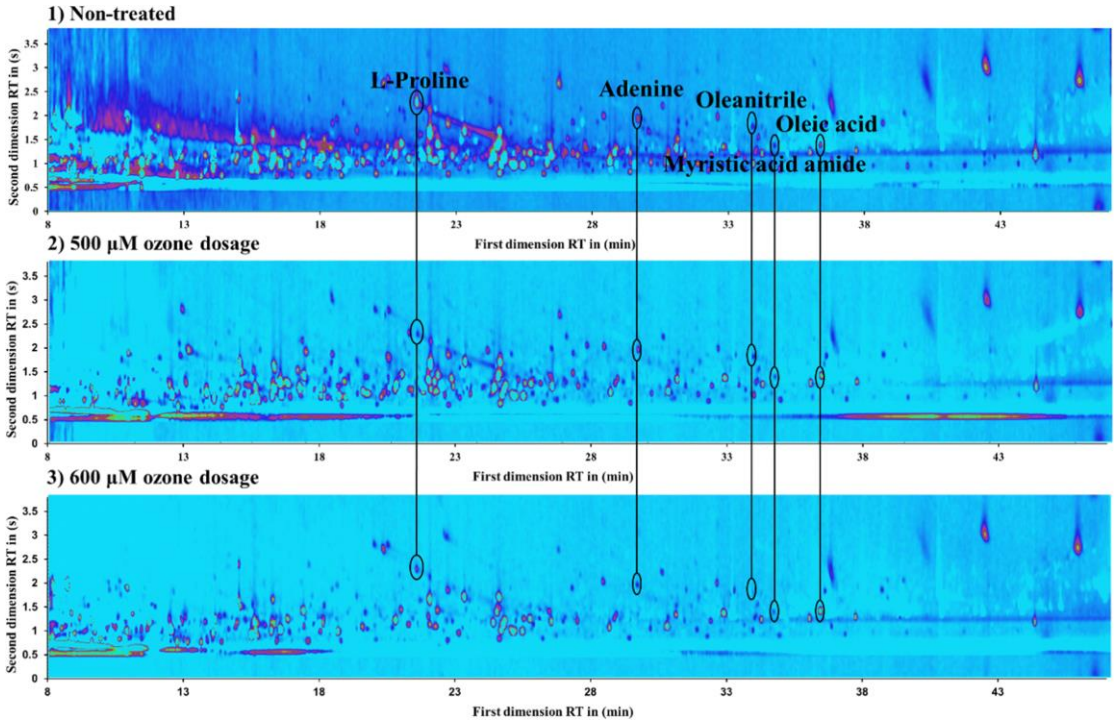

Figure 27 Contour plots with potential intracellular metabolites of *C. marina* (1) non-treated and treated with (2) 500 µM and (3) 600 µM of ozone

In figure 27, five spots were circled and identified according to the mass spectra, which are presented in each contour plot. The substances suggested by the NIST database were included in table 2. Since the contour plots were adjusted into the same contrast parameters, the color of the spots could be used to compare the signal intensity that the

higher intensive signal has a larger spot area. Thus, the trend of these five compounds after ozone dosage could be easily derived by comparing colors.

Amino acids, L-proline (68), and adenine (121) in figure 28 showed a decreasing trend after ozone treatment. Mudd *et al*. described that the amino acid class could be easily attacked and oxidized by ozone [166].

In contrast, oleic acid (152) showed inverse activity in ozone-treated samples. As a typical long-chain fatty acid (LCFA), the concentration of oleic acid was found to grow slightly, according to Belenky *et al*. [153]. They proposed that the cell toxicity of treating *E. coli* with three different antibiotics and its behavior were similar to those under oxidative stress. Therefore, oleic acid might be an up-regulated metabolic factor under such ozone stress.

Hazel *et al*. reported that the fatty acid composition in the cell membrane could improve the ability to survive under the physical change of living conditions [154]. For example, a reduction of saturated fatty acids and an increase of unsaturated fatty acids in some bacteria were found during cold exposure [154]. Recently, it was also proved that cell-derived fatty acids of some bacteria such as *E. coli* and *P. aeruginosa* were changed in constituents when exposed to different stresses and external contaminants [155]. As described by Santos *et al*., an increase of saturated and branched fatty acids was found once the bacteria were exposed to toxic compounds [155].

Interestingly, the intensity of oleanitrile (143), a fatty nitrile derived from oleic acid, also decreased in the treated samples. For myristic acid amide (149), a reducing abundance was also observed after oxidative stress by ozone. Furthermore, except for oleic acid, the other four selected compounds showed a difference between 500-μM and 600-μM ozone dosage, indicated in the plots with distinct spot areas.

4.2.3 Comparison for ozone treatment via GasPedal

To get a more distinct overview of the difference between treated and non-treated samples, a warping image was generated by the GasPedal software to compare the contour plots of both samples and shown in figure 28.

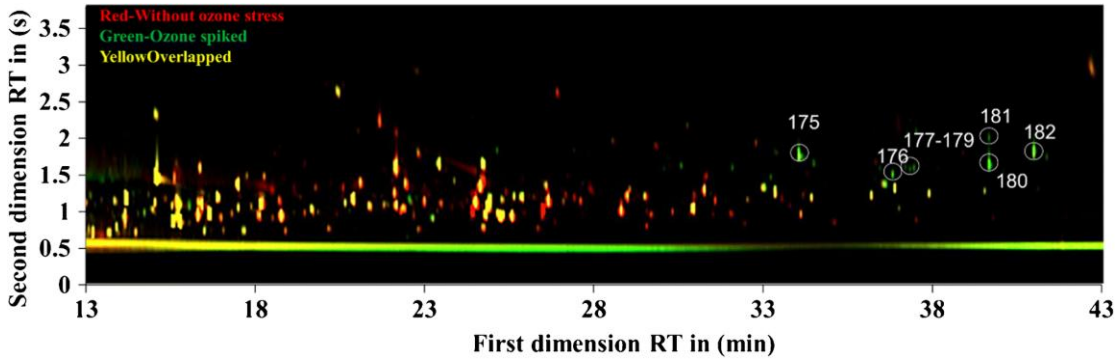

Figure 28 Comparison by overlaying the contour plots performed by the GasPedal software. Red: sample without ozone stress; green: sample with 600-µM ozone dosage; yellow: formed by the overlap of both contour plots

As indicated in figure 28, the spots colors are red for non-ozone treated samples and green for treated once imported the acquired data to the GasPedal. By overlaying these two images, the color of a certain spot in both plots at the same position turned into yellow at the overlap area. At first, most of the spots are overlapped (yellow) in figure 28 and are still present after the ozone treatment. However, some spots are yellow but surrounded by red color. It means that the abundance of these compounds is decreased. The other spots in red or green represent metabolites, which are completely decreased or newly generated, respectively, due to the ozone treatment. As a result, the ozone effect is better visualized by such a warping image, which allows the fast inter-plot comparison without time-consuming observation with the naked eyes in a conventional way. As shown in figure 28, the green spots represent those substances that occurred due to ozone stress. According to the database, the suggested compounds were listed in table 3.

Table 3 List of suggested substance according to the NIST database occurred after ozone stress

No.	Substance	Match factor	No.	Substance	Match factor
175	cis-9-Hexdecenal	91	**176**	Unknown	Not in NIST
177	Unknown	Not in NIST	**178**	Unknown	Not in NIST
179	Unknown	Not in NIST	**180**	Unknown	Not in NIST
181	13-Docosenamide	85	**182**	9-octadecenal	80

Such fatty aldehydes as cis-9-hexdecenal (**175**) and 9-octadecenal (**182**) could be intermediate metabolic products generated by reducing fatty acyl-CoA with acyl-CoA reductase. On the other hand, such aldehydes could not be reduced to fatty alcohols if the fatty aldehyde reductase is lacking. Yao *et al.* has proposed that the fatty alcohols are produced under environmental stress [156]. However, the ozone stress might block the aldehyde reduction pathway, which causes the fatty aldehydes to accumulate as the "snap" of the fatty alcohol biosynthesis pathway. 13-docosenamide (**181**) was reported to be released by the bacteria in response to fluorescein quenching by Tamilmani *et al*. [157]. In this case, 13-docosenamide was detected after the ozone treatment, which might be a stress response to the environmental change.

The other compounds in table 3 do not show sufficient correspondence with the NIST database, and therefore the identification is not possible. The spectra of these unknown compounds were shown in figure 29. First of all, all these five compounds have the fragment of m/z 73, a specific ion fragment of $Si^{+}(CH_3)_3$ in silylation. It implies these unknown compounds could be silylated metabolites not including in the database. The m/z of 252 was presented in the spectra of compounds (173) (178) (179), which is close to the m/z of muramic acid after elimination of the silylation group, typically presented in the bacteria cell wall [158]. The fragment with m/z of 144 could be one product of the m/z 252 after dehydration (m/z of 18) and loss of lactic acid (m/z of 90).

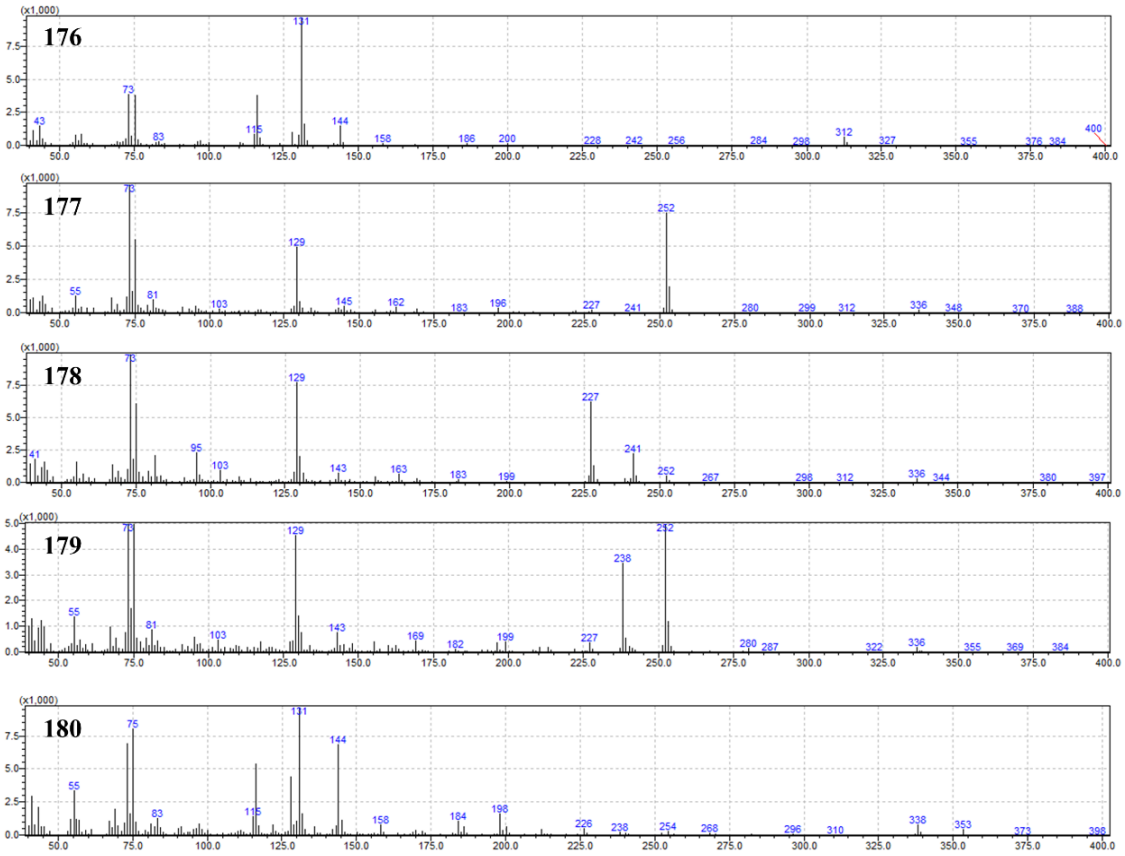

Figure 29 Spectra of unknown substances occurred after ozone treatment found with the help of GasPedal

To summarize, the effect of ozone stress could be visualized and evaluated by the metabolic change of microbial state, which is revealed by the intracellular metabolites.

These findings could not have been possible without the help of the proper sample preparation, the two-dimensional gas chromatography separation coupled with MS, and the visualization via GasPedal. Some identified signals corresponding to specific fatty acids (with the exception of oleic acid) and amino acids from *C. marina* showed to be decreased by increasing the ozone dosage. With the help of GasPedal, compounds such as 9-hexdecenal, 9-octadecenal, and 13-docosenamide were found to respond to environmental changes.

4.3 Metabolic response to starving stress

To evaluate the metabolic state of *C. marina* at starving condition, an overnight culture was treated as described in section 3.2.2. Besides, *C. marina* regrown in different solutions, ASW and MB, were compared before analyzing nutrients starvation.

4.3.1 Comparison of regrowing and resuspension

At first, the behavior of *C. marina* was observed by regrowing in the artificial seawater. In figure 30a, the ASW was almost limpid after 5 h cultivation for diluted *C. marina*. In contrast, regrowth of *C. marina* in MB led to relative turbidity, which might be due to the increase of bacteria quantity. Therefore, it could be proved that *C. marina* could barely survive and reproduce in ASW without nutrients after several hours at room temperature.

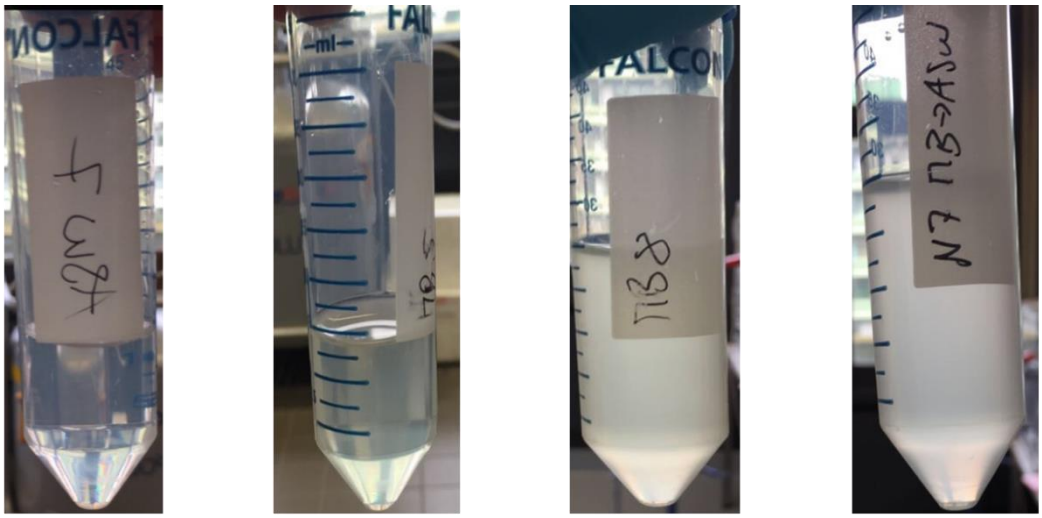

a) regrow in ASW b) regrow in MB c) regrow in MB resuspend in MB d) regrow in MB resuspend in ASW

Figure 30 Bacteria culture of *C. marina* at condition: regrown a) in ASW b) in MB after dilution and resuspended c) in MB d) in ASW after regrowth

The regrowth of *C. marina* in MB was followed by the resuspension in ASW, which is to artificially create starving stress for *C. marina* and compare it with a control

resuspended in MB. Thus, the regrown *C. marina* from different batches was combined then resuspended in MB (Fig. 30c) and ASW (Fig. 30d). Both resuspensions were 20 mL with the same amount of bacteria. Therefore, they have similar turbidity once uniformly distributed in the solution. After a 30-minute starving treatment, they underwent the routine protocol for further analysis.

4.3.2 Comparison of starved and non-starved state

With the quenching step, the normal and starving states of *C. marina* were snapped right after 30 minutes since starving started. The derivatized samples were then analyzed with GCxGC-MS. The resulting contours plots are shown in figure 31.

For the overview, *C. marina* lived in MB with sufficient nutrients (Fig. 31(1)) indicates more intensive signals compared to those lacking nutrient supply (Fig. 31(2)). It implies that corresponding metabolites have changed under such starving stress. Thus, L-cystine (**50**), alanine (**78**), L-phenylalanine (**90**), and L-tyrosine (**132**) were selected for detailed comparison.

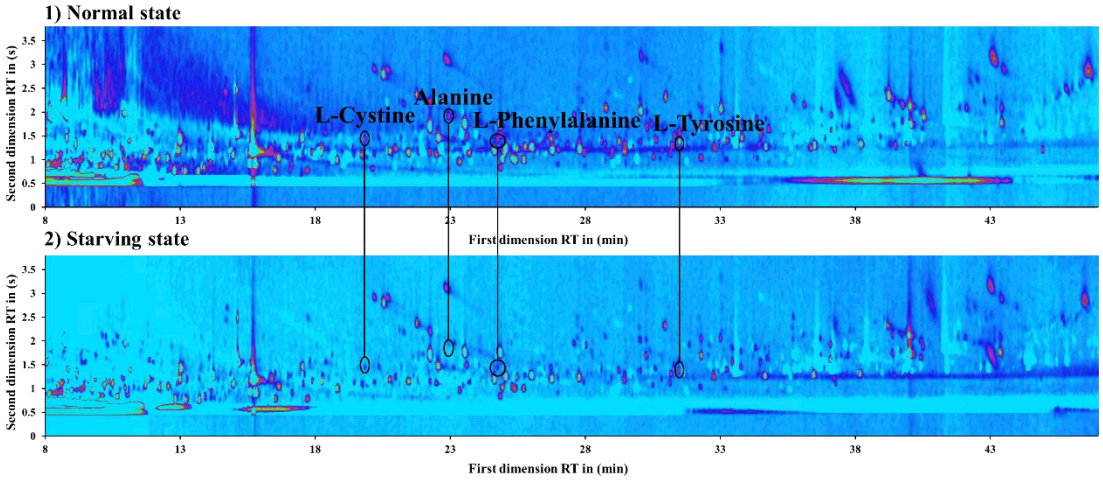

Figure 31 Comparison with contour plots of *C. marina* at (1) normal state and (2) starving state

As reported by Zhou *et al.*, most bacteria have cystine importers to uptake cystine as its sulfur source for the bacteria cells [159]. The imported cystine will be reduced to

cysteine for further biosynthetic pathways such as glutathione redox cycles [160]. L-cystine, in this case, decreasing might be due to lack of uptake from environment culture at nutritional starvation. In addition, the bacterial activity begins to slow down once out of nutrients, which might also lead to biosynthesis disorder with a low reduction rate from cystine to cysteine [161].

By taking *E. coli* as a model, Lee *et al.* described its biological pathway of accumulating alanine [172]. Glucose, as substrate, is metabolized to pyruvate, which then mostly likely converts to alanine by glutamate-pyruvate transaminase. In this case, glucose is limited due to nutritional starvation, which might lead to alanine accumulation failure. Thus, the amount of alanine decreased here might be due to a lack of glucose source [173]. L-phenylalanine and L-tyrosine, the aromatic amino acids, are produced from the intermediate chorismate via enzyme chorismate mutase, prephenate dehydratase, and tyrosine aminotransferase, which are only found in bacteria [162]. As the central intermediate of the shikimate pathway, chorismate is derived after several steps by glycolysis, and therefore its synthesis depends on the nutrient supply from the substrate [163]. It implies that the level of chorismate would drop under starvation conditions. Therefore, the synthesis of L-phenylalanine and L-tyrosine might be influenced by the decrease of chorismate when bacteria are short of nutrients.

4.3.3 Comparison of starved and non-starved state via GasPedal

To get a more distinct overview of the difference between starved and non-starved *C. marina*, a warping image (Fig. 32) was generated by the GasPedal software to compare the contour plots shown in section 4.2.2. Those signals found in both samples were indicated as yellow spots.

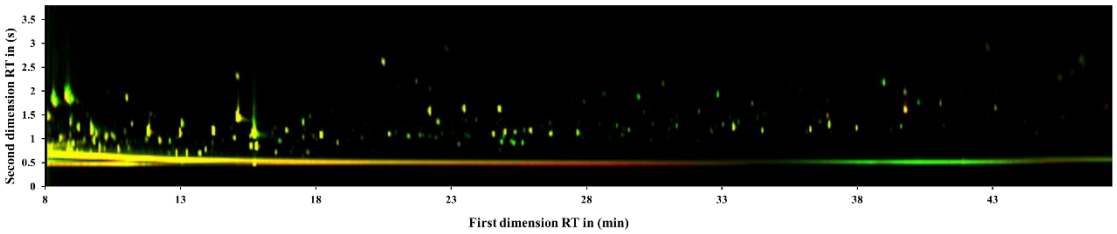

Figure 32 Comparison by overlaying the contour plots performed by the GasPedal software. Green: normal state; red: staving state; yellow: formed by the overlap of both contour plots

As revealed in figure 32, there were barely red spots representing new metabolites for the starving state found on the image. However, many metabolites are showing in green or yellow. The yellow spots were formed by those metabolites relatively less or not influenced by the starving state since the intensities of the spots are comparable in both plots. It is important to mention that the green spots, for example, those circled in white, are not completely “green”(come from the contour plot of normal state). The spots in green have yellow colors, which could not be clearly indicated in this figure. Therefore, the green spots here are not metabolites generate because of the starvation, but those relatively much decreased in intensities.

In conclusion, nutritional starvation seems to have a potential influence on metabolites, especially the amino acid group such as L-cystine, alanine, etc., which mainly play essential roles in the intracellular pathways. With the proposed protocol, the intracellular state could be investigated once the bacteria cells encountered such extreme conditions.

One main limitation of the described metabolome analysis is the needed number of cells. To overcome this limitation preliminary works about single cell analysis were done during this doctorate.

4.4 Sample introduction via inkjet technique

Some advantages of the sample introduction via the inject technique could be derived from previous findings [131, 140, 164]. First of all, the inkjet printing techniques, especially the piezoelectric-based print, could generate the droplets in the picoliter range accurately and reproducibly. Next, the droplet volume is controllable, which means the number of analytes or microorganisms in each drop could be adjusted once the supplied "ink" is uniform during the printing process. Furthermore, sensitive detectors such as MS rely on the signal-to-noise ratio to get reproducible and significant signals. The background noise would be reduced with less solvent matrix in the drops compared to conventional spray. Thus, the sensitivity of the detector could be improved by such a sample introduction method to some extent. Therefore, the inkjet droplets are optimal for those samples with less content or limited bacterial cells for regular sample preparation.

The inkjet technique, as mentioned before, has advantages for the liquid sample introduction. As shown in figure 33, the liquid sample in the red glass tube was

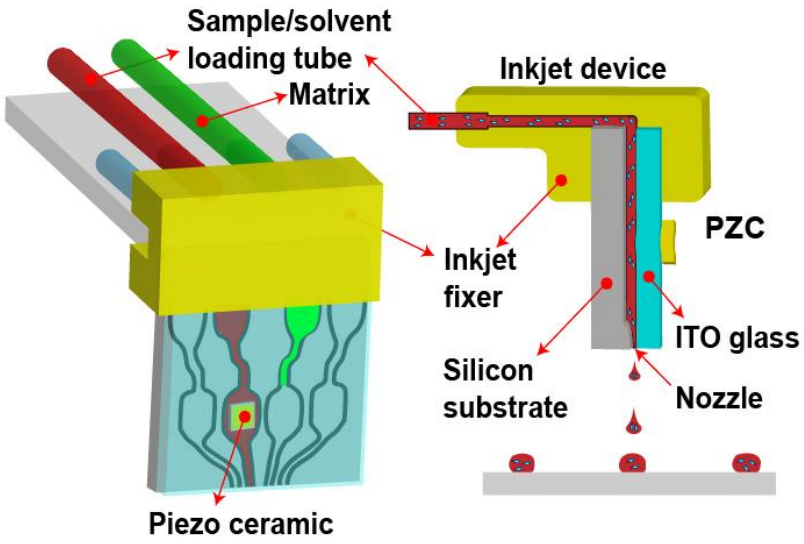

Figure 33 Schematic diagram of the inkjet setup: inkjet printing of bacteria via piezo ceramic onto the MALDI plate for MALDI-QTOF-MS analysis; onto the tungsten needle tip for direct MS detection

squeezed out of the nozzle. The piezo ceramic is responsible for controlling the droplet formation. To adapt it for experimental purposes, the detailed inkjet parameters need to be optimized, such as current pulse, driving voltage, and the number of droplets per ejection. The optimized inkjet was then applied for further use on direct MS or MALDI-MS detection.

4.4.1 Droplets formation and optimization in the matrix

The droplets formed by the inkjet would travel in the air before reaching the MALDI plate or the MS detector. Therefore, it is crucial to find out the optimized parameters to form and drive the droplets and to prevent the quality of droplet formation and the precision of droplet location from air influence. The optimization involved in this section was obtained with water as a sample matrix and with the setup shown in figure 34.

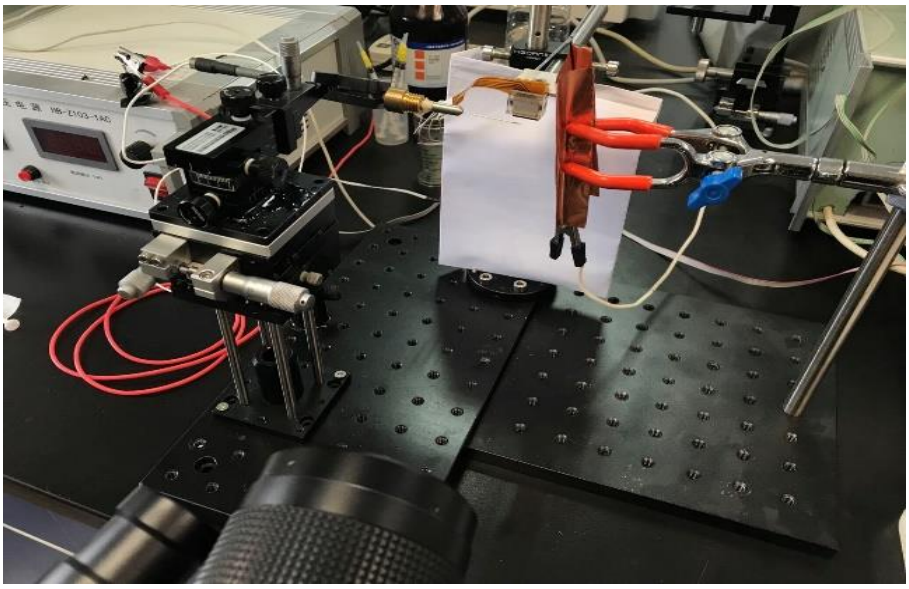

Figure 34 Setup for optimizing inkjet droplets formation

4.4.1.1 Current pulse

The size of the droplets depends mainly on the duration of the pulse, which is usually in the range of μs. In this study, different pulses with a driving voltage of 20 V were

compared through the images recorded by a monochrome camera. The first channel of the inkjet was used to optimize the droplet formation.

Figure 35 shows the droplets from channel 1 in the area circled in red. In figure 35a, the droplets formed by 10 μs pulse were too small to be observed with the camera. With 15-μs pulse, uniform-size and linearly distributed droplets were obtained in figure 35b. In figure 35c and 35d, only some large droplets were produced by increasing the pulses to 20 and 25 μs in the selected area. Therefore, it was evident that the current pulse of 15 μs is the optimum for forming the droplets in the water matrix.

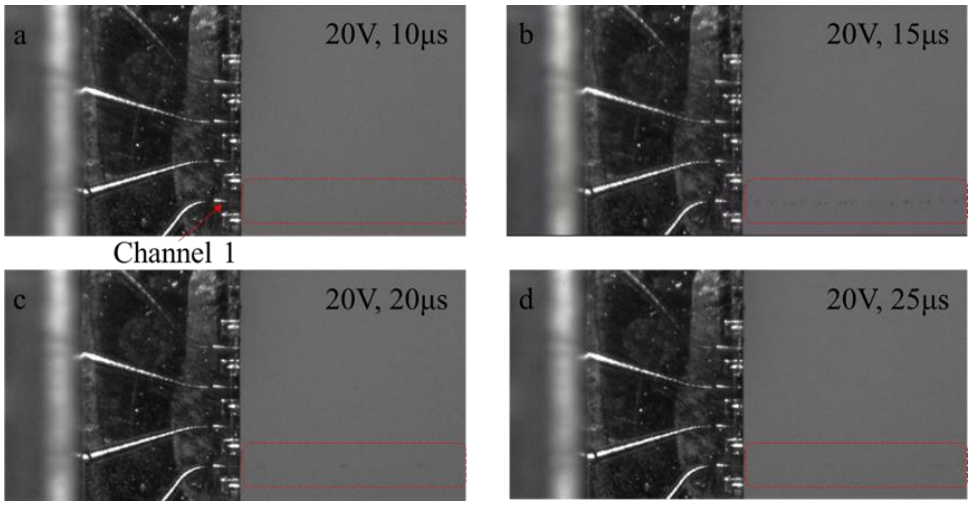

Figure 35 Droplets formation with different current pulses recorded by a monochrome camera; (a) 10 μs (b) 15 μs (c) 20 μs (d) 25 μs

4.4.1.2 Driving voltage

The voltage applied at piezo ceramic decides the driving force for the movement of formed droplets traveling out of the inkjet channel. Since 15 μs was determined to be the best duration for the current pulse, the combinations with different voltages were optimized and detected by the camera. As shown in figure 36, the droplets were driven out of channel 1 in different patterns circled in red. In figure 36a, a voltage of 19 V was applied, which resulted in a well-distributed pattern with a slight shift. With 20-V voltage in figure 36b, the droplets were linearly distributed initially but slanted

afterwards. In figure 36c and 36d, the distribution was linear, and the distance between droplets increased by increasing voltage from 21 V to 22 V. It could be concluded that the moving track of the droplets against air was changing by increasing the driving voltage. The shift patterns were found with 19 V and 20 V, but not that obvious at 21 V. Therefore, the driving voltage needs to be higher than 21 V to prevent offset of the target location.

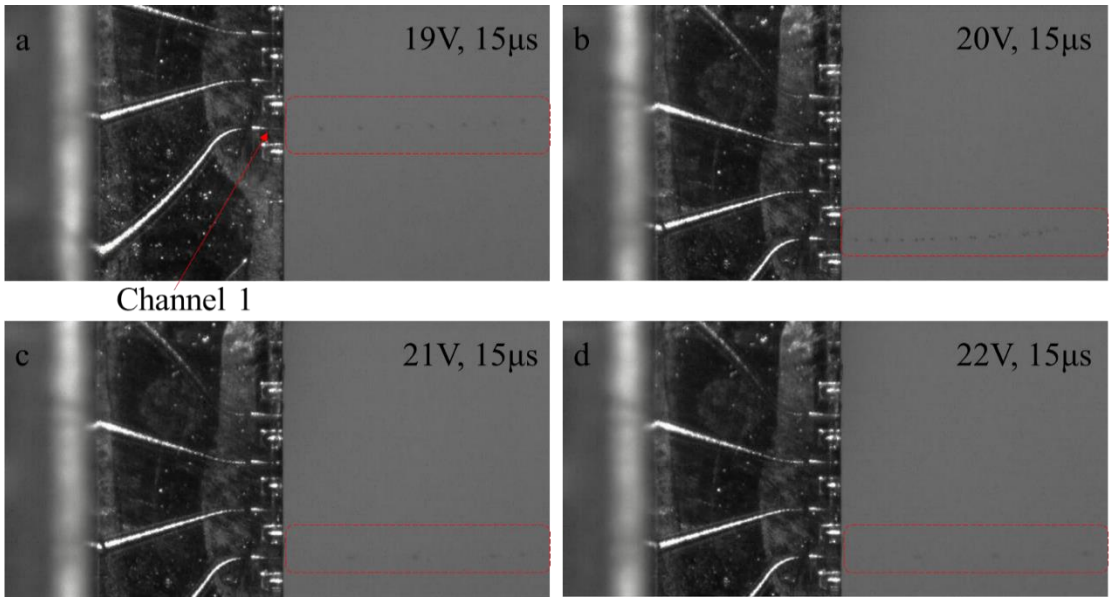

Figure 36 Droplets formation with different driving voltages detected with a monochrome camera (a) 19 V (b) 20 V (c) 21 V (d) 22 V

4.4.1.3 Accumulation of droplets on tungsten needle

The accumulation of the droplets on the tip of the tungsten needle was observed in this test. It is to validate whether the inkjet printer could generate a specified number of droplets in a single printing. As shown in figure 37, more droplets accumulated on the needle tip by increasing from 10 to 100 droplets with a single print. It means that the inkjet nozzle could properly form droplets for study purposes.

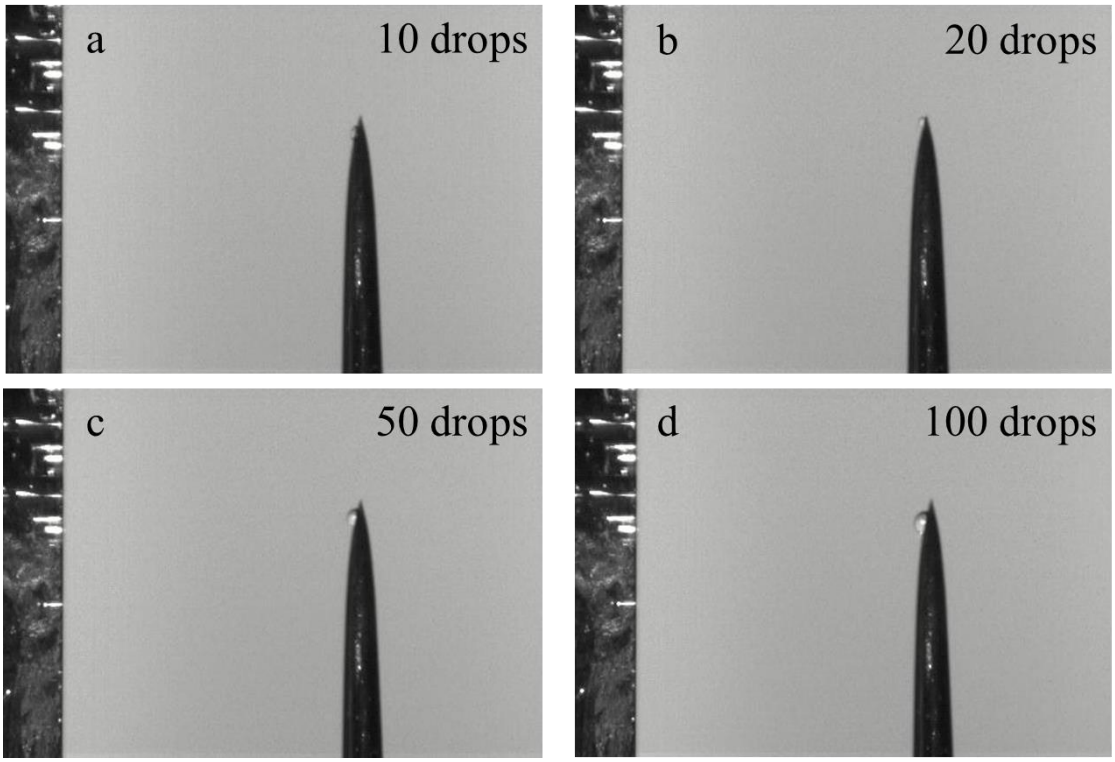

Figure 37 Single printing with (a) 10 (b) 20 (c) 50 (d) 100 droplets accumulated on the tip of the tungsten needle

4.4.2 MALDI-MS detection via sample introduction by inkjet

A multi-layer introduction method in this study was proposed for sample introduction on MALDI plate. According to the optimization, the driving voltage of 30 V was chosen to make sure the droplets landing close to the center of the target area.

4.4.2.1 Sample loading sequence

As reported by Smolira *et al*., the matrix and the ratio of matrix and sample were critical for the MALDI-MS analysis [165]. Similarly, in a multi-layer introduction, the construction of such a two-layer structure would be influenced by the loading procedure [166]. Therefore, the sequence of matrix and sample layer could be quite important to

improve the signal intensity. Taking 1.5-µL sample and 1.5-µL matrix as an example, there were several combinations attempted with the DHB matrix.

1. The "sandwich" structure, which means 0.75-µL matrix was dried on the plate, followed by 1.5-µL sample dried over the matrix then 0.75-µL matrix dropped on the top [178].

2. 1.5-µL sample on the dried 1.5-µL matrix.

3. Opposite to structure 2, which means introducing 1.5-µL sample first, then cover with the 1.5-µL matrix.

Samples prepared in these three ways were analyzed with the MALDI-MS method mentioned in 3.2.7, which were then compared in figure 38 for the m/z range from 20 to 1000.

As shown in figure 38, the intensities of the detected signals differ between the various introduction strategies. In figure 38B, the matrix was placed under the sample, which

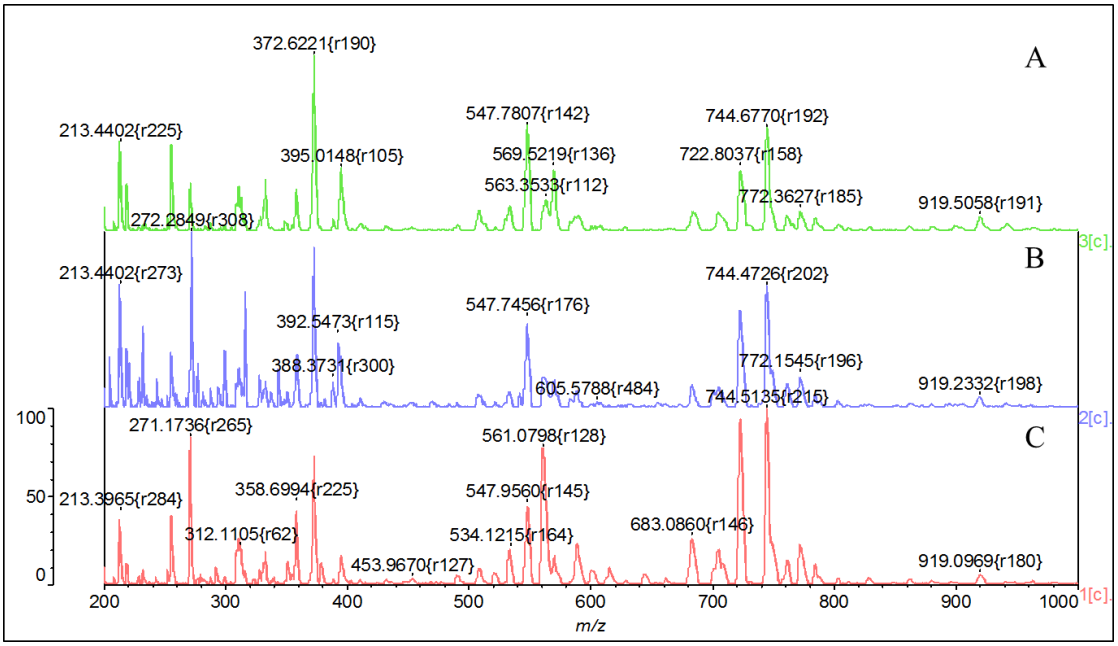

Figure 38 MALDI spectra of different sample loading method in the sequence of (A) "sandwich", 0.75-µL matrix, 1.5-µL sample, 0.75-µL matrix (B) 1.5-µL matrix, 1.5-µL sample (C) 1.5-µL sample, 1.5-µL matrix

leads to relatively fewer signals and intensities. This might be due to the matrix could not be excited properly without direct contact with the laser beam once surrounded by the sample solutions. As a result, the sample molecules were insufficiently ionized. In contrast, the sensitivity increased once the matrix solution was placed above the sample solution, as in figure 38A and 38C.

However, the simple two-layer method with the 1.5-µl sample plus 1.5 µL matrix was considered slightly better than the "sandwich" method. The high relative abundance signals were more in figure 38C, especially for the signals with m/z 722.80 and 744.68. Therefore, the two-layer method that introducing 1.5-µL sample first then 1.5-µL matrix was used for sample introduction in the further study.

4.4.2.2 Matrix concentration

Besides the introduction method, the matrix concentration also influences the sensitivity of MALDI-MS. Commonly used matrices such as DHB, CHCA, and SA were investigated in this study to find out the optimum concentrations for further analyses.

The DHB concentration range was studied from 10 mg/mL to 30 mg/mL in 70 % ACN (ACN:H_2O, 70:30), which were also adopted by other researchers [179, 180]. Figure 39 shows the results of different DHB concentrations in the m/z range from 400 to 1000. At low concentration (10 mg/mL and 15 mg/mL) signals between m/z 500 and 600 and also between 700 and 750 are detected, which are quite similar to the results with 25 mg/mL and 30 mg/mL. In contrast, more signals are observed with DHB at 20 mg/mL, especially in the lower m/z range. Therefore, 20 mg/mL DHB in 70% ACN was used as the matrix for the direct detection of *E. coli*.

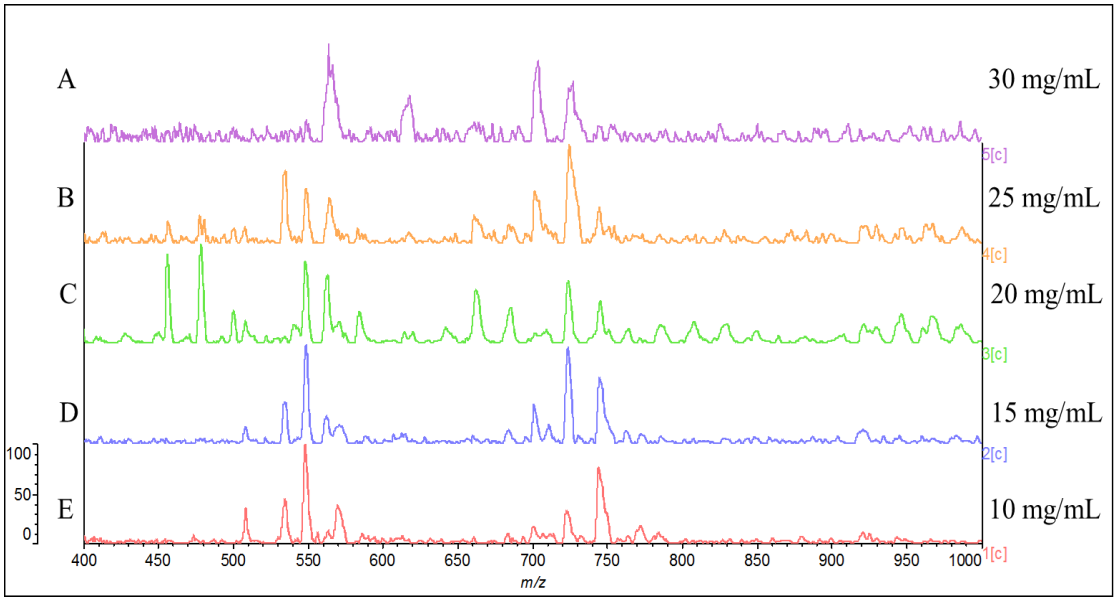

Figure 39 Comparison of different concentration of DHB matrix (A) 30 mg/mL (B) 25 mg/mL (C) 20 mg/mL (D) 15 mg/mL (E) 10 mg/mL

According to former reports, saturated CHCA and SA matrix were also applied for *E. coli* sample analysis [167-169]. Instead of manually pipetting, the difference between saturated and non-saturated CHCA and SA matrix is still unclear for the inkjet printing sample preparation.

Therefore, in this study, saturated and half-saturated (1:1 dilution) matrix dissolved in 70 % ACN (ACN:H_2O, 70:30) were compared for validation. Figure 40A shows that the saturated CHCA matrix could provide more signals with higher sensitivity than the semi-saturated one. Also, in figure 40B, slightly more intense signals in the m/z range from 1000 to 5000 were detected with the saturated SA matrix than with the semi-saturated matrix.

These results show that both the saturated CHCA and saturated SA matrices improve the selectivity and sensitivity of MALDI-MS measurement using inkjet as the sample introduction method.

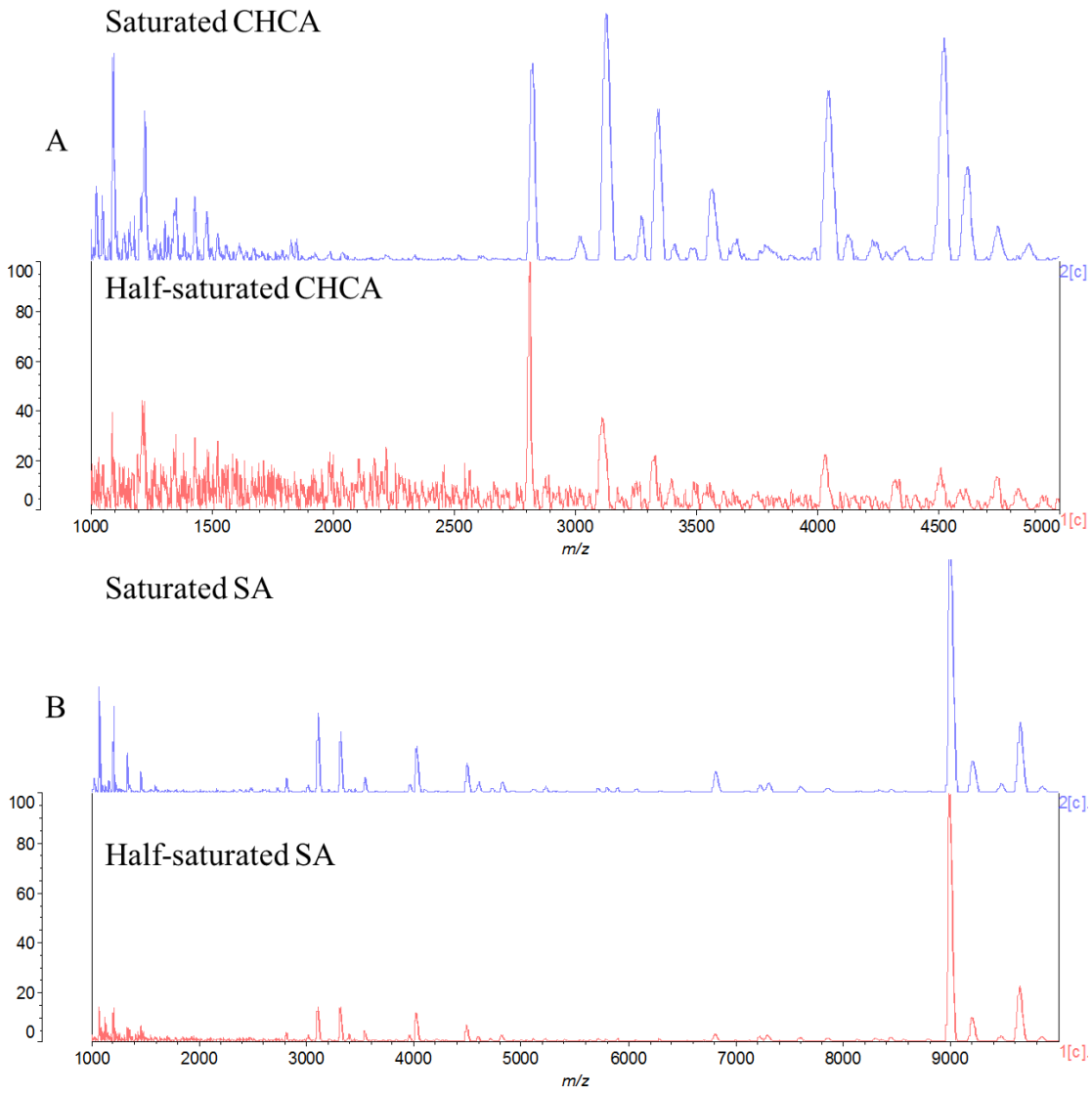

Figure 40 Comparison between saturated and half-saturated matrix of (A) CHCA (B) SA

4.4.2.3 MALDI-MS detection of E. coli with inkjet introduction

The overall system for *E. coli* sample introduction onto the MALDI plate is shown in figure 41. Such a system allows the automatic introduction of required sample volume by printing different amounts of droplets. In the beginning, the red tube was loaded with *E. coli.* sample. In the meanwhile, the matrix was loaded in the green tube. The pulse generator controls droplets' formation and releases them from the nozzle through the piezoceramics for each channel. The printing array was optimized for the distance

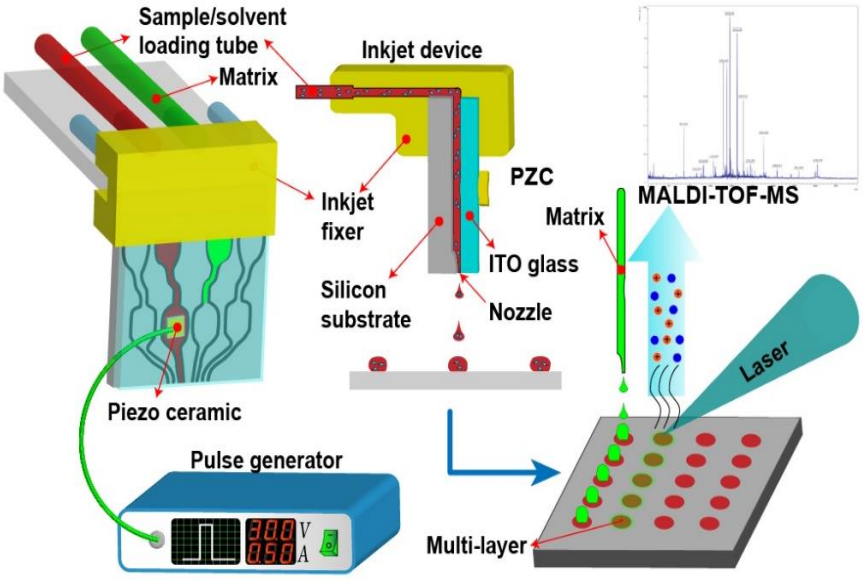

Figure 41 Schematic of inkjet introducing sample on to the MALDI plate with the method of multi-layer introduction (matrix in green as the second layer overlaid on the dried sample in red as the first layer), where culture and matrix were loaded in different loading tube on the inkjet device

between spot areas on the MALDI plate. Therefore, the droplets could be spotted precisely on the targets after leaving the nozzles. *E. coli* sample was first printed, followed by drying in the air at room temperature. The matrix was then printed on top of bacteria dry spots to obtain a two-layer structure.

To get an overview of such a two-layer structure, the crystallization of the spots was observed, as shown in figure 42. Freshly prepared *E. coli* resuspension and SA matrix were used for this investigation. The number of droplets for resuspension and matrix were always equal. For example, the spots were prepared by printed 100-droplet SA on 100-droplet resuspension in 42A and 50-droplets SA on 50-droplet resuspension in 42B. As indicated in figure 42, the crystallization shapes were nearly round for each size, which would help find out the center of the spot and hit it for more signals. Spots formed from 5 to 1 droplet (Fig. 42F to 42H) were relatively small and circled in red. However, even they were formed with relatively fewer droplets, they could still be located in the central area of the target. It implies that the inkjet printer can print samples in a picoliter

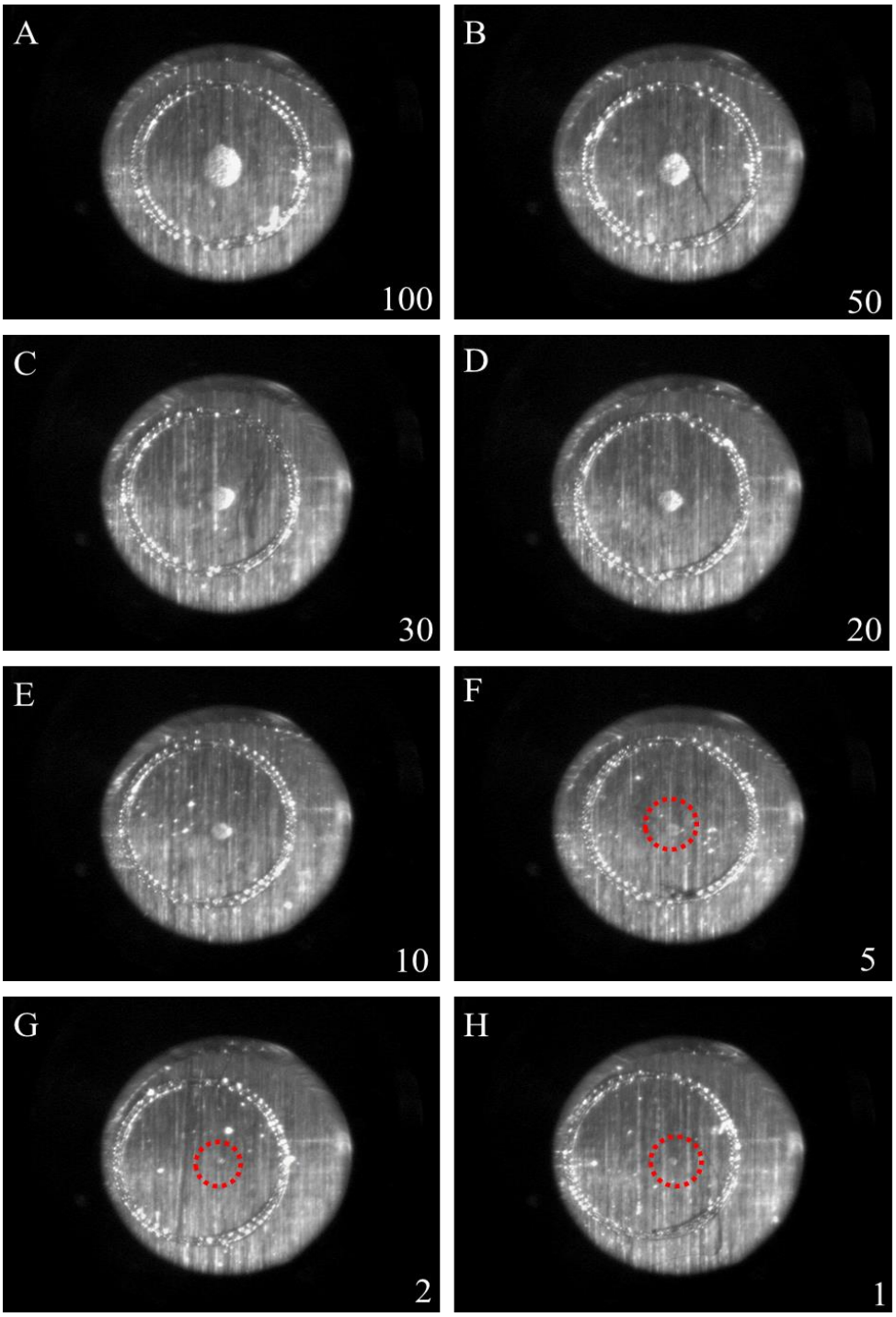

Figure 42 Image of crystallized spot by two-layer inkjet introduction under MALDI camera consisting of (A) 100 drops (B) 50 drops (C) 30 drops (D) 20 drops (E) 10 drops (F) 5 drops (G) 2 drops (H) 1 drop for both bacteria resuspension and SA matrix

scale and locate them at the desired targets against air on the MALDI plate. Furthermore, from figure 42A to 42F, it is clear that the matrix layers distributed uniformly and

covered the whole spot, which indicates the inkjet could precisely and robustly print the second layer on top of the first one.

To investigate the MALDI-MS sensitivity of inkjet-printed *E. coli* samples, sample spots with different numbers of drops and thus bacteria and SA matrix solution were used. MALDI spectra formed by 10 to 100 droplets were compared in figure 43. An *E. coli* culture with $OD_{600} \approx 1$ (5 x 10^8 bacteria/mL) was used, which means that about 10 bacterial cells per 10-pL droplet come out of the inkjet.

As demonstrated in figure 43, the number of signals and intensities increased with increasing number of droplets. There are barely signals of m/z less than 9000 found in the sample with 10 and 20 drops. In contrast, there are more signals detected in the range of m/z from 4500 to 9000 once the drop numbers are more than 30. The sample in figure 43E with 100 drops indicated the most signals and the highest signal-to-noise ratio.

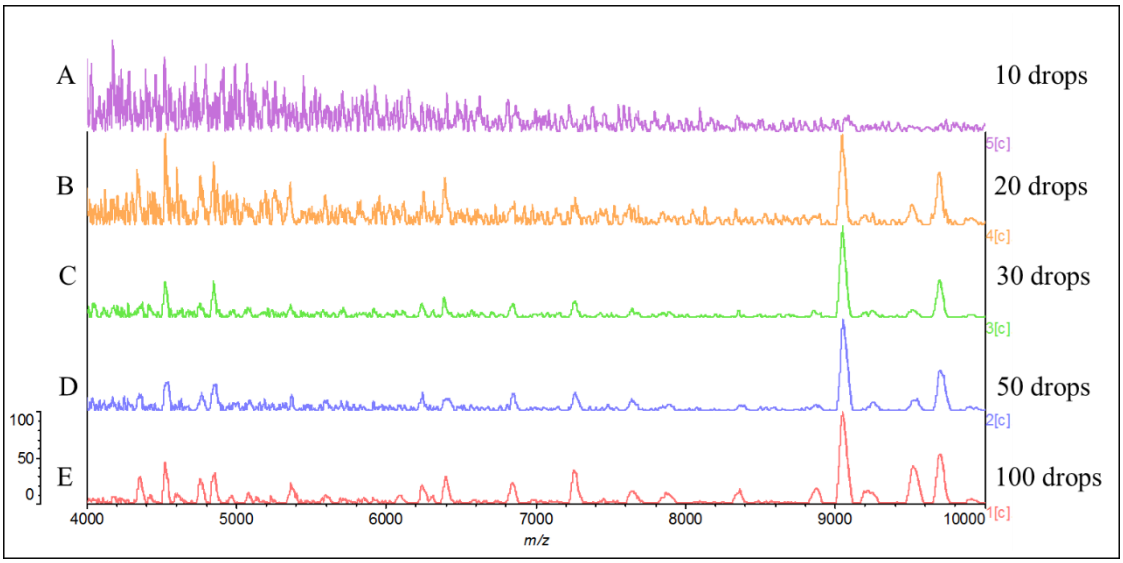

Figure 43 Comparison of MALDI spectra from different amount of bacteria droplets. (A) 10 drops (B) 20 drops (C) 30 drops (D) 50 drops (E) 100 drops (100 drops containing ≈ 1000 bacteria)

The cell density of 10 bacteria per droplet was similar to those proposed by Choi *et al.* [128]. Furthermore, it has been validated that it is hard to detect sufficient signals once

the bacteria containing in a single spot was less than 330 (in 30 drops). On the other hand, the extracted analytes from *E. coli* could be detected with significant abundance with 1000 bacteria (in 100 drops) by such inkjet introduction.

Moreover, the difference between inkjet printing and manually pipetting in a conventional way was also investigated, as shown in figure 44. In figure 44A, 100 droplets of SA matrix were printed on a dried spot formed by 100 droplets of *E. coli* resuspension. 1.5-μL matrix solution was pipetted onto 1.5-μL dried bacteria culture, which formed the spot shown in figure 44B. Due to the different volumes, the inkjet-printed spot was much smaller than the pipetted one. It also has a more uniform shape. The average evaporation time of the inkjet-printed droplets was less than 5 seconds, which is about 120 times faster than a manually pipetted one for 10 min to be completely dry. It means that sample preparation via inkjet printer provides uniform spots and an alternative for reducing sampling time and thereby improves sampling efficiency.

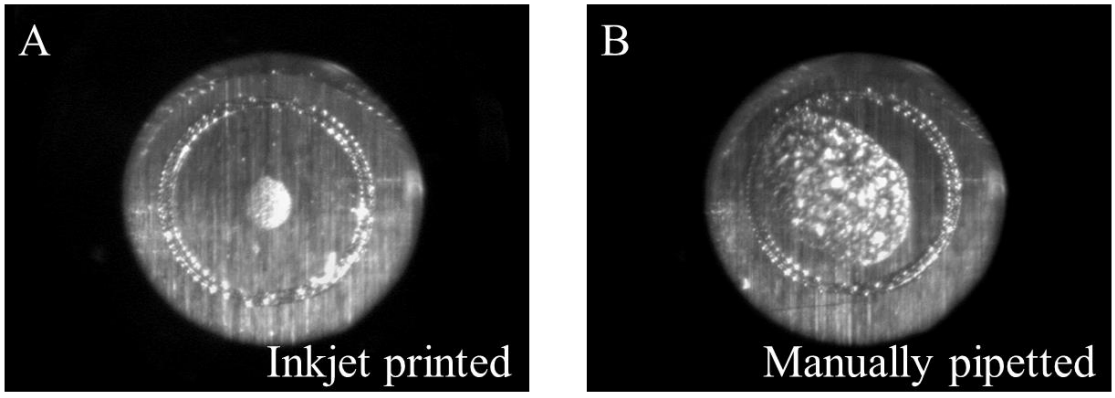

Figure 44 Comparison of inkjet printed spot and manually pipetted one on MALDI plate (A) spot by inkjet printing from 100 drops of bacteria sample and 100 drops of matrix solution (volume of each drop ≈ 10 pL) (B) spot by manually pipetting from 1.5-μL matrix solution on 1.5-μL dried bacteria culture

The spectra of these two spots were compared in figure 45. In figure 45A, the most intensive signals were found in the m/z range from 6000 to 10000 for manually pipetting. On the other hand, the inkjet printing signals in figure 45B were well distributed from m/z 4000 to 10000.

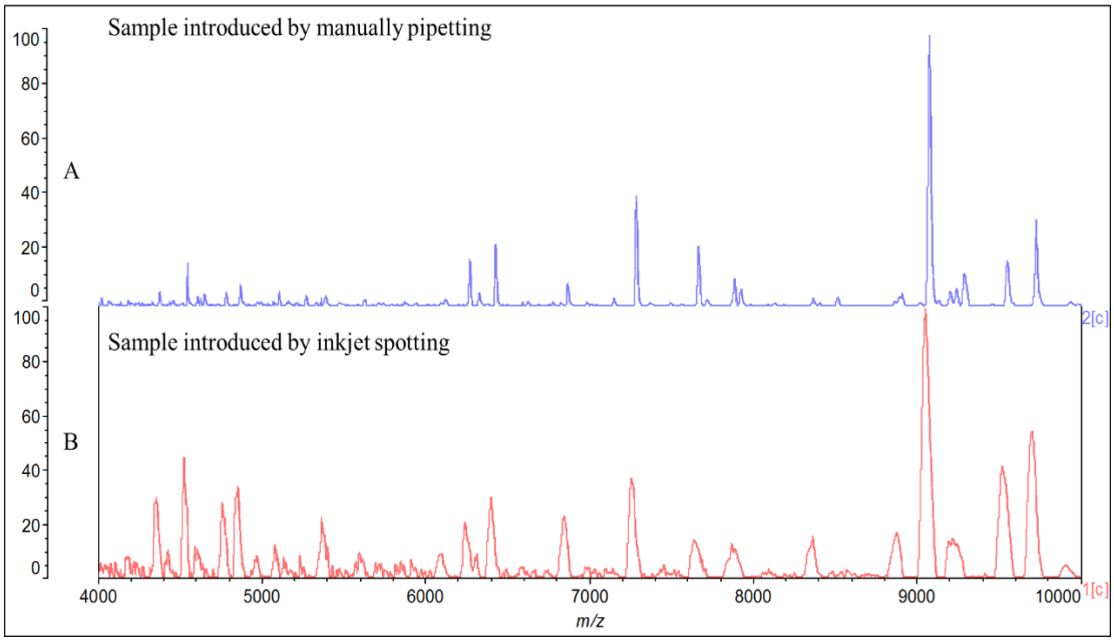

Figure 45 Comparison of different introduction methods (A) manually pipetting (B) inkjet spotting

Therefore, these results demonstrated that the average relative abundance of signals resulted from inkjet printing were comparable to those from pipetting. In contrast to the manually pipetting, relatively small sample volume (≈ 1 nL) was applied in the inkjet printing instead of 1.5 µL, which means sample introduction by inkjet provided sufficient signals even with limited number of bacteria.

4.4.3 Reduction of "coffee-ring" effect via inkjet introduction

The evaporation of droplets containing non-volatile solutes in a volatile solution might lead to the formation of a ring-like pattern of the spot, called "coffee-ring" effect, which typically occurs during the crystallization of sample and matrix in MALDI analysis.

There are several approaches proposed to suppress the "coffee-ring" effect for better homogeneity. One of the possibilities is modifying the surface for different hydrophobicities [170]. A further alternative is the electrowetting, which generates internal flow fields and counter resists the driven flow mentioned above, and then

prevents the diffusion and accumulation of solutes along the droplet rim [171]. However, these two methods are invalid once the surface property of the sample location is fixed.

Another possibility is to focus on the interaction between particles within the droplet. A strategy, depending on the shape of the particles, was demonstrated by Yunker *et al*. [172]. In this case, the interparticle capillary attraction of the ellipsoids forms a packed or arrested structure at the air-water interface, which then stops the movement of suspended particles to the edge. Another idea proposed by Anyfantakis *et al*. was combining anionic nanoparticles and photosensitive cationic surfactants, which enables to control the particle deposition by light-dependent modulation [173].

However, these approaches counteracting the “coffee-ring” effect by modifying the surface, applying an electric field or surfactant additive almost have apparent limitations to become a versatile method for the MALDI analysis.

Furthermore, as mentioned in section 2.4.5, the CS technique is another alternative to avoid the “coffee-ring” effect by solvent-free depositing. Instead of being dissolved in methanol/water and mixed with samples, the DHB, aminopyrazine, and sodium chloride were mixed and homogenized to form a “premix”. The sample was pipetted onto this premix, followed by air-dried and homogenized. Before transferred into the drilling well, the analytes were mixed well with the premix matrix and uniformly distributed due to the homogenization. The detections of peptides with raffinose as the internal standard demonstrated the benefit of post-homogenization and solid-state sample loading [116]. However, it is necessary to keep bacteria intact cell membrane before measuring, which avoids sample loss during the sample preparation. Therefore, such a CS technique might be limited for MALDI detection of microbial samples.

4.4.3.1 Evaporation of E. coli droplets on ITO glass

To evaluate the influence of inkjet on the spotting procedure of MALDI-MS, the ITO glass was applied. It has similar conductivity and surface property as the MALDI plate and transparent to observe droplets evaporation. Different amounts of droplets were printed in the array, as shown in figure 46.

Once being printed, the dried droplets were observed under the microscope with the CCD camera. An overnight culture of *E. coli* was prepared and loaded on an inkjet

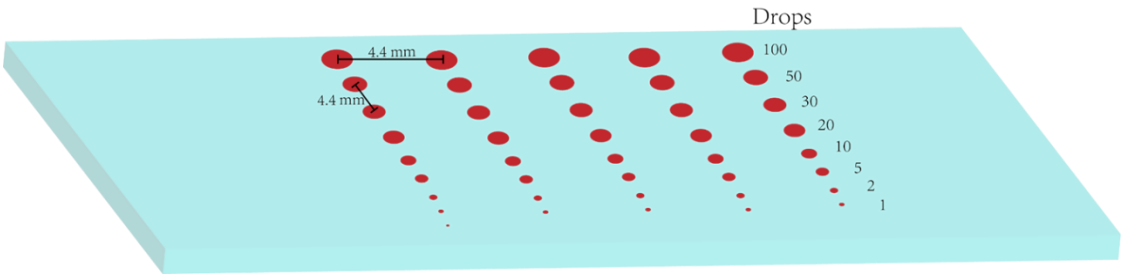

Figure 46 Inkjet printing array on ITO glass

device after resuspension in water. Under the inkjet working condition of 30 V and 15 µs, the droplets of an aqueous solution containing *E. coli* were printed on the ITO glass with the number range from 1 to 100 droplets. The images of dried spots were illustrated in figure 47 in µm-scale. In figure 47A, *E. coli* cells are mainly distributed at the edge of the dried spot, which looks like fine black particles on the image. It is a clear indication of the "coffee-ring" effect because of evaporation. From 47B to 47F, the ring-like distribution of bacteria cells still occurred even for the spot formed by five droplets solution.

In contrast, this phenomenon was not that obvious when the droplet number reduced to 2 and 1. On the other hand, the diameters of dried spots ranged from approximately 700 µm (Fig. 47A, 100 droplets) to 100 µm (Fig. 47H, 1 droplet). The typical beam size of

the MALDI-MS detector is about 100 µm. Therefore, the spots printed with fewer droplets, such as one or two, have a better chance of being ionized completed without concern about the sample heterogeneity after drying.

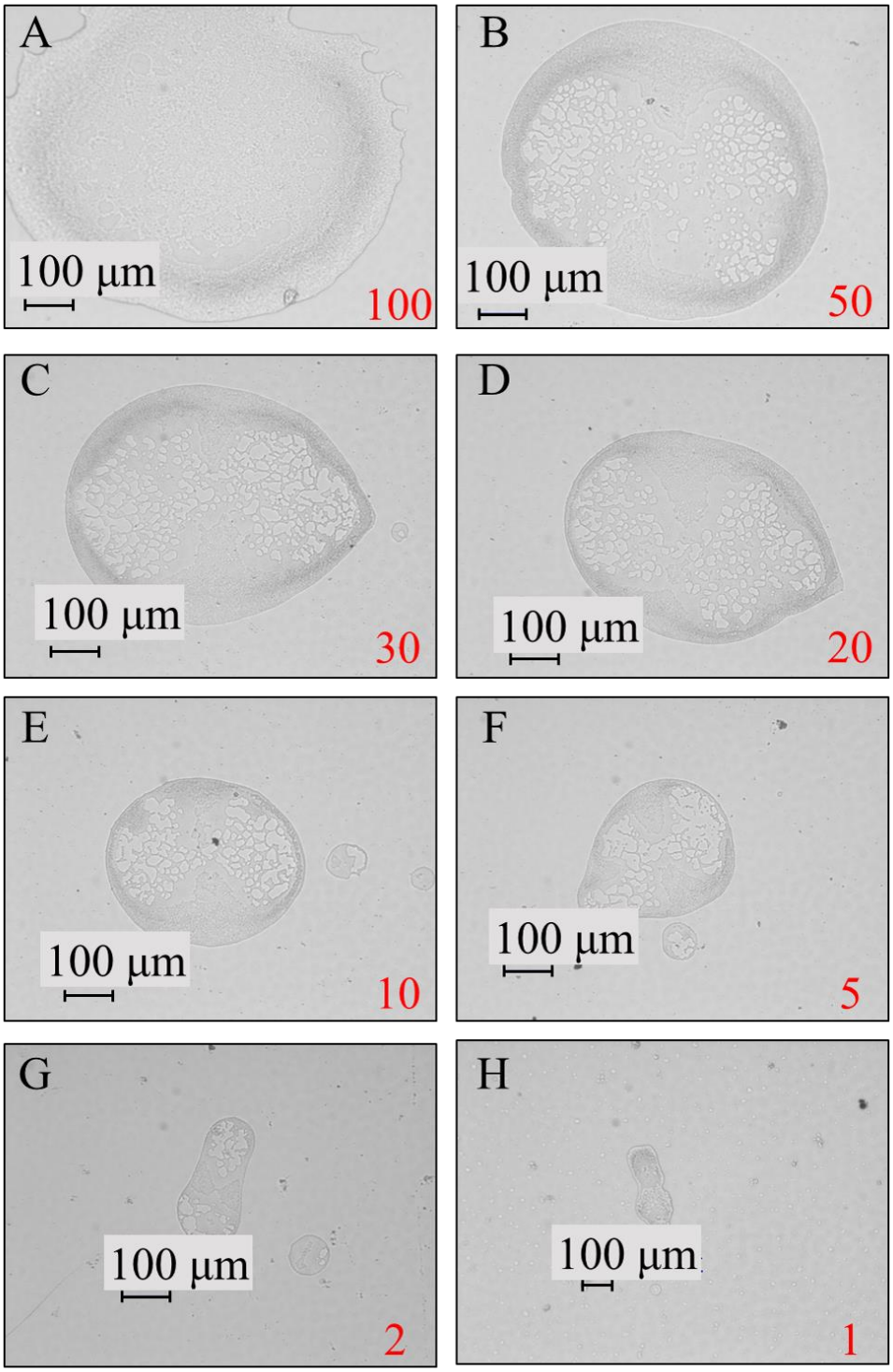

Figure 47 Image of dried bacteria droplets under CCD camera consisting of (A) 100 drops (B) 50 drops (C) 30 drops (D) 20 drops (E) 10 drops (F) 5 drops (G) 2 drops (H) 1 drop of bacteria resuspension (each drop contains ≈ 10 bacteria)

4.4.3.2 Evaporation of MALDI matrix on ITO glass

The crystallization of DHB, CHCA, and SA matrix were investigated in different sizes of droplets. The composition of the matrix solution was ACN:H_2O (70:30, v/v). The "coffee-ring" effect was evaluated through the images from a CCD camera.

DHB matrix

The concentration of the DHB matrix was 20 mg/mL. After loading into the inkjet device, the droplets were printed with matrix solution from 100 drops to 1 drop. As shown in figure 48, for the DHB matrix, all images revealed ring-like crystallization that the solid particles focused on the spots' edges. The middle of each spot was relatively empty because of the outward capillary flow. Due to the high solubility of DHB in water, the crystallized particles of DHB were relatively large and rod-shaped, especially in figure 48A [174]. On the other hand, the crystallization of DHB was relatively slow, that the "coffee-ring" effect was the most significant in this kind of matrix, as demonstrated in figure 48.

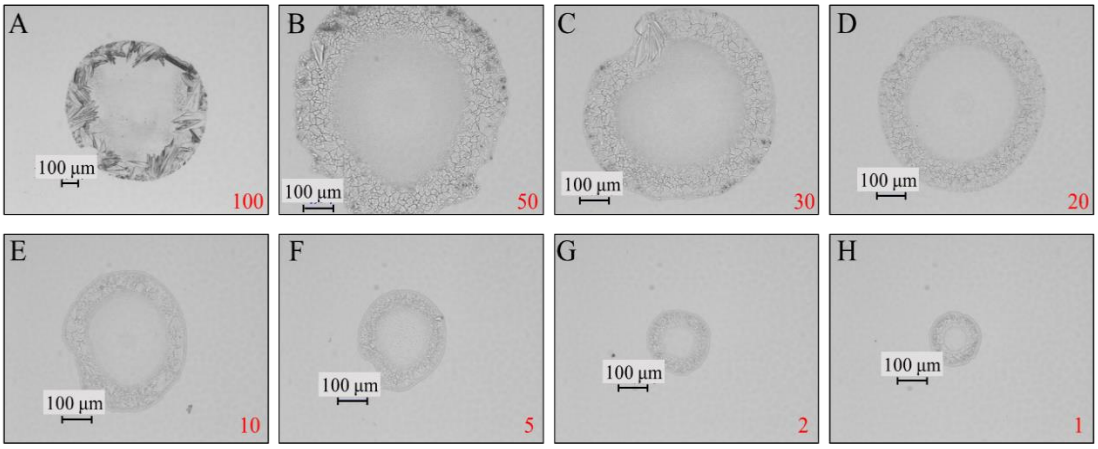

Figure 48 Image of dried DHB matrix droplets under CCD camera consisting of (A) 100 drops (B) 50 drops (C) 30 drops (D) 20 drops (E) 10 drops (F) 5 drops (G) 2 drops (H) 1 drop of matrix solution

CHCA matrix

The saturated CHCA matrix solution was utilized for the assay printing. Similar to the work reported by Sleno *et al*., the crystallization of CHCA forms small fine particles [175]. In figure 49A, the spot was about 800 µm with fine particles of CHCA after evaporation. The spot size decreased with the decreasing number of droplets. The gap between each particle becomes relatively small started from figure 49E (a spot formed by ten droplets). The spot in figure 49H seems to be even solid without gaps due to its 100-µm diameter. Therefore, the inkjet introduction might help CHCA overcome its discrete distribution and increase homogeneity against evaporation.

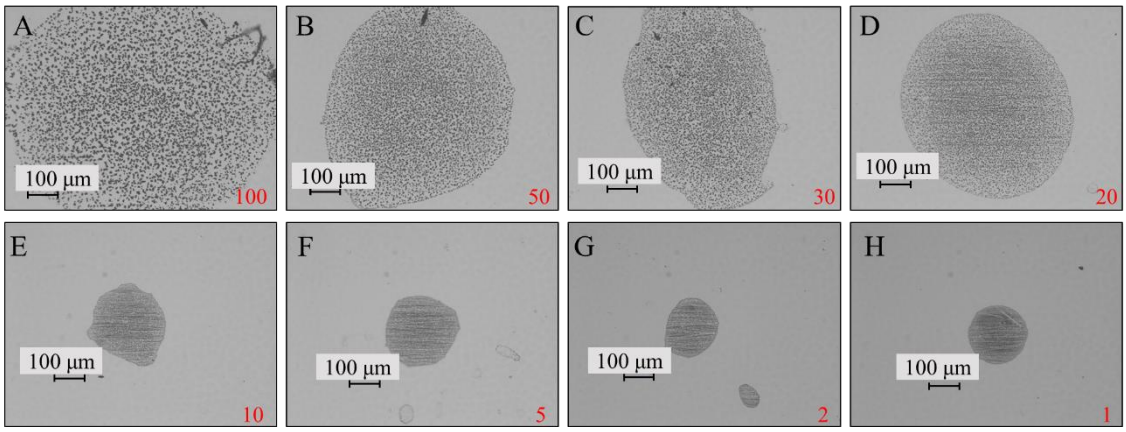

Figure 49 Image of dried CHCA matrix droplets under CCD camera consisting of (A) 100 drops (B) 50 drops (C) 30 drops (D) 20 drops (E) 10 drops (F) 5 drops (G) 2 drops (H) 1 drop of matrix solution

SA matrix

As Sleno *et al*. [185] reported, the crystallization of the SA matrix leads to needle-shaped and relatively large particles, as shown in figure 50. Similar to the DHB matrix, it was influenced by the outward capillary flow, which was especially indicated from figure 50C to 50H. Interestingly, the particles at the edge of the dried spot were smaller than those close to the middle region. This might be due to the faster crystallization of SA compared to DHB. In fact, instead of crystallizing at the spot edge, SA started to crystalize before transportation of the capillary flow; thus, the growth of crystallization

was faster and more in the middle area.

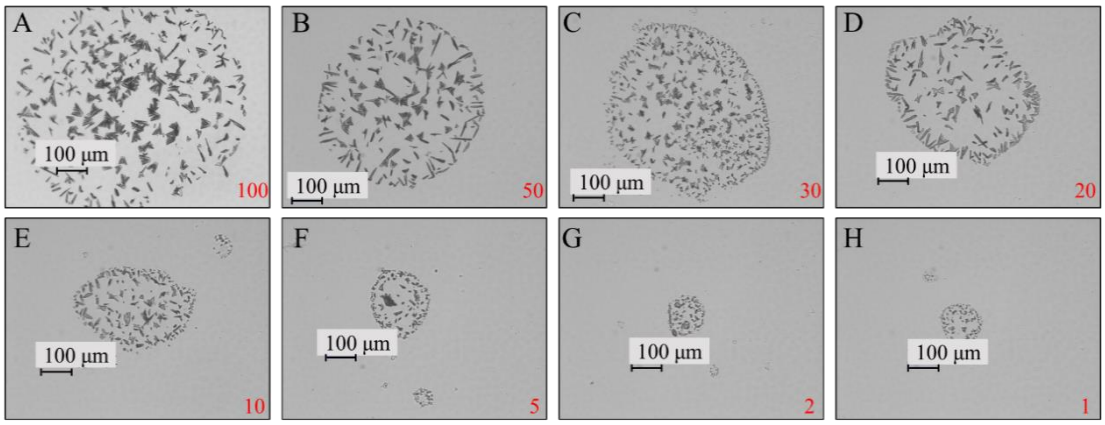

Figure 50 Image of dried SA matrix droplets under CCD camera consisting of (A) 100 drops (B) 50 drops (C) 30 drops (D) 20 drops (E) 10 drops (F) 5 drops (G) 2 drops (H) 1 drop of matrix solution

Multi-introduction strategies

In addition to the fast-evaporation characteristic of the SA matrix, inkjet printing provides another approach to reduce the "coffee-ring" effect. The fast the evaporation is, the less time remains for the outward capillary flow to transport the matrix. It means the crystallization of the SA matrix will take place in a limited area if the matrix volume is relatively small and evaporates very fast. In this case, the droplets of the SA matrix were printed by inkjet repeatedly at the same position in a small number.

In figure 51, different strategies with various waiting time intervals were applied for the SA matrix introduction by inkjet printing. The waiting time is the time needed for the matrix evaporation between each round of printing, which was necessary to assure that the printed droplets could be dried before the next round. The waiting time between each round of printing was proportional to the number of droplets printed per round. For example, the waiting time in figure 51A is one second because, in each round, only one droplet came out of the inkjet. Similarly, the waiting time for the inkjet printing between each round is 10 seconds (10 droplets printed per round) in figure 51D.

As demonstrated in figure 51, such multi-printing strategies changed the evaporation patterns of the SA matrix. The distribution of crystallized particles was more intensive and uniform for those spots printed with more rounds. For example, the spot in figure 51B printed (5 rounds with 2 droplets in each round) has a smaller diameter than that in figure 51C (2 rounds with 5 droplets in each round). This phenomenon could also be found within comparison between figure 51D and 51E. It implies that the multi-introduction strategy leads to more concentrated evaporation due to less volume and evaporation time in a single round.

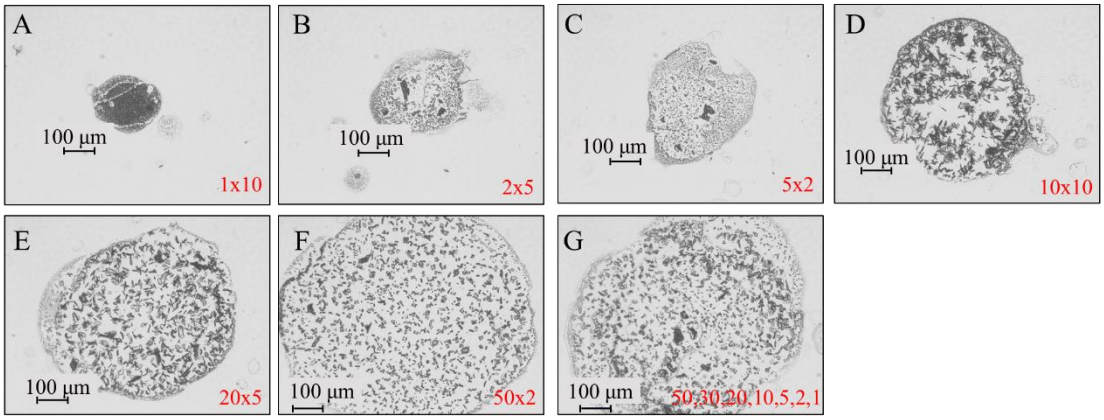

Figure 51 Image of dried SA matrix droplets in multi-introduction strategies (A) 10 rounds with 1 droplet (B) 5 rounds of 2 droplets (C) 2 rounds of 5 droplets (D) 10 rounds of 10 droplets (E) 5 rounds of 20 droplets (F) 2 rounds of 50 droplets (G) 6 rounds with decreasing number of droplets from 50 to 1 per round

As mentioned before, the evaporation of SA solution was relatively fast for a single droplet with a volume of about 10 picoliters formed by the inkjet nozzle. By programming the inkjet printing, it was possible to create droplets with reproducible volume and with a fixed frequency. The droplet in figure 52A was generated by 10-round printing with the help of these programming features. It has the same total number as the droplet in figure 52C but shows a clear difference in the crystallization pattern with a much more uniform distribution.

On the other hand, the crystallization was more homogeneous in figure 52B than in 52D though both of them were formed by 100 drops of the matrix solution. Therefore, there

is clear evidence that the multi-introduction strategy with inkjet printing could help to reduce the influence of the “coffee-ring” effect on the evaporation of MALDI spotting.

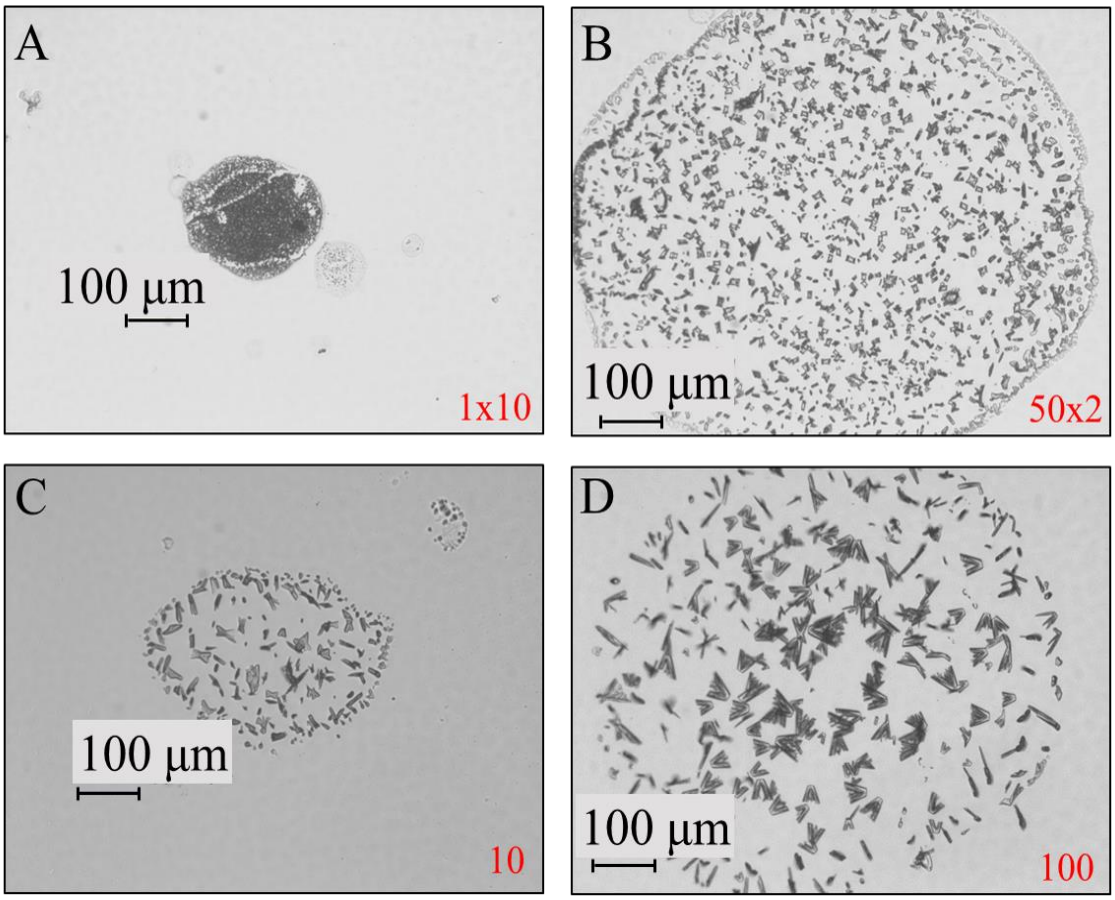

Figure 52 Comparison between droplets by multi-printing (A) 10 rounds of 1 droplet (B) 2 rounds of 50 droplets and normal printing of (C) 10 droplets (D) 100 droplets with SA matrix

As shown in figure 52B and 52D, it demonstrated that the evaporation of matrix spots was improved even with two-round printing instead of single printing. Therefore, there is clear evidence that the multi-introduction strategy with inkjet printing could reduce the influence of the “coffee-ring” effect on the evaporation of MALDI spotting.

5 Conclusion and Outlook

The purpose of this thesis was to develop a method for microbial sample preparation, which could be applied for the MS-based metabolic analysis. A sample preparation protocol for the analysis of the intracellular metabolites of a gram-negative bacteria, *C. marina* as the study object, was carefully optimized in particular from the quenching step to the derivatization with the mixture of BSTFA and TMCS. As a result, it was possible to detect more than 170 intensive signals corresponding to specific metabolites representing a "snapshot" of intracellular metabolic state, which were identified according to the NIST library. These analytes included three main groups of amino acids, alkane, and fatty acids. Repeatability analysis revealed that most of the signals have RSDs less than 20%, which implies superiority compared to previous work. Furthermore, this protocol was applied for the evaluation of intracellular state variation under different stresses. Oxidative stress inducing by treatment with ozone leads to a decrease of metabolites belonging to different groups such as L-proline, adenine and an increase of oleic acid. Moreover, it has been revealed that intermediate metabolic products such as cis-9-hexdecenal and 9-octadecenal could not be reduced due to the blockage of the enzyme by the stress as determined via visualization by GasPedal. Furthermore, the metabolic change of *C. marina* under artificially nutritional starvation was evaluated. There were significant changes in the signals of some metabolites, mainly amino acids, which are involved in metabolic pathways such as the glutathione redox cycles, the glucose pathway, and the shikimate pathway. Thus, it has been demonstrated that the proposed protocol and evaluation procedure could be utilized as a "toolkit" for the fingerprint MS-based analysis of such gram-negative bacteria. With the GasPedal software, it was much easier to find significant differences between images instead of naked eyes.

In the second part of this thesis, the use of the inkjet technique for introducing samples in MALDI-MS was evaluated and compared to traditional pipetting. To accomplish this,

the formation of the droplets by an inkjet device was optimized in current pulse and driving voltage to get the optimum condition. After optimization, a voltage of 30 V and a pulse of 15 μs were chosen for the loading procedure with the multi-layer introduction method. It has been demonstrated that the induction sequence of 1.5-μL sample followed by 1.5-μL matrix was superior as compared to the "sandwich" method, which indeed locates the sample in between the matrix. Due to the fast evaporation of relatively small volume, the multi-layer method enables the spots on the MALDI plate to be prepared about 120 times faster than manual preparation with satisfying homogeneity. It has shown that a minimum of approximately 1000 bacteria is necessary for analyzing some analytes with MALDI-MS. Spotting by using an inkjet device has its obvious advantages, including precise location, adjustable volume, and uniform operation. Moreover, the multi-printing method for SA matrix by using the inkjet device could be applied to reduce the typical "coffee-ring" effect observed after the crystallization of different matrices by the CCD camera. It could be a potential way to reduce the influence of outward capillary flow.

In summary, the protocol for *C. marina* provides a routine procedure to search for the significance and the possibility for potential biomarkers in biological pathways. In case of limited microbial samples, the inkjet technique could be an alternative for the sample preparation before MS detection. In the future, the inkjet device could be coupled with a detector such as ESI-Q-TOF for real-time and direct measurement instead of crystallization for MALDI analysis.

6 Appendix

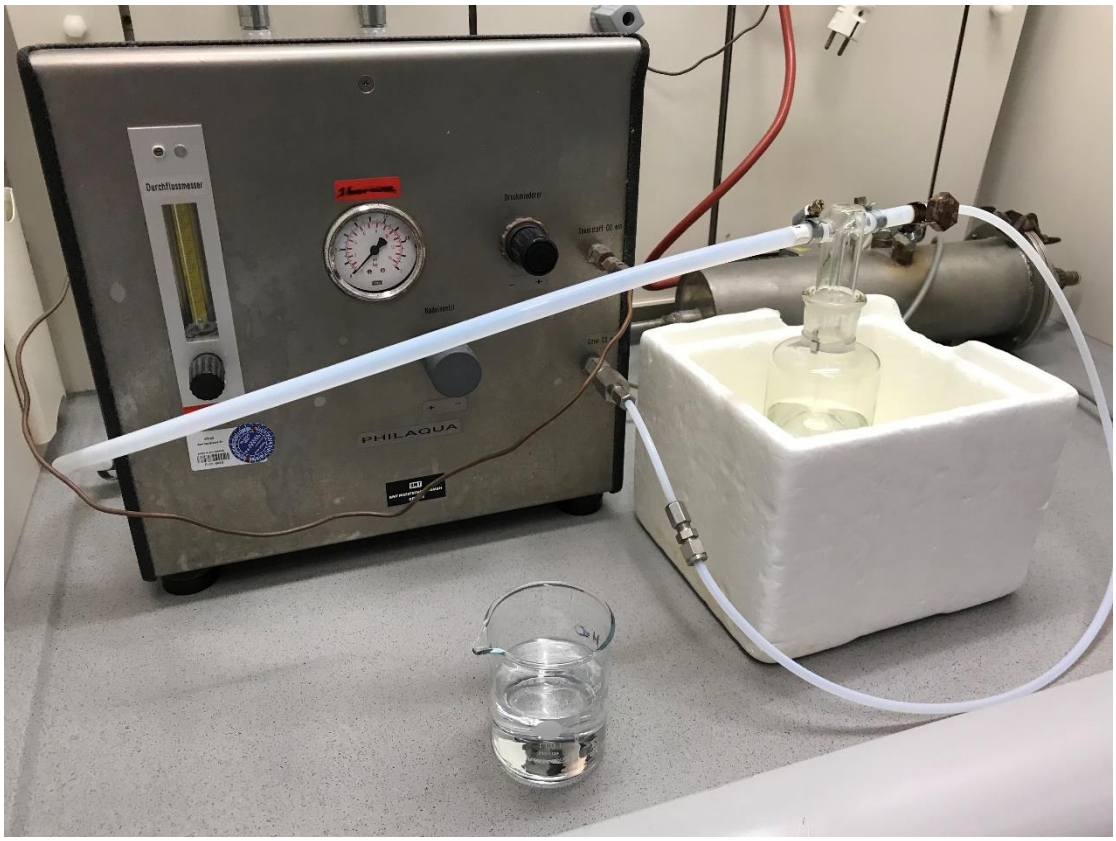

Fig S 1 Appearance of Ozone generator

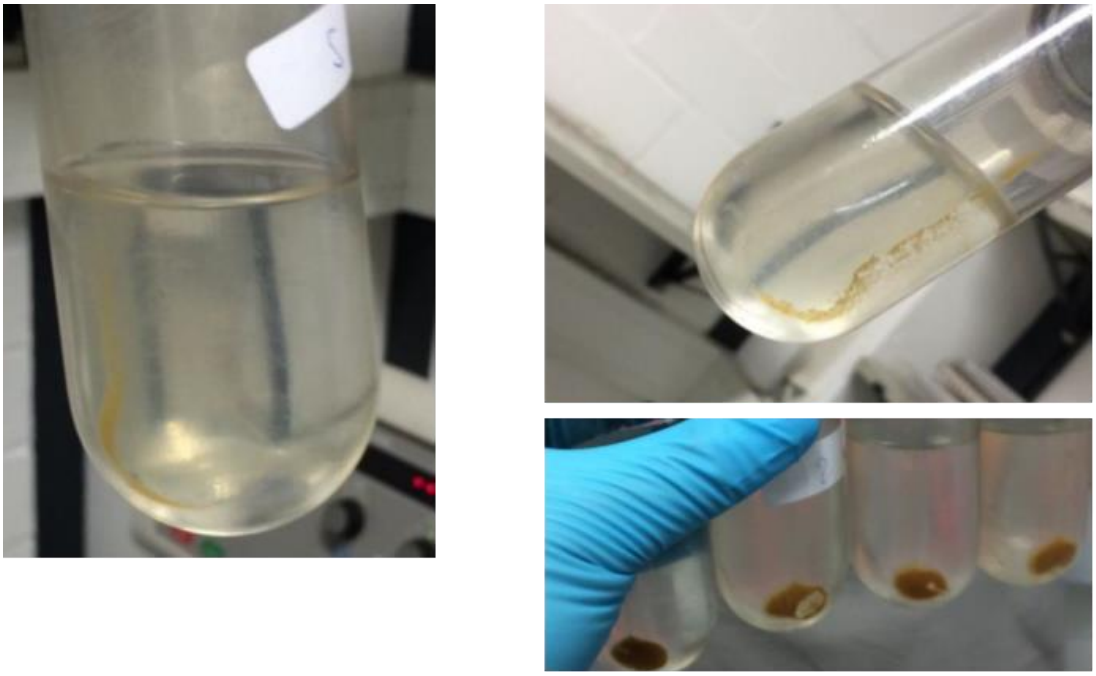

Fig S 2 Comparison of centrifugation in different speed

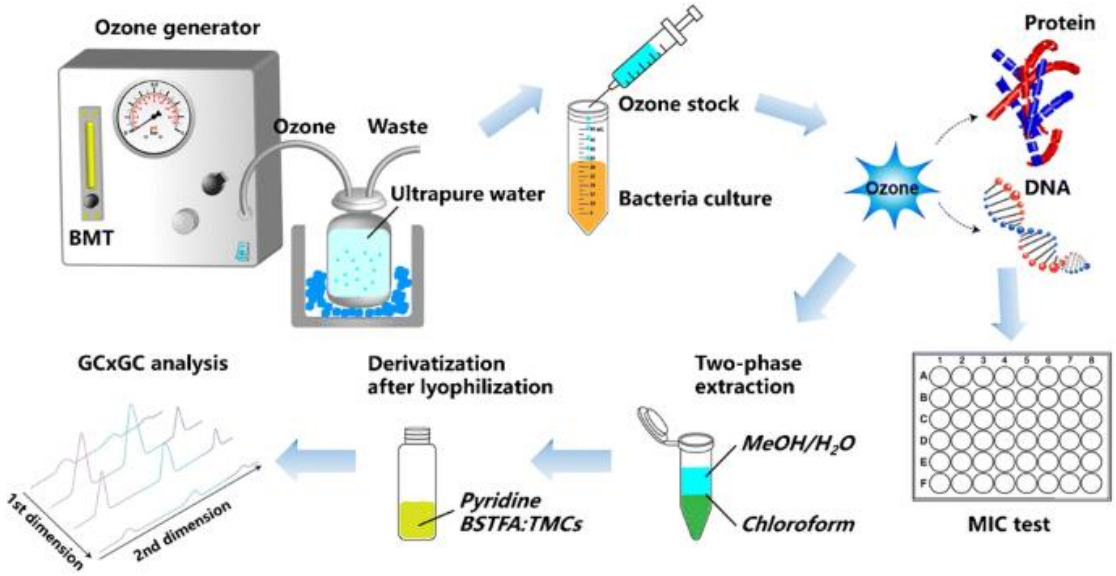

Fig S 3 Workflow of bacteria sample analysis with ozone stress treatment

6.1 Sample preparation protocol for the ozone depletion

The indigotrisulfonate stock solution was prepared by dissolving indigotrisulfonate in deionized water for 50 mL indigotrisulfonic acid solution at 10 mM. The indigo stock solution was then diluted at a ratio of 1:20 to get a working solution at 0.5 mM with a total volume of 250 mL. Phosphoric acid was added into the working solution at 65 mM, reducing the pH value of the final indigo solution below 4.

As shown in figure 34, prepared was in a screw-neck bottle with a magnetic stirrer mounted by a dispenser. The procedure is as below:

1. Purge dispenser two times

2. Dispense two samples into reagent vessels containing indigotrisulfonic acid as reference samples (Blank)

3. Turn on the magnetic stir by adjusting rotating speed to slightly mixing but without air bubbles sucked into the solution.

4. Make the counting timer ready

5. Dose ozone by merging the stainless steel cannula into the water sample and inject the ozone stock solution into the sample after 30 seconds for turning on the timer

6. After 10 s, immediately dispense two times

7. Dispense ozone dosed solution to get depletion samples at the following time point after starting the timer: 50 s (20 s after addition of the ozone into the screw-neck bottle), 60 s, 1 min 10 s, 1 min 20 s, 1 min 30 s, 2min 0 s, 2 min 30 s, 3 min 0 s, 3 min 30 s, 5 min 0 s, 7 min 0 s, 10 min 0 s, 15 min 0 s, 20 min 0 s.

8. Check the pH value of the reference sample to make sure it is below 4

9. Measure the reference samples and depletion samples at UV 600 nm

6.2 List of abbreviation

ΔA	Ratio of the UV absorption of reference and sample
µs	Microsecond
$O_2^{\cdot -}$	Superoxide radical
^{13}C	Isotope of carbon with isotope mass of 13
CS	Compressed sample
ACN	Acetonitrile
ASW	Artificial seawater
BF_3	Boron trifluoride
C. marina	*Cobetia Marina*
C18 column	Columns bonding octadecyl alkyl-groups
CCD	Charged-coupled device
CHCA	α-cyano-4-hydroxycinnamic acid
CoA	Coenzyme A
DBP	Direct bacterial profiling
DCM	Dichloromethane
DHB	2,5-dihydroxy benzoic acid
DNA	Deoxyribonucleic acid
E. coli	*Escherichia coli*
EtOH	Ethanol
FAMEs	Fatty acid methyl esters
g	G force
GC-MS	Gas chromatography - mass spectrometry
GCxGC	Two-dimensional gas chromatography
h	Hour
H_2O_2	Hydrogen peroxide
HILIC	Hydrophilic liquid interaction chromatography
$HO_2^{\cdot}$	Hydroperoxy radical
HPLC	High-performance liquid chromatography
Hz	Hertz
IP-LC-ESI-MS	Ion pair liquid chromatography coupled to electrospray ionization mass spectrometry
IS	Internal standard
ITO	Indium tin oxide
LB	Lysogeny broth
LCFA	Long-chain fatty acid
LC-MS	Liquid chromatography - mass spectrometry
m	Meter
m/z	Mass-to-charge ratio
MA	Marine agar
MALDI-TOF	Matrix-assisted laser desorption/ionization time-of-flight

MB	Marine broth
MeOH	Methanol
mg	Milligram
MIC	Minimal inhibitory concentration
min	Minute
mL	Milliliter
mm	Millimeter
MSTFA	N-methyl-N-(trimethylsilyl) trifluoroacetamide
nm	Nanometer
O^{2-}	Superoxide anion
OD_{600}	Optical density at 600 nm wavelength
$OH^{\cdot}$	Hydroxyl radical
PBS	Phosphate-buffered saline
pH	Potential of hydrogen
pL	Picoliter
PZC	Piezo ceramic
ROS	Reactive oxygen species
ROS	Reactive oxygen species
RP	Reversed phase
rpm	Revolutions per minute
rRNA	Ribosomal ribonucleic acid
RSD	Relative standard deviations
RT	Retention time
SA	3,5-dimethoxy-4-hydroxycinnamic acid
spp.	Several species
TetR	Tetracycline repressor protein
TFA	Trifluoroacetic acid
Tg	Thymine glycol
TIC	Total ion current
TMCS	Trimethyl-chlorosilane
TMS	Trimethylsilyl
V	Volt
ε	Absorption coefficient
µg	Microgram
µL	Microliter
µm	Micrometer
µM	Micromole per liter

6.3 List of figures

6.4 List of tables

7 Literature

1. Collar, C., et al., *Amino acid metabolism by yeast and lactic acid bacteria during bread dough fermentation*. J Food Sci, 1992. **57**: 1423-1427.
2. Montel, E., et al., *An integrated approach to Phoma systematics*. Mycopathologia, 1991. **115**(2): 89-103.
3. Collar, C., *Review: Biochemical and technological assessment of the metabolism of pure and mixed cultures of yeast and lactic acid bacteria in breadmaking applications*. Food Sci Technol Int, 1996. **2**: 349-367.
4. Smedsgaard, J. and Frisvad, J., *Using direct electrospray mass spectrometry in taxonomy and secondary metabolite profiling of crude fungal extracts*. J Microbiol Methods, 1996. **25**: 5-17.
5. Lund, F. and Frisvad, J., *Chemotaxonomy of Penicillium aurantiogriseum and related species*. Mycological Res, 1994. **98**: 481-492.
6. Andersen, B., et al., *Metabolite profiles of common Stemphylium species*. Mychological Res, 1995. **99**: 672-676.
7. Oliver, S.G., et al., *Systematic functional analysis of the yeast genome*. Trends Biotechnol, 1998. **16**(9): 373-378.
8. Tweeddale, H., et al., *Effect of slow growth on metabolism of Escherichia coli, as revealed by global metabolite pool ("metabolome") analysis*. J Bacteriol, 1998. **180**(19): 5109-5116.
9. Tweeddale, H., et al., *Assessing the effect of reactive oxygen species on Escherichia coli using a metabolome approach*. Redox Rep, 1999. **4**(5): 237-241.
10. Tang, J., *Microbial metabolomics*. Curr Genomics, 2011. **12**(6): 391-403.
11. Castrillo, J., et al., *An optimized protocol for metabolome analysis in yeast using direct infusion electrospray mass spectrometry*. Phytochemistry, 2003. **62**: 929-939.
12. Allen, J., et al., *High-throughput classification of yeast mutants for functional genomics using metabolic footprinting*. Nat Biotech, 2003. **21**: 692-696.
13. Liebeke, M. and Lalk, M., *Staphylococcus aureus metabolic response to changing environmental conditions - a metabolomics perspective*. Int J Med Microbiol, 2014. **304**(3-4): 222-229.
14. Hiller, J., et al., *Fast sampling and quenching procedures for microbial metabolic profiling*. Biotechnol Lett, 2007. **29**(8): 1161-1167.
15. Tian, J., et al., *Optimization of a GC-MS metabolic fingerprint method and its application in characterizing engineered bacterial metabolic shift*. J Sep Sci, 2009. **32**(13): 2281-2288.
16. Faijes, M., et al., *Comparison of quenching and extraction methodologies for metabolome analysis of Lactobacillus plantarum*. Microb Cell Fact, 2007. **6**: 27.
17. Winder, C.L., et al., *Global metabolic profiling of Escherichia coli cultures: an evaluation of methods for quenching and extraction of intracellular metabolites*. Anal Chem, 2008. **80**(8): 2939-2948.
18. Tredwell, G.D., et al., *The development of metabolomic sampling procedures for Pichia pastoris, and baseline metabolome data*. PLoS One, 2011. **6**(1): e16286.
19. Wang, X., et al., *A metabolomics-based method for studying the effect of yfcC gene in Escherichia coli on metabolism*. Anal Biochem, 2014. **451**: 48-55.
20. Orr, H.A., *The genetic theory of adaptation: a brief history*. Nat Rev Genet, 2005. **6**(2): 119-127.

21. Ray, B., *Impact of Bacterial Injury and Repair in Food Microbiology: its Past, Present and Future*. J Food Prot, 1986. **49**(8): 651-655.
22. Guan, N., et al., *Microbial response to environmental stresses: from fundamental mechanisms to practical applications*. Appl Microbiol Biotechnol, 2017. **101**(10): 3991-4008.
23. Jones, P.G., et al., *Induction of proteins in response to low temperature in Escherichia coli*. J Bacteriol, 1987. **169**(5): 2092-2095.
24. Mihoub, F., et al., *Cold adaptation of Escherichia coli: microbiological and proteomic approaches*. Int J Food Microbiol, 2003. **89**(2-3): 171-184.
25. Winkler, J.D., et al., *Evolved osmotolerant Escherichia coli mutants frequently exhibit defective N-acetylglucosamine catabolism and point mutations in cell shape-regulating protein MreB*. Appl Environ Microbiol, 2014. **80**(12): 3729-3740.
26. Castanie-Cornet, M.P., et al., *Acid stress response in Escherichia coli: mechanism of regulation of gadA transcription by RcsB and GadE*. Nucleic Acids Res, 2010. **38**(11): 3546-3554.
27. Ramos, J.L., et al., *Mechanisms of solvent resistance mediated by interplay of cellular factors in Pseudomonas putida*. FEMS Microbiol Rev, 2015. **39**(4): 555-566.
28. Carmel-Harel, O. and Storz, G., *Roles of the glutathione- and thioredoxin-dependent reduction systems in the Escherichia coli and saccharomyces cerevisiae responses to oxidative stress*. Annu Rev Microbiol, 2000. **54**: 439-461.
29. Ezraty, B., et al., *Oxidative stress, protein damage and repair in bacteria*. Nat Rev Microbiol, 2017. **15**(7): 385-396.
30. Schieber, M. and Chandel, N.S., *ROS function in redox signaling and oxidative stress*. Curr Biol, 2014. **24**(10): R453-462.
31. Imlay, J.A., *Pathways of oxidative damage*. Annu Rev Microbiol, 2003. **57**: 395-418.
32. Xu, P., et al., *Wastewater disinfection by ozone: main parameters for process design*. Water Res, 2002. **36**(4): 1043-1055.
33. Facile, N., et al., *Evaluating bacterial aerobic spores as a surrogate for Giardia and Cryptosporidium inactivation by ozone*. Water Res, 2000. **34**(12): 3238-3246.
34. Tomiysu, H., et al., *Kinetics and Mechanism of Ozone Decomposition in Basic Aqueous Solution*. Inorg Chem, 1985. **24**: 2962-2966.
35. Eddy, M., et al., *Wastewater engineering: Treatment and reuse*. 2003.
36. Patil, S., et al., *Assessing the microbial oxidative stress mechanism of ozone treatment through the responses of Escherichia coli mutants*. J Appl Microbiol, 2011. **111**(1): 136-144.
37. Jung, T., et al., *Oxidized proteins: intracellular distribution and recognition by the proteasome*. Arch Biochem Biophys, 2007. **462**(2): 231-237.
38. Hohn, A., et al., *Protein oxidation in aging and the removal of oxidized proteins*. J Proteomics, 2013. **92**: 132-159.
39. Teoule, R., et al., *Thymine fragment damage retained in the DNA polynucleotide chain after gamma irradiation in aerated solutions. II*. Radiat Res, 1977. **72**(2): 190-200.
40. Hayes, R.C. and LeClerc, J.E., *Sequence dependence for bypass of thymine glycols in DNA by DNA polymerase I*. Nucleic Acids Res, 1986. **14**(2): 1045-1061.
41. Dickson, J.S. and Frank, J.F., *Bacterial starvation stress and contamination of beef*. Food Microbiol, 1993. **10**: 215-222.

42. Morita, R.Y., *Bioavailability of energy and its relationship to growth and starvation survival in nature*. Can J Microbiol, 1988. **34**: 436-441.
43. Stucki, D., et al., *Stress responses upon starvation and exposure to bacteria in the ant Formica exsecta*. 2019. **7**: 1-17.
44. Morita, R.Y., *The starvation-survival state of microorganisms in nature and its relationship to the bioavailable energy*. Experientia, 1990. **46**: 813–817.
45. Amy, P.S. and Morita, R.Y., *Starvation-survival patterns of sixteen freshly isolated open-ocean bacteria*. Appl Environ Microbiol, 1983. **45**(3): 1109-1115.
46. Cobet, A.B., et al., *The effect of nickel on a marine bacterium: fine structure of Arthrobacter marinus*. J Gen Microbiol, 1971. **66**(2): 185-196.
47. Baumann, L., et al., *Description of Deleya gen. nov. Created to Accommodate the Marine Species Alcaligenes aestus, A. pacijicus, A. cupidus, A. venustus, and Pseudomonas marina*. Int J Syst Bacteriol, 1983. **33**: 793-802.
48. Shea, C., et al., *Comparison of the adhesion properties of Deleya marina and the exopolysaccharide-defective mutant strain DMR*. Appl Environ Microbiol, 1991. **57**(11): 3107-3113.
49. Shea, C., et al., *Deleya marina as a model organism for studies of bacterial colonization and biofilm formation*. J Ind Microbiol, 1995. **15**(4): 290-296.
50. Mata, J.A., et al., *A detailed phenotypic characterisation of the type strains of Halomonas species*. Syst Appl Microbiol, 2002. **25**(3): 360-375.
51. Dobson, S.J. and Franzmann, P.D., *Unification of the genera Deleya (Baumann et al. 1983), Halomonas (Vreeland et al. 1980), and Halovibrio (Fendrich 1988) and the species Paracoccus halodenitrificans (Robinson and Gibbons 1952) into a single genus, Halomonas, and placement of the genus Zymobacter in the family Halomonadaceae*. Int J Syst Bacteriol, 1996. **46**: 550-558.
52. Mormile, M.R., et al., *Halomonas campisalis sp. nov., a denitrifying, moderately haloalkaliphilic bacterium*. Syst Appl Microbiol, 1999. **22**(4): 551-558.
53. Duckworth, A.W., et al., *Halomonas magadii sp. nov., a new member of the genus Halomonas, isolated from a soda lake of the East African Rift Valley*. Extremophiles, 2000. **4**(1): 53-60.
54. Bouchotroch, S., et al., *Halomonas maura sp. nov., a novel moderately halophilic, exopolysaccharide-producing bacterium*. Int J Syst Evol Microbiol, 2001. **51**(Pt 5): 1625-1632.
55. Yoon, J.H., et al., *Halomonas marisflavae sp. nov., a halophilic bacterium isolated from the Yellow Sea in Korea*. Int J Syst Evol Microbiol, 2001. **51**(Pt 3): 1171-1177.
56. Yoon, J.H., et al., *Halomonas alimentaria sp. nov., isolated from jeotgal, a traditional Korean fermented seafood*. Int J Syst Evol Microbiol, 2002. **52**(Pt 1): 123-130.
57. Arahal, D.R., et al., *Phylogeny of the family Halomonadaceae based on 23S and 165 rDNA sequence analyses*. Int J Syst Evol Microbiol, 2002. **52**(Pt 1): 241-249.
58. Arahal, D.R., et al., *Proposal of Cobetia marina gen. nov., comb. nov., within the family Halomonadaceae, to include the species Halomonas marina*. Syst Appl Microbiol, 2002. **25**(2): 207-211.
59. van der Greef, J., et al., *Metabolomics-based systems biology and personalized medicine: moving towards n = 1 clinical trials?* Pharmacogenomics, 2006. **7**(7): 1087-1094.
60. Vila, J., et al., *Escherichia coli: an old friend with new tidings*. FEMS Microbiol Rev, 2016. **40**(4): 437-463.
61. Meric, G., et al., *From Escherich to the Escherichia coli genome*. Lancet Infect Dis, 2016. **16**(6): 634-636.

62. Escherich, T., *The intestinal bacteria of the neonate and breast-fed infant. 1884*. Rev Infect Dis, 1988. **10**(6): 1220-1225.
63. Shulman, S.T., et al., *Theodor Escherich: the first pediatric infectious diseases physician?* Clin Infect Dis, 2007. **45**(8): 1025-1029.
64. *Etymologia: Escherichia coli*. Emerg Infect Dis, 2015. **21**: 1310.
65. Blattner, F.R., et al., *The complete genome sequence of Escherichia coli K-12*. Science, 1997. **277**(5331): 1453-1462.
66. Adamczyk, P.A. and Reed, J.L., *Escherichia coli as a model organism for systems metabolic engineering*. Curr Opin Sys Biol, 2017. **6**: 80-88.
67. Wang, Z., et al., *Ion suppression effect in desorption electrospray ionization and electrospray ionization mass spectrometry*. Rapid Commun Mass Spectrom, 2017. **31**(23): 1957-1962.
68. Jeong, S., et al., *Real-time quantitative analysis of metabolic flux in live cells using a hyperpolarized micromagnetic resonance spectrometer*. Sci Adv, 2017. **3**(6): e1700341.
69. Lindon, J.C., et al., *So what's the deal with metabonomics?* Anal Chem, 2003. **75**(17): 384A-391A.
70. Palama, T.L., et al., *Identification of bacterial species by untargeted NMR spectroscopy of the exo-metabolome*. Analyst, 2016. **141**(15): 4558-4561.
71. Emwas, A.H., et al., *NMR Spectroscopy for Metabolomics Research*. Metabolites, 2019. **9**(7).
72. Segers, K., et al., *Analytical techniques for metabolomic studies: a review*. Bioanalysis, 2019. **11**(24): 2297-2318.
73. Coulier, L., et al., *Simultaneous quantitative analysis of metabolites using ion-pair liquid chromatography-electrospray ionization mass spectrometry*. Anal Chem, 2006. **78**(18): 6573-6582.
74. Gu, L., et al., *LC-MS/MS assay for protein amino acids and metabolically related compounds for large-scale screening of metabolic phenotypes*. Anal Chem, 2007. **79**(21): 8067-8075.
75. Fei, F., et al., *Comprehensive and simultaneous coverage of lipid and polar metabolites for endogenous cellular metabolomics using HILIC-TOF-MS*. Anal Bioanal Chem, 2014. **406**(15): 3723-3733.
76. Baidoo, E.E., et al., *Mass spectrometry-based microbial metabolomics*. Methods Mol Biol, 2012. **881**: 215-278.
77. Orata, F., *Derivatization Reactions and Reagents for Gas Chromatography Analysis. Advanced Gas Chromatography - Progress in Agricultural, Biomedical and Industrial Applications*. 2012. 91.
78. Kataoka, H., *Gas chromatography of amines as various derivatives. Quantitization of amino acids and amines by chromatography - methods and protocols*. Journal of Chromatography Library, 2005. **70**: 364-404.
79. Lin, D.L., et al., *Chemical derivatization for the analysis of drugs by GC-MS - A conceptual review*. Journal of Food and Drug Analysis, 2008. **16**(1): 1-10.
80. Chen, B.G., et al., *GC-MS analysis of multiply derivatized opioids in urine*. J Mass Spectrom, 2007. **42**(8): 1012-1023.
81. Villas-Boas, S.G., et al., *Alkylation or Silylation for Analysis of Amino and Non-Amino Organic Acids by GC-MS?* Metabolites, 2011. **1**(1): 3-20.
82. Strelkov, S., et al., *Comprehensive analysis of metabolites in Corynebacterium glutamicum by gas chromatography/mass spectrometry*. Biol Chem, 2004. **385**(9): 853-861.
83. Koek, M.M., et al., *Microbial metabolomics with gas chromatography/mass spectrometry*. Anal Chem, 2006. **78**(4): 1272-1281.

84. Liu, Z. and Philips, J., *Comprehensive two-dimensional gas chromatography using an on-column thermal modulator interface*. J Chromatogr Sci, 1991. **29**(6): 227-231.
85. Almstetter, M.F., et al., *Integrative normalization and comparative analysis for metabolic fingerprinting by comprehensive two-dimensional gas chromatography-time-of-flight mass spectrometry*. Anal Chem, 2009. **81**(14): 5731-5739.
86. Simmons, M.C. and Snyder, L.R., *Two-Stage Gas-Liquid Chromatography*. Anal Chem, 1958. **30**: 32−35.
87. Zhu, S., *Effect of column combinations on two-dimensional separation in comprehensive two-dimensional gas chromatography: estimation of orthogonality and exploring of mechanism*. J Chromatogr A, 2009. **1216**(15): 3312-3317.
88. Boswell, H.A., et al., *Comparison of Thermal and Flow-Based Modulation in Comprehensive Two-Dimensional Gas Chromatography—Time-of-Flight Mass Spectrometry (GC × GC-TOFMS) for the Analysis of Base Oils*. Separations, 2020. **7**(4): 70.
89. Gorecki, T., et al., *The evolution of comprehensive two-dimensional gas chromatography (GC x GC)*. J Sep Sci, 2004. **27**(5-6): 359-379.
90. Seeley, J.V. and Seeley, S.K., *Multidimensional gas chromatography: fundamental advances and new applications*. Anal Chem, 2013. **85**(2): 557-578.
91. Dallüge, J., et al., *Comprehensive two-dimensional gas chromatography with time-of-flight mass spectrometric detection applied to the determination of pesticides in food extracts*. J chromatogr A, 2002. **965**(1-2): 207–217.
92. Gray, M., et al., *Two dimensional reversed-phase-reversed-phase separations isomeric separations incorporating C18 and carbon clad zirconia stationary phases*. J Chromatogr A, 2002. **975**(2): 285-297.
93. Slonecker, P.J., et al., *Informational orthogonality of two-dimensional chromatographic separations*. Anal Chem, 1996. **68**(4): 682-689.
94. Johnson, K.J., et al., *Quantification of naphthalenes in jet fuel with GC x GC/Tri-PLS and windowed rank minimization retention time alignment*. J Sep Sci, 2004. **27**(5-6): 410-416.
95. Fraga, C.G., et al., *Comprehensive two-dimensional gas chromatography and chemometrics for the high-speed quantitative analysis of aromatic isomers in a jet fuel using the standard addition method and an objective retention time alignment algorithm*. Anal Chem, 2000. **72**(17): 4154-4162.
96. Fiehn, O., et al., *Metabolite profiling for plant functional genomics*. Nat Biotechnol, 2000. **18**(11): 1157-1161.
97. David, F., et al., *Chemotaxonomy of bacteria by comprehensive GC and GC-MS in electron impact and chemical ionisation mode*. J Sep Sci, 2008. **31**(19): 3395-3403.
98. Yang, S., et al., *Liquid chromatography-tandem quadrupole mass spectrometry and comprehensive two-dimensional gas chromatography-time-of-flight mass spectrometry measurement of targeted metabolites of Methylobacterium extorquens AM1 grown on two different carbon sources*. J Chromatogr A, 2009. **1216**(15): 3280-3289.
99. Okubo, Y., et al., *Alternative route for glyoxylate consumption during growth on two-carbon compounds by Methylobacterium extorquens AM1*. J Bacteriol, 2010. **192**(7): 1813-1823.
100. Gu, Q., et al., *Analysis of bacterial fatty acids by flow modulated comprehensive two-dimensional gas chromatography with parallel flame ionization detector/mass spectrometry*. J Chromatogr A, 2010. **1217**(26): 4448-4453.

101. Karas, M., et al., *Matrix-assisted ultraviolet laser desorption of non-volatile compounds*. Int J Mass Spectrom Ion Process, 1987. **78**: 53-68.
102. Karas, M. and Hillenkamp, F., *Laser desorption ionization of proteins with molecular masses exceeding 10,000 daltons*. Anal Chem, 1988. **60**(20): 2299-2301.
103. Mann, M., et al., *Analysis of proteins and proteomes by mass spectrometry*. Annu Rev Biochem, 2001. **70**: 437-473.
104. Kaufmann, R., *Matrix-assisted laser desorption ionization (MALDI) mass spectrometry: a novel analytical tool in molecular biology and biotechnology*. J Biotechnol, 1995. **41**(2-3): 155-175.
105. Hanan, A., et al., *Mass Spectrometry, Review of the Basics: Ionization*. Applied Spectroscopy Reviews, 2014. **50**(2): 158-175.
106. Carbonnelle, E., et al., *MALDI-TOF mass spectrometry tools for bacterial identification in clinical microbiology laboratory*. Clin Biochem, 2011. **44**(1): 104-109.
107. Singhal, N., et al., *MALDI-TOF mass spectrometry: an emerging technology for microbial identification and diagnosis*. Front Microbiol, 2015. **6**: 791.
108. Kostrzewa, M., et al., *MALDI-TOF MS: an upcoming tool for rapid detection of antibiotic resistance in microorganisms*. Proteomics Clin Appl, 2013. **7**(11-12): 767-778.
109. Zhang, L., et al., *Biomarker- and similarity coefficient-based approaches to bacterial mixture characterization using matrix-assisted laser desorption ionization time-of-flight mass spectrometry (MALDI-TOF MS)*. Sci Rep, 2015. **5**: 15834.
110. Horneffer, V., et al., *Localization of analyte molecules in MALDI preparations by confocal laser scanning microscopy*. Anal Chem, 2001. **73**(5): 1016-1022.
111. Holland, R.D., et al., *Rapid identification of intact whole bacteria based on spectral patterns using matrix-assisted laser desorption/ionization with time-of-flight mass spectrometry*. Rapid Commun Mass Spectrom, 1996. **10**(10): 1227-1232.
112. Eddabra, R., et al., *Rapid discrimination of environmental Vibrio by matrix-assisted laser desorption ionization time-of-flight mass spectrometry*. Microbiol Res, 2012. **167**(4): 226-230.
113. Stephan, R., et al., *Rapid species specific identification and subtyping of Yersinia enterocolitica by MALDI-TOF mass spectrometry*. J Microbiol Methods, 2011. **87**(2): 150-153.
114. Ilina, E.N., et al., *Direct bacterial profiling by matrix-assisted laser desorption-ionization time-of-flight mass spectrometry for identification of pathogenic Neisseria*. J Mol Diagn, 2009. **11**(1): 75-86.
115. Liu, H., et al., *Universal sample preparation method for characterization of bacteria by matrix-assisted laser desorption ionization-time of flight mass spectrometry*. Appl Environ Microbiol, 2007. **73**(6): 1899-1907.
116. Hyzak, L., et al., *Quantitative matrix-assisted laser desorption ionization-time-of-flight mass spectrometry analysis of synthetic polymers and peptides*. Anal Chem, 2011. **83**(24): 9467-9471.
117. Hyzak, L., et al., *Improvements to the compressed-sample (CS) technique for MALDI-TOF mass spectrometry*. Anal Bioanal Chem, 2013. **405**(4): 1417-1424.
118. Klebe, R.J., *Cytoscribing: a method for micropositioning cells and the construction of two- and three-dimensional synthetic tissues*. Exp Cell Res, 1988. **179**(2): 362-373.
119. Lemmo, A.V., et al., *Inkjet dispensing technology: applications in drug discovery*. Curr Opin Biotechnol, 1998. **9**(6): 615-617.
120. Liberski, A.R., et al., *"One cell-one well": a new approach to inkjet printing single cell microarrays*. ACS Comb Sci, 2011. **13**(2): 190-195.

121. Tasoglu, S., et al., *Manipulating biological agents and cells in micro-scale volumes for applications in medicine*. Chem Soc Rev, 2013. **42**(13): 5788-5808.
122. Tasoglu, S. and Demirci, U., *Bioprinting for stem cell research*. Trends Biotechnol, 2013. **31**(1): 10-19.
123. Xu, T., et al., *Construction of high-density bacterial colony arrays and patterns by the ink-jet method*. Biotechnol Bioeng, 2004. **85**(1): 29-33.
124. Xu, T., et al., *Inkjet printing of viable mammalian cells*. Biomaterials, 2005. **26**(1): 93-99.
125. Saunders, R.E., et al., *Delivery of human fibroblast cells by piezoelectric drop-on-demand inkjet printing*. Biomaterials, 2008. **29**(2): 193-203.
126. Nakamura, M., et al., *Biocompatible inkjet printing technique for designed seeding of individual living cells*. Tissue Eng, 2005. **11**(11-12): 1658-1666.
127. Merrin, J., et al., *Printing multistrain bacterial patterns with a piezoelectric inkjet printer*. PLoS One, 2007. **2**(7): e663.
128. Choi, W.S., et al., *Synthetic multicellular cell-to-cell communication in inkjet printed bacterial cell systems*. Biomaterials, 2011. **32**(10): 2500-2507.
129. Sandler, N., et al., *Inkjet printing of drug substances and use of porous substrates-towards individualized dosing*. J Pharm Sci, 2011. **100**(8): 3386-3395.
130. Delvolve, A.M. and Woods, A.S., *Optimization of automated matrix deposition for biomolecular mapping using a spotter*. J Mass Spectrom, 2011. **46**(10): 1046-1050.
131. Luo, C., et al., *Generation of picoliter droplets of liquid for electrospray ionization with piezoelectric inkjet*. J Mass Spectrom, 2013. **48**(3): 321-328.
132. Riba, J., et al., *Label-free isolation and deposition of single bacterial cells from heterogeneous samples for clonal culturing*. Sci Rep, 2016. **6**: 32837.
133. Zheng, Q., et al., *Application of inkjet printing technique for biological material delivery and antimicrobial assays*. Anal Biochem, 2011. **410**(2): 171-176.
134. Vorm, O., et al., *Improved Resolution and Very High Sensitivity in MALDI TOF of Matrix Surfaces Made by Fast Evaporation*. Anal Chem, 1994. **66**: 3281-3287.
135. Nicola, A.J., et al., *Application of the fast-evaporation sample preparation method for improving quantification of angiotensin II by matrix-assisted laser desorption/ionization*. Rapid Commun Mass Spectrom, 1995. **9**(12): 1164-1171.
136. Han, W. and Lin, Z., *Learning from "coffee rings": ordered structures enabled by controlled evaporative self-assembly*. Angew Chem Int Ed Engl, 2012. **51**(7): 1534-1546.
137. Deegan, R.D., et al., *Capillary flow as the cause of ring stains from dried liquid drops*. Nature, 1997. **389**.
138. Arpa-Sancet, M.P., et al., *Microfluidic assay to quantify the adhesion of marine bacteria*. Biointerphases, 2012. **7**(1-4): 26.
139. Bader, H. and Hoigné, J., *Determination of ozone in water by the indigo method*. Water Res, 1981. **15**(4): 449-456.
140. Chen, F., et al., *Single-Cell Analysis Using Drop-on-Demand Inkjet Printing and Probe Electrospray Ionization Mass Spectrometry*. Anal Chem, 2016. **88**(8): 4354-4360.
141. Gao, P. and Xu, G., *Mass-spectrometry-based microbial metabolomics: recent developments and applications*. Anal Bioanal Chem, 2015. **407**(3): 669-680.

142. Wang, X., et al., *Evaluation and optimization of sample preparation methods for metabolic profiling analysis of Escherichia coli*. Electrophoresis, 2015. **36**(18): 2140-2147.
143. Shin, M.H., et al., *Evaluation of sampling and extraction methodologies for the global metabolic profiling of Saccharophagus degradans*. Anal Chem, 2010. **82**(15): 6660-6666.
144. Maharjan, R.P. and Ferenci, T., *Global metabolite analysis: the influence of extraction methodology on metabolome profiles of Escherichia coli*. Anal Biochem, 2003. **313**(1): 145-154.
145. Li, X., et al., *Sample preparation for the metabolomics investigation of poly-gamma-glutamate-producing Bacillus licheniformis by GC-MS*. J Microbiol Methods, 2013. **94**(1): 61-67.
146. Fischer, T., *Lyophilizer qualification: Some practical advice*. Drugs Pharm Sci, 2004. **135**: 517-534.
147. Fiehn, O., *Metabolomics by Gas Chromatography-Mass Spectrometry: Combined Targeted and Untargeted Profiling*. Curr Protoc Mol Biol, 2016. **114**: 30 34 31-30 34 32.
148. Schummer, C., et al., *Comparison of MTBSTFA and BSTFA in derivatization reactions of polar compounds prior to GC/MS analysis*. Talanta, 2009. **77**(4): 1473-1482.
149. Blau, K. and Halket, J.M., *Handbook of Derivatives for Chromatography, 2nd Edition*. 1993.
150. Maifiah, M.H., et al., *Global metabolic analyses identify key differences in metabolite levels between polymyxin-susceptible and polymyxin-resistant Acinetobacter baumannii*. Sci Rep, 2016. **6**: 22287.
151. Purcaro, G., et al., *Characterization of bacterial lipid profiles by using rapid sample preparation and fast comprehensive two-dimensional gas chromatography in combination with mass spectrometry*. J Sep Sci, 2010. **33**(15): 2334-2340.
152. Li, Y., et al., *Differentiation of bacteria using fatty acid profiles from gas chromatography-tandem mass spectrometry*. J Sci Food Agric, 2010. **90**(8): 1380-1383.
153. Belenky, P., et al., *Bactericidal Antibiotics Induce Toxic Metabolic Perturbations that Lead to Cellular Damage*. Cell Rep, 2015. **13**(5): 968-980.
154. Hazel, J.R. and Williams, E.E., *The role of alterations in membrane lipid composition in enabling physiological adaptation of organisms to their physical environment*. Prog Lipid Res, 1990. **29**(3): 167-227.
155. Santos, I.C., et al., *Analysis of bacteria stress responses to contaminants derived from shale energy extraction*. Environ Sci Process Impacts, 2019. **21**(2): 269-278.
156. Yao, L., et al., *Improved production of fatty alcohols in cyanobacteria by metabolic engineering*. Biotechnol Biofuels, 2014. **7**: 94.
157. Tamilmani, E., et al., *13-Docosenamide release by bacteria in response to glucose during growth-fluorescein quenching and clinical application*. Appl Microbiol Biotechnol, 2018. **102**(15): 6673-6685.
158. Black, G.E., et al., *Electrospray tandem mass spectrometry for analysis of native muramic acid in whole bacterial cell hydrolysates*. Anal Chem, 1994. **66**(23): 4171-4176.
159. Zhou, Y. and Imlay, J.A., *Escherichia coli K-12 Lacks a High-Affinity Assimilatory Cysteine Importer*. mBio, 2020. **11**(3).
160. Chonoles Imlay, K.R., et al., *Physiological Roles and Adverse Effects of the Two Cystine Importers of Escherichia coli*. J Bacteriol, 2015. **197**(23): 3629-3644.
161. Watson, S.P., et al., *Characterization of the starvation-survival response of Staphylococcus aureus*. J Bacteriol, 1998. **180**(7): 1750-1758.
162. Parthasarathy, A., et al., *A Three-Ring Circus: Metabolism of the Three Proteogenic Aromatic Amino Acids and Their Role in the Health of Plants and Animals*. Front Mol Biosci, 2018. **5**: 29.

163. Averesch, N.J.H. and Kromer, J.O., *Metabolic Engineering of the Shikimate Pathway for Production of Aromatics and Derived Compounds-Present and Future Strain Construction Strategies*. Front Bioeng Biotechnol, 2018. **6**: 32.
164. Delaney, J.T., et al., *Combinatorial optimization of multiple MALDI matrices on a single tissue sample using inkjet printing*. ACS Comb Sci, 2011. **13**(3): 218-222.
165. Smolira, A. and Wessely-Szponder, J., *Importance of the matrix and the matrix/sample ratio in MALDI-TOF-MS analysis of cathelicidins obtained from porcine neutrophils*. Appl Biochem Biotechnol, 2015. **175**(4): 2050-2065.
166. Zhang, N., et al., *Two-layer sample preparation method for MALDI mass spectrometric analysis of protein and peptide samples containing sodium dodecyl sulfate*. Anal Chem, 2001. **73**(13): 2968-2975.
167. Ojima-Kato, T., et al., *Assessing the performance of novel software Strain Solution on automated discrimination of Escherichia coli serotypes and their mixtures using matrix-assisted laser desorption ionization-time of flight mass spectrometry*. J Microbiol Methods, 2015. **119**: 233-238.
168. Chui, H., et al., *Rapid, Sensitive, and Specific Escherichia coli H Antigen Typing by Matrix-Assisted Laser Desorption Ionization-Time of Flight-Based Peptide Mass Fingerprinting*. J Clin Microbiol, 2015. **53**(8): 2480-2485.
169. Shell, W.S., et al., *Matrix-assisted laser desorption-ionization-time-of-flight mass spectrometry as a reliable proteomic method for characterization of Escherichia coli and Salmonella isolates*. Vet World, 2017. **10**(9): 1083-1093.
170. Mujawar, L.H., et al., *Spot morphology of non-contact printed protein molecules on non-porous substrates with a range of hydrophobicities*. Analyst, 2013. **138**(2): 518-524.
171. Eral, H.B., et al., *Control of evaporating complex fluids through electrowetting*. Soft Matter, 2012. **8**: 10614–10617.
172. Yunker, P.J., et al., *Suppression of the coffee-ring effect by shape-dependent capillary interactions*. Nature, 2011. **476**(7360): 308-311.
173. Anyfantakis, M. and Baigl, D., *Dynamic photocontrol of the coffee-ring effect with optically tunable particle stickiness*. Angew Chem Int Ed Engl, 2014. **53**(51): 14077-14081.
174. Nguyen, H.Q., et al., *Recrystallization of dried droplets using acetonitrile to improve surface homogeneity in matrix-assisted laser desorption/ionization mass spectrometric analysis with 2,5-dihydroxybenzoic acid matrix*. Rapid Commun Mass Spectrom, 2019. **33**(18): 1481-1484.
175. Sleno, L. and Volmer, D.A., *Some fundamental and technical aspects of the quantitative analysis of pharmaceutical drugs by matrix-assisted laser desorption/ionization mass spectrometry*. Rapid Commun Mass Spectrom, 2005. **19**(14): 1928-1936.

List of Publication

Publication

Li, J., Rumancev, C., Lutze, H.V., Schmidt T.C., Axel R., Schmitz O.J., *Effect of ozone stress on the intracellular metabolites from Cobetia marina*. Anal Bioanal Chem. 2020; 412: 5853–5861

Ayala-Cabrera, J.F., Lipok, C., Li, J., Moyano, E., Schmitz, O.J., Santos, F. J., *Ionic Liquid Stationary Phase for Improving Comprehensive Two-dimensional Gas Chromatographic Separation of Polychlorinated Naphthalenes*. Accepted in Journal of Chromatography A

Chen, Y., Montero, L., Luo, J., Li, J., Schmitz O. J., *Application of the new at-column dilution (ACD) modulator for the two-dimensional RPxHILIC analysis of Buddleja davidii*, Anal Bioanal Chem. 2020; 412:1483–1495

Chen, Y., Li, J., Schmitz, O.J., *Development of an at-column dilution modulator for flexible and precise control of dilution factors to overcome mobile phase incompatibility in comprehensive two-dimensional liquid chromatography.* Anal Chem. 2019; 91:10251-10257

Posters

9th Shanghai International Symposium on Analytical Chemistry, Shanghai/China, 2018, participation with poster, "*Ozone Stress Effect on the Intracellular Metabolites from Cobetia Marina measured by GCxGC-MS"*.

8th Shanghai International Symposium on Analytical Chemistry, Shanghai/China, 2018, participation with poster, "*Determination of Intracellular Metabolites from Cobetia Marina by Two-Dimensional Gas Chromatography with Mass Spectrometer"*.

Curriculum Vitae

For data protection reasons the Curriculum Vitae is not included in the online version.

Acknowledgment

First of all, I would like to thank my doctoral supervisor Prof. Oliver J. Schmitz very much for sparing no effort to supervise this work. Thank you for offering me such an opportunity to pursue my scientific dream and all the arrangements to enrich my experience. Thank you for the tremendous support, guidance, and encouragement during the period of work and enlightening discussions. I would also thank Prof. Dr. Torsten Schmidt for igniting and allowing me to take ozone treatment as a critical part of this thesis.

My special thanks go to Dr. Christoph Rumancev from Prof. Dr. Rosenhahn's working group, who helped me prepare the *C. marina* during the whole thesis time. Thank you for supporting me with the background knowledge and helping me with the MIC test for the livability validation. I would particularly like to thank Prof. Dr. Holger Lutze, who explained the ozonation process and discussed with me for the lab feasibility of ozone stress. Thanks to Katharina from Prof. Dr. Torsten Schmidt's group for the hand on ozone depletion and spiking to the bacteria culture. I would like especially to thank all my colleagues for always listening to my questions or problems and offering in-time help.

I would also like to thank my family and especially my wife Puyu, who encouraged me to pursue the PhD and always supported me no matter when and no matter what I need to accomplish my work. I could not reach here without her patience and love.

Sincerely

Thanks.